Vortex-to-Polarization Phase Transformation in $Pb(ZrTi)O_3$ Nanoparticles

Ivan I. Naumov and Huaxiang Fu
Department of Physics, University of Arkansas, Fayettville, AR 72701

I. INTRODUCTION

Vortex is a circularly ordered structure phase of broad interest, which has been found in ferromagnets, superconductors, and Bose-Einstein condensated atoms. Recently, the vortex phase formed by *electric* dipoles was revealed to exist in ferroelectric (FE) nanoparticles.[1]. In FEs, another ordered structure of general concern is the ferroelectric phase with an *out-of-plane* polarization[2]. Transformation between these two ordered structures in FE nanoparticles, by electric fields perpendicular to the vortex plane, is a phase transition of fundamental relevance, since this vortex-to-polarization transformation involves two phases of completely different order parameters (namely, toroid moment in vortex phase versus polarization in ferroelectric phase), and is a critical example to study collective mechanism in terms of how order parameter nucleates and/or disappears *within a single domain*.

Here we perform *ab-initio* based simulations[3–5] on vortex-to-polarization phase transformation, induced by homogeneous electric fields normal to the vortex plane, in nanoparticles made of technologically important $Pb(Zr_{0.5}Ti_{0.5})O_3$ (PZT) solid solution. These studies lead to (1) the finding of a new structure that bridges the transformation between two phases of unlike order parameters, (2) the existence of a new type of hysteresis, and (3) a possibly interesting approach for reading FE toroid moment.

II. RESULTS

Figure 1a depicts the collective behaviors of toroid moment, $\mathbf{G} = \frac{1}{2\mathrm{N}}\sum_i \mathbf{r}_i \times \mathbf{p}_i$, and net polarization, $\mathbf{P} = \frac{1}{\mathrm{N}\Omega}\sum_i \mathbf{p}_i$ (where N is the number of bulk cells and Ω is the cell volume), that develop in a d=19 nanodisk as the strength of electric field varies. When electric field is small and below a critical value $\mathrm{E}_{c,1} = 1.5\mathrm{V/nm}$, the disk shows only a G_z toroid component while G_x and G_y are null. The system in the $\mathrm{E} \leq \mathrm{E}_{c,1}$ field region thus retains the same macroscopic toroid symmetry as in zero field (this structure phase will be denoted as phase I hereafter). As the field reaches $\mathrm{E}_{c,1}$, the G_z moment declines only slightly as compared to the initial zero-field value, and meanwhile, a net polarization of $0.3\mathrm{C/m}^2$ develops. The vortex response of phase I is thus characterized by the coexistence of strong toroid moment and large polarization, *both pointing along the cylindrical z-axis*. We further numerically find that the toroid moment in phase I responds to the **E** field by accurately following a quadratic scaling law as $\mathrm{G_z}(E) = \mathrm{G}_0 - \sigma\mathrm{E}^2$.

The system behaves in a different fashion as the electric field exceeds $\mathrm{E}_{c,1}$, manifested in Fig.1a by the dramatic occurrence of a nonzero G_y component and simultaneously a sharp decline of the G_z. Being perpendicular to the initial G_z moment, the appearance of the G_y moment deviates the system from continuing to possess macroscopic cylindrical symmetry, and the resulting symmetry-broken new structure is to be denoted as phase II. This phase acts as the intermediate state for bridging the transformation from phase I (of the same cylindrical symmetry as the initial vortex) to the destination phase of uniform polarization (that also has cylindrical symmetry). Finally, when electric field continues to increase, the phase II eventually disappears above a critical value $\mathrm{E}_{c,2} = 2.8\mathrm{V/nm}$.

Turning off electric fields when the system is in a phase II leads to hysteresis which is caused by toroid moment. Our simulations reveal that, regardless of whether the field is gradually reduced or suddenly switched off, the system in phase II does not transform back to the initial state of G_z moment, and instead is trapped in the G_y vortex state (Fig.1b, left plot). Trapping of the system in the G_y state also suggests that this state is stable and surrounded by energy barrier. To confirm this, the system of the G_y phase is heated at zero field to a chosen temperature $\tilde{T}$ and then cooled down to 64K. We found that only when $\tilde{T}$ is above 500K the G_y phase is able to overcome the barrier and becomes the G_z phase (see the right plot of Fig.1b).

Our analysis shows that, in addition to the reduction of the depolarizing field, there is another factor that facilitates the transformation from phase I into phase II, that is, the interaction between local mode and strain. Fig.1c depicts the strain components at different fields. At zero field the lattice of the vortex state is pseudo-tetragonal with c/a ratio less than 1, i.e., with strain components $\eta_{xx} = \eta_{yy} > \eta_{zz}$, because all dipoles are laying in the xy plane. As the field increases, the c/a rises as a result of the polarization-strain coupling. Notably, the field at which c/a becomes 1 (i.e., the system becomes pseudocubic) is very close to the critical $\mathrm{E}_{c,1}$ field where phase I is transformed into phase II. The mode-strain coupling[3] $-\sum_i |B|(\eta_{xx}u_{ix}^2 + \eta_{yy}u_{iy}^2 + \eta_{zz}u_{iz}^2)$ (where B is the coupling strength) advances the transition into phase II largely due to the increase in atomic volume, $\Delta\Omega/\Omega_0 = \eta_{xx} + \eta_{yy} + \eta_{zz}$, which is nearly a constant in phase I and rises sharply for $\mathrm{E}>\mathrm{E}_{c,1}$ (Fig.1c).

We next address how the diameter of nanodisk may influence the vortex transformation. We find that there is a critical size d_c=17, below which the transformation path turns out to be different. Simulation results of a

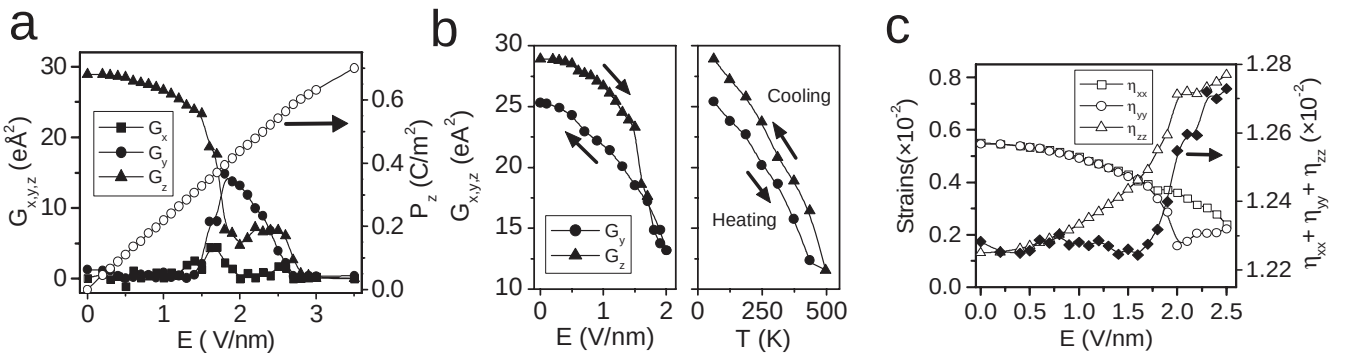

FIG. 1: (a) Toroid moment **G** (using the left vertical axis) and net polarization P_z (using the right vertical axis) in a d=19 disk. (b) Left: hysteresis of toroid moment caused by increasing and then decreasing the electric field in d=19 disk; Right: transformation of the G_y vortex into a G_z vortex by heating the system to 500K and then cooling down. (c) Strain components η_{xx}, η_{yy} and η_{zz} (using the left vertical axis) and volume expansion $\eta_{xx} + \eta_{yy} + \eta_{zz}$ (filled symbols, using the right vertical axis). The horizontal axis in (a) and (c) is the strength of electric field.

d=9 disk (not shown here) reveal that the vortex undergoes a continuous transformation into a single domain ferroelectric phase, without the bridging phase II. The critical $E_{c,2}$ field in the d=9 disk decreases to 1.3V/nm. One main difference between d=9 and d=19 nanodisks is the depolarizing effect which is small in the former and thus allows a symmetry conforming transformation.

We also like to point out that the predicted FE-vortex responses may have some technological implication. The quadratic law, $G_z(E) = G_0 - \sigma E^2$, tells us that, when a FE nanodisk is exposed to an alternating field $\mathbf{E}(t) = \mathbf{E}_0 \cos \omega t$, the toroid moment $\mathbf{G}(t)$ will respond with a double frequency 2ω, and its radiation field can be separated from the field of the vibrating polarization which responds only with ω. The signal with 2ω frequency may further tell us whether it is associated with moment **G** or $-\mathbf{G}$, since the latter field is phase shifted by π.[6] This may thus open an approach by using electromagnetic fields of pulse lasers to probe and/or read FE vortex state. Compared to mechanical approach using piezoelectric force microscope tips, the optic approach is fast and can be performed simultaneously in a large quantity.

III. ACKNOWLEDGEMENTS

This work was supported by the Office of Naval Research and the Army Congressional Fund. The computing facility was provided by the Center for Piezoelectrics by Design.

[1] I.I. Naumov, L. Bellaiche, and H. Fu, Nature **432**, 737 (2004).
[2] D.D. Fong, G.B. Stephenson, S.K Streiffer, J.A. Eastman, O. Auciello, P.H. Fuoss, and C. Thompson, Science **304**, 1650 (2004).
[3] W. Zhong, D. Vanderbilt, and K. M. Rabe, Phys. Rev. Lett. **73**, 1861 (1994).
[4] L. Bellaiche, A. Garcia, and D. Vanderbilt, Phys. Rev. Lett. **84**, 5427 (2000).
[5] A. Garcia and D. Vanderbilt, Appl. Phys. Lett. **72**, 2981 (1998).
[6] V.M. Dubovik, M.A. Martsenyk, N.M. Martsenyk, J. Magn. Magn. Mater. **145**, 211 (1995).

Ferroelectricity in charge-ordered $LuFe_2O_4$ from first principles

Takeshi Nishimatsu, David Vanderbilt, Karin M. Rabe, and Yoichi Horibe
Department of Physics and Astronomy, Rutgers University
136 Frelinghuysen Road, Piscataway, NJ 08544-8019
Phone: 732-445-4197; Fax: 732-445-4343; e-mail: takeshi@physics.rutgers.edu
Claude Ederer
Department of Physics, Columbia University
538 West 120th Street, New York, NY 10027

Electron and x-ray diffraction experiments [1, 2, 3] suggest that $LuFe_2O_4$ develops ferroelectricity via a novel electronic mechanism based on a $\sqrt{3} \times \sqrt{3}$ charge ordering in which equal numbers of Fe^{2+} and Fe^{3+} are ordered in such a way as to break inversion symmetry (Fig. 1). However, the precise nature of the charge and magnetic orders and their coupling to structural distortions remain poorly understood. With this motivation, we have undertaken a first-principles study of $LuFe_2O_4$ using DFT-based methods, specifically LDA+U as implemented in VASP.

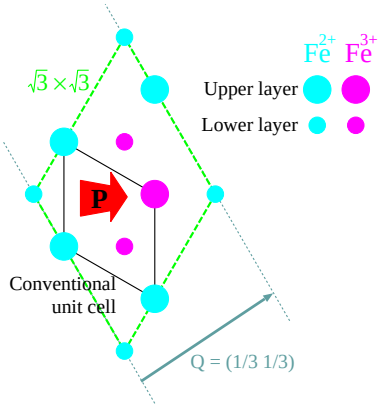

Figure 1. Charge-ordering in a $\sqrt{3}\times\sqrt{3}$ structure on the Fe-ion double-layer of $LuFe_2O_4$. (After [3])

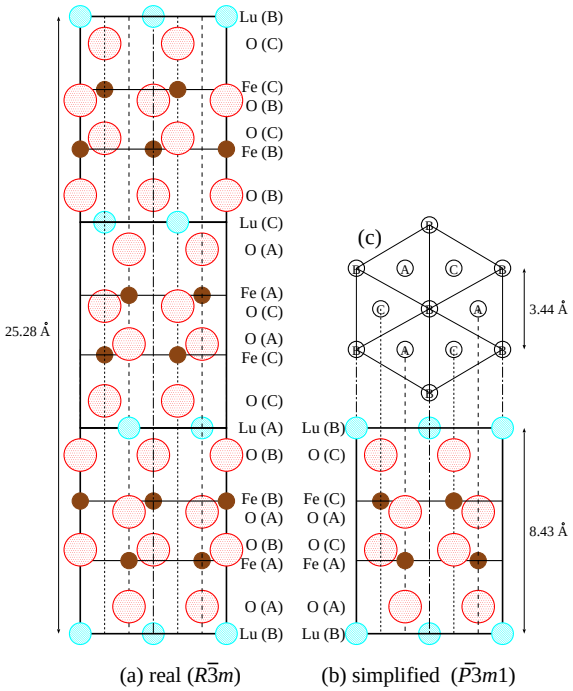

Figure 2. Schematically illustrated stackings along c-axis of (a) real and (b) simplified structures of $LuFe_2O_4$. In (c), three kinds of sites, A, B, and C, are projected and depicted onto xy-plane. (After [4])

The high-symmetry reference structure of $LuFe_2O_4$ can be regarded as a stacking of Fe_2O_2 double layers and LuO_2 layers, as depicted in Fig 2(a), with space group $R\bar{3}m$ and 3 formula units per hexagonal conventional unit cell (1 formula unit per rhombohedral primitive cell). Calculations for configurations with charge and magnetic orderings require the use of supercells containing multiple reference unit cells. To allow for the investigation of

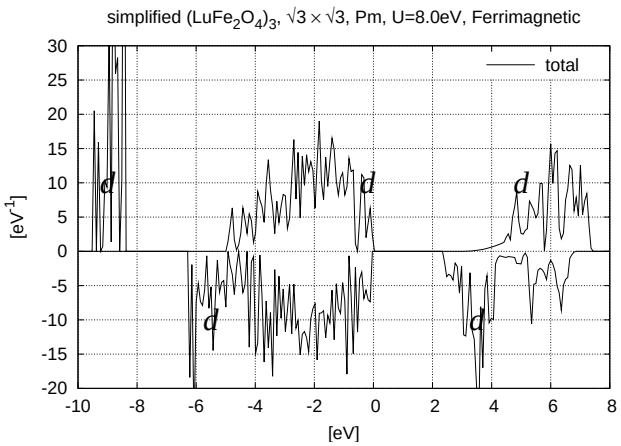

Figure 3. Spin polarized density of states of $LuFe_2O_4$ with $\sqrt{3} \times \sqrt{3}$ charge and magnetic ordering of the simplified reference structure discussed in the text. Bands mainly comprised of $3d$ electrons of Fe are indicated with "d".

the widest possible variety of ordering with available computational resources, we consider a simplified reference structure with a different stacking arrangement, shown in Fig. 2(b), with space group $P\bar{3}m1$ and 1 formula unit per unit cell. As this modification preserves the Fe_2O_2 double layer structure, the results for the charge and magnetic ordering are expected to be relevant to the real system; in addition we note that the calculated difference in cohesive energy between the two structures is less than 5 meV/formula unit.

We performed calculations for selected charge and magnetic orderings for a range of values of U, allowing relaxation of atomic coordinates in the supercells. In general, the configurations considered were found to be metallic, inconsistent with the observed ferroelectricity. We did identify one insulating configuration, with density of states shown in Fig. 3, for $U = 8.0$ eV; it has $\sqrt{3} \times \sqrt{3}$ charge and ferrimagnetic spin ordering, resulting in a Pm symmetry with 3 formula units per unit cell. Calculations of the induced structural distortions and polarization and their relation to experiment, and explorations to identify other insulating configurations, are in progress.

Despite the limitations of a DFT-based approach, these results provide useful guidance in the quest to develop an understanding of the novel form of ferroelectricity displayed by this material.

References

[1] Y. Yamada, S. Nohdo and N. Ikeda: J. Phys. Soc. Jpn. **66** (1997) 3733.

[2] Y. Yamada, K. Kitsuda, S. Nohdo and N. Ikeda: Phys. Rev. B **62** (2000) 12167.

[3] N. Ikeda, H. Ohsumi, K. Ohwada, K. Ishii, T. Inami, K. Kakurai, Y. Murakami, K. Yoshii, S. Mori, Y. Horibe and H. Kito: Nature **436** (2005) 1136.

[4] N. Ikeda, K. Kohn, N. Myouga, E. Takahashi, H. Kitoh and S. Takeawa: J. Phys. Soc. Jpn. **69** (2000) 1526.

Epitaxial stabilization of artificial hexagonal RMnO$_3$ (R = Dy, Tb, and Gd) thin films and their physical properties

T. W. Noh, J. H. Lee, D. Lee, S. Y. Jang

ReCOE, School of physics and astronomy, Seoul National University, Seoul 151-747, Korea

Phone: 82-2-880-6616; Fax: 82-2-875-1222; E-mail: twnoh@snu.ac.kr

The lanthanide based RMnO$_3$ (R=Tb,Dy,..., and Lu) have been attractive materials for researchers because of their richness in physics due to the interplay between charge, spin and lattice degrees of freedom. Especially, the orthorhombic RMnO$_3$ (R = Dy, Tb, and Gd) compounds are recently found to have large magneto-electric couplings, but their ferroelectric and antiferromagentic transition temperatures are quite low (typically, much below 77 K). On the other hand, hexagonal RMnO$_3$ (R = Ho, ..., and Lu) have high ferroelectric transition temperatures (typically, above room temperature) and their remnant polarization values are much larger than those of the orthorhomic phase materials. Note that the difference between the formation energies of the orthorhombic and the hexagonal RMnO$_3$ phases could be small. Therefore, as schematically shown in Fig. 1, it might be possible to stabilize orthorhombic RMnO$_3$ into a metastable hexagonal phase using a suitable substrate, such as Pt/Al_2O_3(0001) or YSZ(111), which has a hexagonal symmetry.

In this presentation, we will report the fabrication of the artificial hexagonal RMnO$_3$ (R = Dy, Tb, and Gd) thin films using the epitaxial stabilization technique[1]. From the P-E hysterisis loops, shown in Fig. 2, we could observe enhanced ferroelectric properties: for example, h-TbMnO$_3$ thin film has maximum polarization of 1.6 $\mu C/cm^2$, which is 20 times higher than that of the orthorhombic phase, and its Curie temperature is about 60 K. Above 65 K, we found an antiferroelectric-like phase. As shown in Fig. 3, magnetic property studies showed that they have antiferromagnetic Néel temperatures around 60 K and a spin reorientation transition around 40 K. And, we also observed intriguing spin–glass-like behaviors, which could arise from the geometric frustration of antiferromagnetically-coupled Mn spins with an edge-sharing triangular lattice.[2] We also found experimental evidences for the second-order magnetoelectric effects. As displayed in Fig. 4, the magnetoelectric coefficients decrease below the spin reorientation transition temperature, but increases above it, suggesting a moderate coupling between spin and charge. These intriguing findings suggest the uniqueness of the artificial h-RMnO$_3$ compounds in multiferroic materials and a possible extention of this approach to find new multiferroic materials.

[1] J.-H. Lee *et al*. Adv. Mater. **18**, 3125 (2006).
[2] J.-H. Lee *et al*. Appl. Phys. Lett. (in press) / cond-mat/0610681

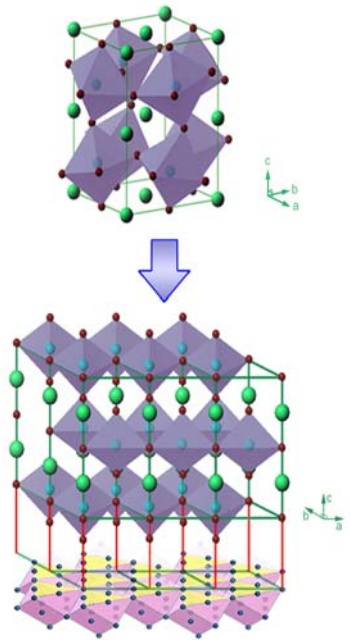

Figure 1 Schematic representation of epitaxial stabilization into hexagonal structure from bulk orthorhombic structure.

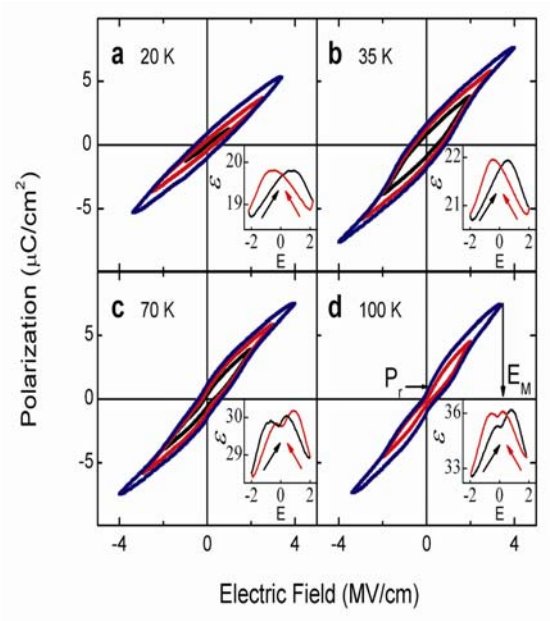

Figure 2 Ferroelectric polarizations *vs*. Electric field hysteresis loops of *h*-$TbMnO_3$ thin film measured at (a) 20 K, (b) 35 K, (c) 70 K, and (d) 100 K.

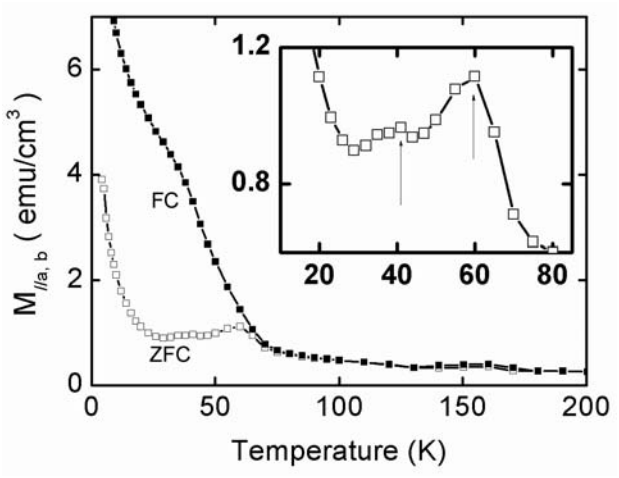

Figure 3 Temperature-dependent magnetization curves of *h*-$DyMnO_3$ thin film measured with a 100 Oe magnetic field along the in-plane axes after zero-field cooling (ZFC) and field cooling (FC).

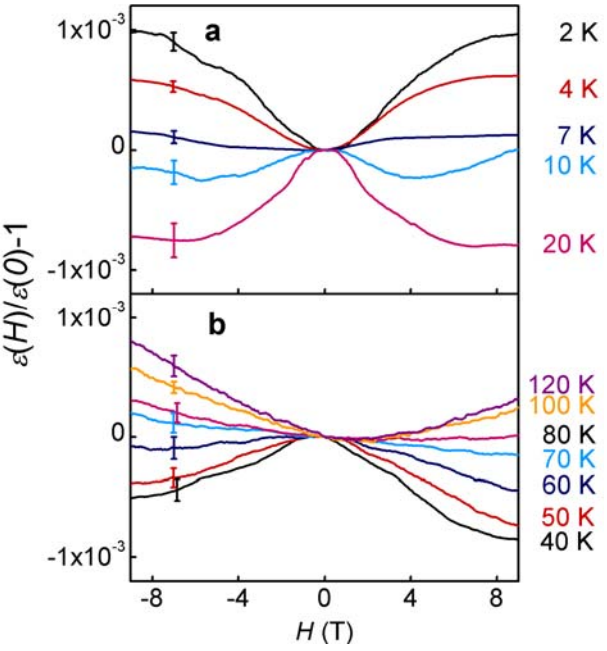

Figure 4 Magnetocapacitance of hexagonal $TbMnO_3$. The magnetic field dependence of $\varepsilon(H)/\varepsilon(0) - 1$ at temperatures (a) below 20 K, and (b) from 40 to 120 K.

Modelling Thickness-Dependence of Ferroelectric Thin Film Properties

L. Pálová, P. Chandra and K. Rabe
Department of Physics and Astronomy, Rutgers University, Piscataway, NJ 08854

Increasing demands for high-density data storage with ultra-fast accessibility present tremendous challenges. In parallel to the characterization of new materials, important size-dependent effects must be understood to optimize design. This is particularly true for ferroelectric memories [1]; their dielectric properties are strongly dependent on electromechanical boundary conditions due to the long-range nature of their underlying electrostatic interactions. In ferroelectric thin films, the effects of homogeneous misfit strain have been identified [2], studied and controlled to the point that particular systems have been strain-engineered to have spontaneous polarizations significantly larger than those in the bulk [3]. Despite these impressive achievements, several authors [4, 5, 6, 7] have suggested that homogeneous epitaxial strain cannot qualitatively account for all the observed effects in ferroelectric films. In particular, the thickness-dependence of their dielectric properties has been attributed to defect-induced strain gradients [4, 6].

Broadening of the temperature-dependent dielectric constant in thin films near the paraelectric-ferroelectric transition is reported by several experimental groups [8, 9]; this observed smearing, accompanied by an overall reduction in the dielectric permittivity, is more pronounced with decreasing film thickness, Fig. 2. This feature is characteristic of dielectric behavior in applied bias field that breaks the symmetry $P \rightarrow -P$. As an example, it has been noted that flexoelectric coupling of strain gradients to the polarization implies a spatially-varying effective field term due to the underlying inhomogeneous strain; the resulting phenomenological model successfully reproduces key thickness-dependences of the dielectric properties [6].

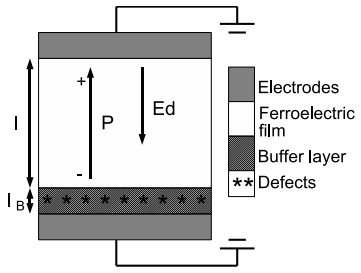

Figure 1: A schematic of the modelled ferroelectric capacitor under study with the key length-scales and regions clearly demarcated. Note that the mismatch defects are segregated in a buffer layer of thickness l_B on the substrate, and that the polarization is homogeneous in the majority of the film. Incomplete charge compensation at the ferroelectric-electrode interfaces results in a depolarization field as shown.

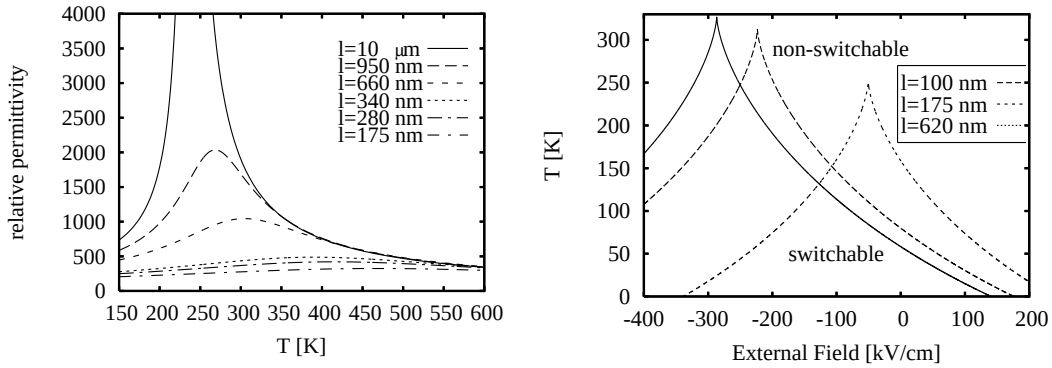

Figure 2: Calculated relative permittivity as a function of temperature for $BaSrTiO_3$ (BST) films of thicknesses $l = 10\mu m$, 950, 660, 340, 280 and 175 nm. The highest permittivity corresponds to the thickest film; it diverges at the bulk Curie temperature at 235 K. Reduction of the permittivity for thin films is observed.

Figure 3: Phase-transition temperature as a function of applied external electric field for BST films of thicknesses 100 (solid), 175 (dashed) and 620 nm (dotted line); non-switchable and switchable phases denote one or two possible polarization states, respectively.

Lattice mismatch between the film and the substrate is a key source of macroscopic strain in these systems [2]. In our phenomenological treatment, we assume that the misfit dislocations created by the lattice mismatch reside within a thin buffer layer next to the film-substrate interface. The majority of the film, which is relatively defect-free, is then elastically relaxed and homogeneous, as depicted schematically in Fig. 1; we describe it using a Landau-Ginzburg approach that includes depolarization effects and an effective field term [7]. Representative results for $BaSrTiO_3$ are displayed in Figs. 2 and 3, and this approach is also applied to strained $SrTiO_3$ with comparison to first-principles calculation and experiment whenever possible. Finally we discuss "smoking gun" probes for inhomogeneous strain in ferroelectric thin films.

References

[1] O. Auciello et al., *Physics Today* **51**, 22 (1998).

[2] N.A. Pertsev et al., *Phys. Rev. B* **80**, 1988 (1998).

[3] K.J. Choi et al. *Science* **306**, 1005 (2004).

[4] D. Balzar et al., *Phys. Rev. B* **70**, 092103 (2004).

[5] S.P. Alpay et al., Appl. Phys. Lett. **8**5 2044 (2004).

[6] G. Catalan et al., *J. Phys. Condens. Mat.* **16**, 2253 (2004); G. Catalan et al., Phys. Rev. B **72**, 020102 (2005).

[7] A.M. Bratkovsky and A.P. Levanyuk, *Phys. Rev. Lett.* **9**4, 107601 (2005).

[8] C.B. Parker et al., *Appl. Phys. Lett.* **81** 340 (2002).

[9] L.J. Sinnamon et al., Appl. Phys. Lett. **81**, 889 (2002).

NMR Chemical Shielding in Perovskites: Embedded Cluster Calculations

D. L. Pechkis, E. J. Walter, H. Krakauer
Department of Physics, College of William and Mary, Williamsburg, VA, 23187-8795
Phone: 757-221-3557; Fax: 757-221-3540; email: dlpech@wm.edu

NMR spectroscopy is an important probe of local structure, which can be applied equally well in crystalline and disordered materials. NMR spectra reflect the distribution of environments of the target nuclear species as manifested by the chemical shielding of the external magnetic field and (for quadrupole nuclei) by coupling to the electric field gradient (EFG) The EFGs are easily obtained using any first-principles all-electron electronic structure method. While the calculation of chemical shieldings has long been available using mature molecular codes such as Gaussian and NWCHEM, it has only recently been implemented for periodic boundary condition (PBC)[1]. While the PBC codes are limited to the LDA and GGA levels of density functional theory, the molecular codes additionally allow calculations of chemical shielding using higher levels of theory, such as B3LYP, MP2 and coupled cluster methods. This may be important, since there is evidence that LDA and GGA are inadequate in materials where O(2p)-cation(d) hybridization is present (see Table II below). We have therefore investigated the use of embedded clusters to calculate chemical shielding tensors in perovskites. Material properties can be accurately determined from embedded clusters if the properties of interest depend strongly on the local structure and weakly on longer-range atomic arrangements. Experience with other materials indicates that this is true for EFGs and chemical shieldings. In this regard, the embedded cluster approach may also be more efficient than the PBC approach for calculating properties of disordered systems, since the local environment need not be modeled by large supercells as with PBC.

An embedded cluster for the ionic materials considered here consists of a small number of real or "quantum" (QM) atoms, typically centered on the target atom. The QM atoms are embedded in a large array of point charges (PC) placed at the appropriate atomic positions. The first $\simeq 500-700$ PC adjacent to the QM have the nominal charge of the ion they represent (e.g. Ti^{+4}, O^{-2}), while the charge of the remaining $\simeq 6000-14,000$ PC can be adjusted so that the Madelung potential on and surrounding the QM atoms is exact[3]. In addition to the above, cation PC's that are nearest neighbors (NN) of O atoms are replaced by large-core pseudopotentials of the same charge (total ion pseudopotentials - TIPs), to better mimic the quantum mechanical Pauli core repulsion of the cations [4]. This method has been successfully applied to calculating the energy level structure of doped rock salts [4] and has also been used calculate ligand-metal charge transfer excitations, crystal field spectra, photoemission spectra [5], NQR spectra [6], and EFGs of high temperature superconductors [7].

	Mg		O		
	V_{zz}	Force	V_{zz}	Force	σ_{iso}
MgO_6-Mg^*_{18}	-3.32	-1.28			
$Mg_{19}O_6$	-2.92	-1.29			
OMg_6			-0.80	1.42	357.5
$O_{19}Mg_6$-Mg^*_{36}			-0.75	0.85	180.0
$O_{19}Mg_{44}$			-0.72	1.31	189.0
LAPW	-3.12	-1.28	-0.79	1.28	

Table 1: Embedded cluster tests for distorted rock salt MgO. The electric field gradient, V_{zz} (in units of $10^{21}V/m^2$) and the force (in units of eV/Å) are given for the central atom. Results for Mg- and O-centered clusters are shown. X* refers to a TIP for atom type X. Forces and EFGs are at the LDA level of theory and the isotropic chemical shielding is at the GGA level [2]

The convergence of various LDA [8] calculated properties in MgO is shown in Table 1. Results using embedded clusters and Gaussian98 [9] representing a distorted MgO structure ([111] frozen optic phonon) are compared to PBC calculations using the LAPW method [10]. EFGs and forces on the central atom are compared, and the ^{17}O isotropic chemical shift is also given for the O-

centered cluster. Convergence of basis set size was tested for both atoms with the OMg_6 and MgO_6 clusters. Convergence was achieved with Mg and O having the cc-pCVTZ [11] and IGLO-III [12] basis sets respectively. Both the forces and the EFGs calculated with embedded clusters compare favorably to LAPW. Even the 7 atom Mg center cluster is in good agreement. The EFGs and isotropic chemical shielding values are converged with the 25 atom O centered cluster.

To further validate our method, we compared ^{17}O chemical shifts in undistorted MgO and CaO to PBC projector augment wave (PAW) values computed by Profeta and coworkers [13] (Table II). The cluster method ^{17}O chemicals shifts are in good agreement with PAW. However, both methods give an ^{17}O CaO chemical shift value that is in poor agreement with experiment. Profeta *et al.* [13] attributed this to the tendency of GGA to overestimate the effects of O(2p)-Ca(3d) hybridization on the ^{17}O chemical shielding. This indicates that higher levels of theory may be required to accurately predict chemical shifts in perovskite piezoelectrics, where O(2p)-cation(d) hybridization effects are large, *e.g.* as seen in large anomalous Z* values.

	This work	PBC-PAW	Experiment
MgO	58.4	58.8	47.0
CaO	426.64	418.05	294.0

Table 2: ^{17}O isotropic chemical shifts in ppm (relative to liquid water for MgO and CaO. $O_{19}X_6$-X^*_{36} clusters were used for these calculations, where X = Ca, Mg. PBC-PAW refers to Ref.[1] which used periodic boundary conditions and the projector augmented wave method [13].

Preliminary GGA results for $PbTiO_3$ and $SrTiO_3$ QM clusters containing up to 27 QM atoms have been obtained. The calculated ^{17}O chemical shifts in $PbTiO_3$ do not show the $\simeq$ 200 ppm O1-O2 difference seen in the only available experimental measurement[14]. Barring possible experimental issues, this discrepancy could result from the GGA p-d hybridization problem, as in CaO. Calculated GGA ^{47,49}Ti chemical shifts are, however, in reasonable agreement with experiment[15]. We are in the process of verifying convergence of these results with larger QM clusters.

Acknowledgments: Supported by ONR, CPD, and VSGC

References

[1] C. J. Pickard and F. Mauri. *Phys. Rev. B*, 63:245101, 2001.

[2] K. Burke, J. P. Perdew, and Y. Wang. *Electronic Density Functional Theory: Recent Progress and New Directions*. Plenum, 1998.

[3] M. K. Klintenberg, S. E. Derenzo, and M. J. Weber. *Comput. Phys. Commun.*, 131:120, 2000.

[4] N. W. Winter, R. M. Pitzer, and D. K. Temple. *J. Chem. Phys.*, 86:3549, 1987.

[5] R. L. Martin and P. J. Hay. *J. Chem. Phys.*, 98:8680, 1993.

[6] R. L. Martin. *Phys. Rev. Lett.*, 75:744, 1995.

[7] P. Husser, H. U. Suter, E. P. Stoll, and P. F. Meier. *Phys. Rev. B*, 61:1567, 61.

[8] J. P. Perdew and A. Zunger. *Phys. Rev. B*, 23:5048, 1981.

[9] M. J. Frisch et al.. Gaussian 03, Revision C.02. Gaussian, Inc., Wallingford, CT, 2004.

[10] D. Singh. *Planewaves, Pseudopotentials, and the LAPW Method*. Kluwer Academic Publishers, 1994.

[11] D. Woon and Jr. T. H. Dunning. *J. Chem. Phys.*, 103:1995, 1995.

[12] W. Kutzelnigg, U. Fleischer, and M. Schindler. *NMR Basic Principles and Progress Vol. 213, p. 165-262*. Springer Verlag, 1991.

[13] M. Profeta, M. Benoit, F. Mauri, and C. J. Pickard. *J. Phys. Chem. B*, 109:6052, 2005.

[14] A. Baldwin, P. A. Thomas, and R. Dupree. *J. Phys.: Condens. Matter*, 17:7159, 2005.

[15] D. Padro, V. Jennings, M. E. Smith, R. Hoppe, P. A. Thomas, and R. Dupree. *J. Phys. Chem. B*, 106:13176, 2002.

Properties of ferroelectric ultrathin films grown along [001], [110] and [111] directions

I. Ponomareva and Laurent Bellaiche
Physics Department, University of Arkansas, Fayetteville, Arkansas 72701, USA
Phone: 479-575-5596; Fax: 479-575-4580; e-mail: iponoma@uark.edu

Ferroelectric thin films have been intensively studied recently (see Refs. [1–4] and references therein) because of their potential applications in miniaturized devices. The dependencies of their properties on thickness, electrical and mechanical boundary conditions have been widely investigated. However, an overwhelming majority of past studies focused on films grown along the [001] direction, while it was found that the properties of ferroelectric films can be dramatically influenced by the growth direction [5–7].

Here, we report the results of first-principles-based Monte Carlo calculations of $Pb(Zr_{0.4}Ti_{0.6})O_3$ ferroelectric thin films of 48 Å thickness that are grown along [001], [110] and [111] directions and subject to different electrical and mechanical boundary conditions [8]. Electrical boundary conditions are simulated by partial or full screening of the depolarizing field inside the film with the screening strength being controlled by a coefficient β. The full screening of the depolarizing field corresponds to ideal short-circuit (SC) boundary conditions and is associated with $\beta = 1$. When no screening is applied ($\beta = 0$ in our simulations) we have ideal open-circuit (OC) boundary conditions. β in-between correspond to partial screening. Mechanical boundary conditions corresponding to epitaxially grown films are simulated by freezing some homogeneous strain components.

Fig.1 shows the results of our simulations, and reveals a wide variety of dipole pattern. Such variety can be explained by the following simple rules: *Rule 1: Close to SC conditions*, the films are *homogeneously* polarized with the polarization: $\mathbf{P} = \lambda_1 \mathbf{e_g} + \lambda_2 \mathbf{e_b}$, where $\mathbf{e_g}$ is the unit vector along the growth direction while $\mathbf{e_b}$ is the unit vector along the direction of the polarization in the corresponding *bulk* that is the *closest* one to $\mathbf{e_g}$. λ_1 and λ_2 are scalars that depend on the material, the epitaxial strain δ, the magnitude of the depolarizing field and the growth direction. Rule 1 expresses the simultaneous desires of the films to enhance their polarization component along the growth direction under SC-like conditions (in order to reduce short-range energy costs near the surfaces [4]) *and* to have a polarization similar to the bulk. *Rule 2: For OC-like conditions*, the films adopt patterns for which the out-of-plane component of the spontaneous polarization vanishes, in order to fight against the large depolarizing field associated with such boundary conditions.

The first rule predicts the formation of monoclinic phases in the non-[001] films under SC-like boundary conditions. The second rule suggests two possible arrangements for the dipole configuration under OC-like conditions: 1) homogeneous in-plane polarization; 2) domains with alternating "up" and "down" out-of-plane dipole component. The occurrence of these two states depends on the interplay between crystal anisotropy and uniaxial anisotropy induced by an applied strain. For example, crystal anisotropy favors [100],[010] or [001] direction in $Pb(Zr_{0.4}Ti_{0.6})O_3$ material. Applying compressive strain to [001] film will single out the out-of-plane [001] direction forcing the 180° degrees domain to form (left part of Fig.1c). Whereas tensile strain will favor either [100] or [010] direction resulting in homogeneous in-plane polarization (left part of Fig.1b). Note that for [111] films under OC-like conditions, the competition between the crystal and strain induced anisotropy results in the formation of $\approx 90°$ domains (see schematizations in Fig.1).

This work is supported by NSF grants DMR-0404335 and DMR-0080054 (C-SPIN), by

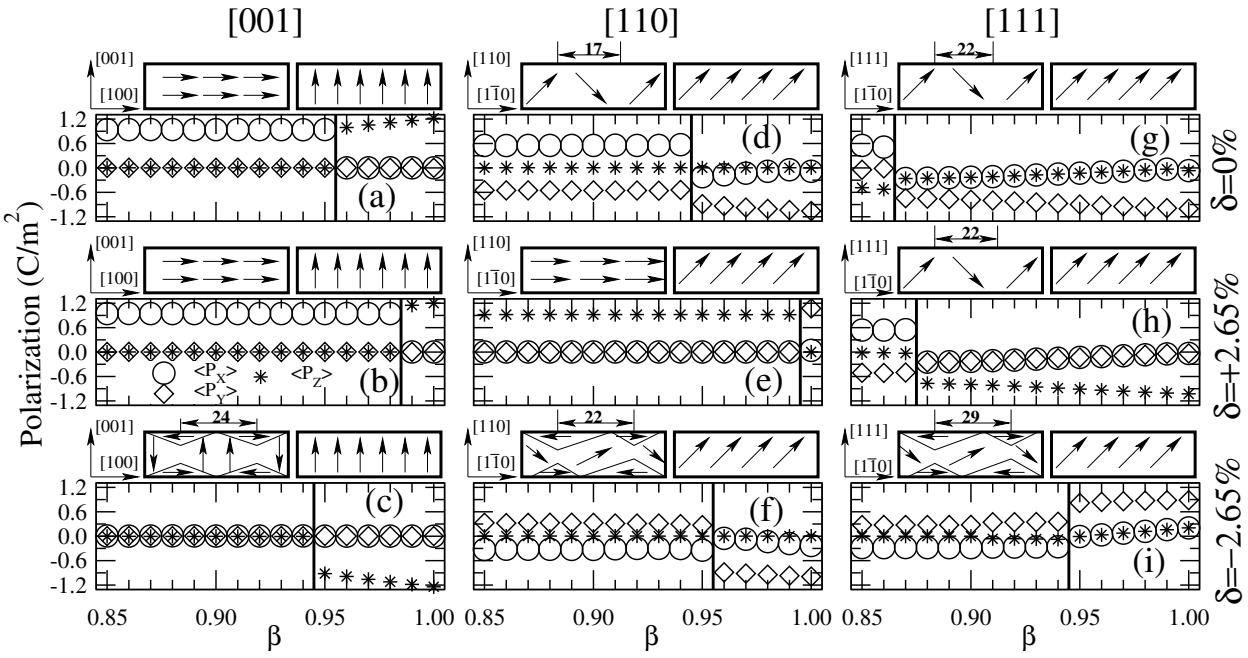

FIG. 1: x-, y- and z-components of the ground-state spontaneous polarization in $Pb(Zr_{0.4}Ti_{0.6})O_3$ ($\simeq$ 46-48 Å-thick) films as a function of the screening coefficient β. x-, y- and z-directions correspond to the [100], [010] and [001] crystallographic directions Parts (a), (b) and (c): [001] films under stress free, 2.65% tensile strain and -2.65% compressive strain, respectively; Parts (d-f): same as Parts (a-c) but for a [110] film; Parts (h-g): same as Parts (a-c) but for a [111] film. The vertical lines characterize the transition of the dipoles pattern from SC-like conditions to OC-like conditions. The schematization of these two different patterns is given above each part. The width of the stripe domains is given in Å.

ONR grants N00014-01-1-0365 (CPD) and N00014-04-1-0413, and by DOE grant DE-FG02-05ER46188.

---

[1] A. V. Bune, Nature (London) **391**, 874 (1998).

[2] D. Fong, G. Stephenson, S. Streiffer, J. Eastman, O. Auciello, P. Fuoss, and C. Thompson, Science **304**, 1650 (2004).

[3] I. Kornev, H. Fu, and L. Bellaiche, Phys. Rev. Lett. **93**, 196104 (2004).

[4] P. Ghosez and K. M. Rabe, Appl. Phys. Lett. **76**, 2767 (2000).

[5] C. Zybill, B. Li, F. Koch, and T. Graf, Phys. Stat. Sol. **177**, 303 (2000).

[6] I. Kanno, H. Kotera, T. Matsunaga, T. Kamada, and R. Takayama, J. Appl. Phys. **93**, 4091 (2003).

[7] M. B. Kelman, L. F. Schloss, P. C. McIntyre, B. C. Hendrix, S. M. Bilodeau, and J. F. Roeder, Appl. Phys. Lett. **80**, 1258 (2001).

[8] I. Ponomareva and L. Bellaiche, Phys. Rev. B **74**, 064102 (2006).

Probing Ferroelectricity in Cyanopolymer Systems

Matt Poulsen[1], Stephen Ducharme[1], James M. Takacs[2], Sahadeva Reddy[2], V.M. Fridkin[3]

[1] Department of Physics and Astronomy, Nebraska Center for Materials and Nanoscience University of Nebraska, Lincoln, Nebraska

[2] Department of Chemistry, Nebraska Center for Materials and Nanoscience University of Nebraska, Lincoln, Nebraska

[3] Institute of Crystallography, Russian Academy of Sciences, Moscow, RUSSIA

Phone: (402) 472-8218; email; mpoulsen@bigred.unl.edu

We report evidence for ferroelectricity in newly synthesized cyanopolymer systems. These systems are chemical analogs to the well known ferroelectric polymer poly(vinylidene fluoride), PVDF. Various chemical groups have been used to replace the electronegative fluorine and electropositive hydrogen atoms found in PVDF. This substitution maintains the polar nature of the all-trans conformation while increasing the amphiphilic nature of the polymers, enabling the fabrication of ultrathin films using the Langmuir-Blodgett technique. The studied cyanopolymers, shown in Fig. 1, include poly(methyl vinylidene cyanide), PMVC, several of its copolymers, and the previously studied copolymer of poly(vinylidene cyanide) and vinyl acetate, P(VDCN-VAC). [1,2]

Evidence for ferroelectric behavior has been observed in the 50:50 copolymer of poly(methyl vinylidene cyanide) and vinyl acetate, P(MVC-VAC), where, at elevated temperatures, polarization hysteresis, measured using a specialized Chynoweth pyroelectric technique [3], has been observed, Fig. 2. This technique involved the measurement of the remnant polarization, via the pyroelectric current, with the pyroelectric current being measured after the applied voltage was removed. Polarization loops, in the case of P(MVC-VAC), were measured at 130° C which is well below the melting temperature, T_m, of 170° C. In addition, even when maintained at elevated temperature, the polarization states associated to this behavior have been shown to be quite long lived (+100 hours). Similarly, polarization hysteresis has been observed in the P(VDCN-VAC) copolymer, Fig. 2, a long suspected ferroelectric polymer system that, until recently, has lacked unambiguous confirmation of ferroelectric switching.

Consistent with reversible polarization, unsaturated dielectric hysteresis curves (i.e. butterfly curves) have been observed, at T = 25° C, in all of the above mention cyanopolymer systems. However, the results associated to the observed "butterfly curves" are inconclusive as external causes such as injected charged from the associated electrodes can not be ruled out as the source of the observed hysteresis. [4] It should also be noted that no evidence for a phase transition below T_m has been observed in dielectric or differential scanning calorimetry measurements. Observation of reversible remnant polarization at high temperature, below T_m, and a lack of an observed phase transition might suggest a situation analogous to that found in PVDF, in that the related ferroelectric-paraelectric phase transition temperature, in fact, resides above the related melting point. In addition, piezoelectric and pyroelectric properties have been studied

and will be discussed. Piezoelectric, pyroelectric, and ferroelectric properties make this family of cyanopolymers a promising new class of materials for use in electromechanical transducers, nonvolatile memories, and infrared imaging.

References

1. T.T. Wang and Y. Takase, J. Appl. Phys. **62** 3466 (1987).

2. H.S. Nalwa, ed., Ferroelectric Polymers, (Marcel Dekker, New York, 1995), 895 pages.

3. A.V. Bune, Chuanxing Zhu, Stephen Ducharme, L.M. Blinov, V.M. Fridkin, S.P. Palto, N.G. Petukhova, and S.G. Yudin, J. Appl. Phys. **85**, 7869 (1999).

4. Matt Poulsen, Stephen Ducharme, A.V. Sorokin, Sahadeva Reddy, James M. Takacs, Y. Wen, Jihee Kim, and S. Adenwalla, Ferroelectric Letters **32** 91 (2005).

Figures

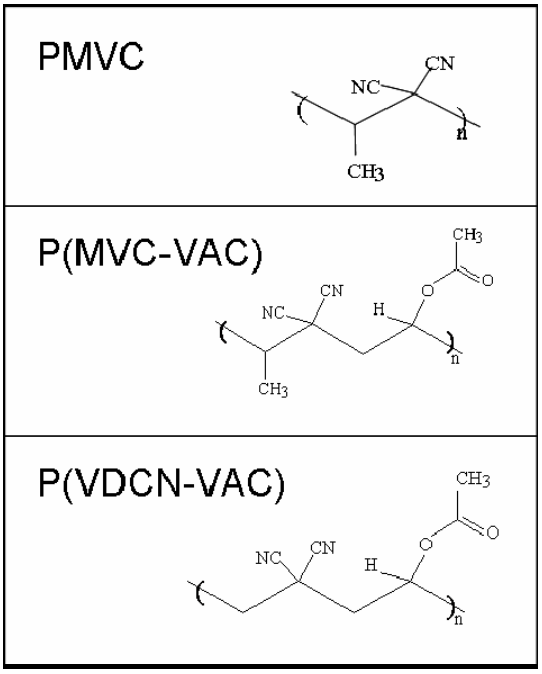

Fig. 1. Chemical structures of poly(methyl vinylidene cyanide), poly(methyl vinylidene cyanide) with vinyl acetate and poly(vinylidene cyanide) with vinyl acetate.

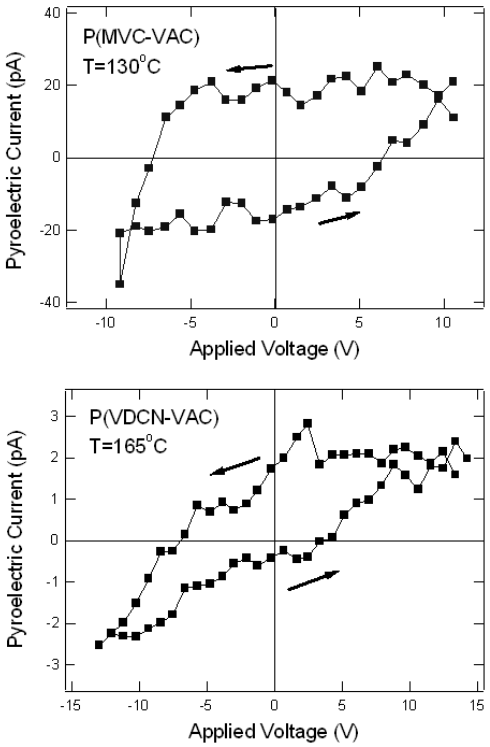

Fig. 2. Polarization versus voltage hysteresis loops taken via the pyroelectric method at 130° C from a 20 monolayer P(MVC-VAC) sample and at 165° C from a spin coated P(VDCN-VAC) sample.

Novel phenomena in ferroelectric nanodots

S. Prosandeev, I. Kornev, and L. Bellaiche

Physics Department, University of Arkansas, Fayetteville, AR 72701

Atomistic simulations are nowadays capable of tackling really complex challenges of fundamental and technological importance. For example, a dipole vortex structure has been discovered, by means of these methods, in isolated nanoparticles of ferroelectrics – which may lead to a new generation of efficient nanoscale memory devices [1].

Here, we use atomistic approaches to address the following issues: (i) what are the elastic signatures and field charateristics of dipole vortices in isolated ferroelectric nanodots? (ii) can these dipole vortices lead to the existence of new material tensors? and (iii) what are the possible phases in arrays of ferroelectric dots *embedded* in a crystal lattice?

Regarding item (i), we found that the tetragonal axial ratio in the vortex state is lower than 1 (unlike in "normal" ferroelectric or antiferrodistortive phases), and that the electric field produced by the dipole vortex outside the dot oscillates in space when changing the polar angle of the cylindrical coordinate system. Such features can serve as fingerprints of the vortex state to experimentally confirm the existence of such unusual state.

Moreover, we demonstrate that new tensors, indeed, exist in ferroelectric nanodots, as a result of the formation of electric dipole vortices. In particular, one tensor represents a new form of electromechanical coupling occurring at the nanoscale, while another tensor can be considered as analogous of dielectric susceptibility when going from bulk to nanoparticles.

Finally, it is predicted that array of embedded dots can adopt novel phases, depending on the temperature and difference in polarizability between the dots and medium [2]. Atomistic details of such phases can be seen in Fig. 1.

This work is supported by ONR grant N00014-04-1-0413, DOE grant DE-FG02-05ER46188, and NSF grant DMR-0404335. Some computations were made possible thanks to the MRI Grant 0421099 from NSF.

1. I. Naumov, L. Bellaiche and H. Fu, "Unusual phase transitions in ferroelectric nanodisks and nanorods", Nature **432**, 737 (2004).

2. S. Prosandeev and L. Bellaiche, "Properties of Ferroelectric Nanodots Embedded in a Polarizable Medium: Atomistic Simulations", Phys. Rev. Lett. **97**, 167601 (2006).

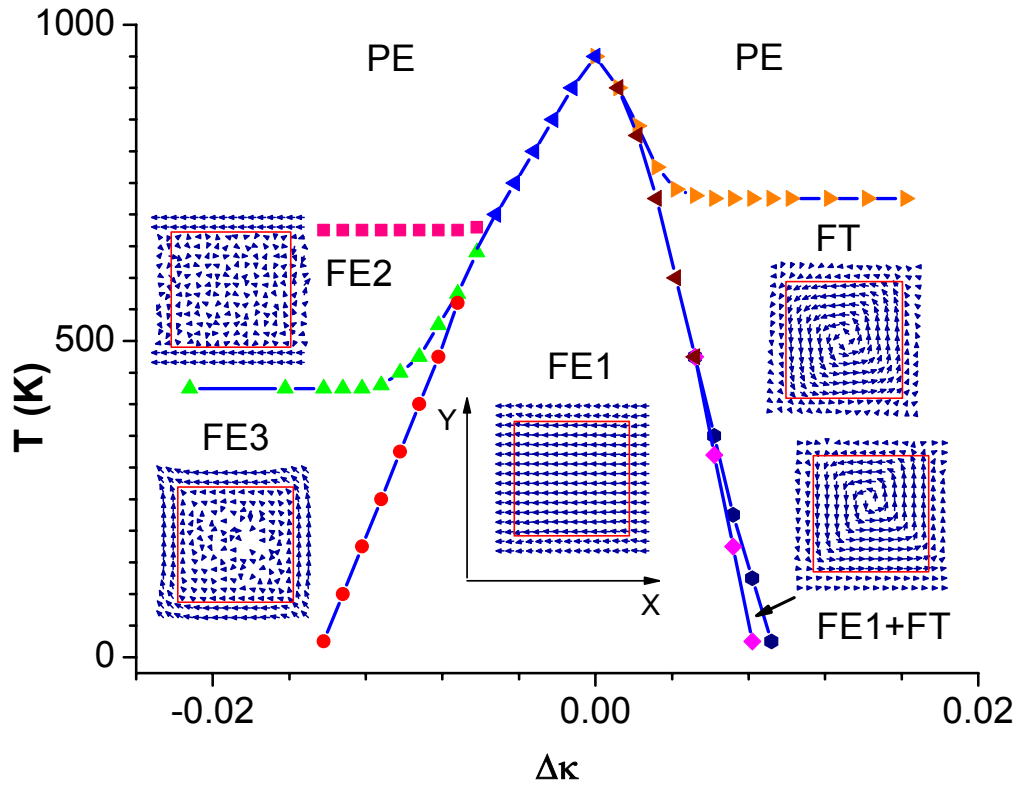

Fig. 1. Temperature-versus-Δκ phase diagram of a 12x12x12 AB"O_3 dot embedded in a AB'O_3 medium within a 16x16x16 periodic supercell. The positive Δκ part of this diagram corresponds to a soft ferroelectric dot immersed in a medium that is ferroelectrically harder than the dot and that has a decreasing ferroelectric instability as Δκ increases. The negative Δκ part of this diagram corresponds to a dot (having a ferroelectric instability that is weaker than those of the medium and that decreases, and then vanishes, as Δκ increases in magnitude) embedded in a ferroelectrically-soft medium. The insets show a (001) cross-section of the dipole configuration in the different phases. The dot surfaces are indicated via thick continuous lines in these insets. The x- and y-axes are chosen along the pseudo-cubic [100] and [010] directions, respectively.

Modeling coherent ferroelectric polarization reorientation in $PbTiO_3$

Tingting Qi[1], Young-Han Shin[1], Keith A. Nelson[2], Andrew M. Rappe[1]
[1] *The Makineni Theoretical Laboratories, Department of Chemistry, University of Pennsylvania, Philadelphia, PA 19104–6323*
[2] *Department of Chemistry, Massachusetts Institute of Technology, Cambridge, Massachusetts 02139*
(Dated: January 17, 2007)

I. MOTIVATION

The potentially high data storage density of ferroelectric remanent storage devices is of interest to many people. Ferroelectrics under tetragonal strain have two polarization orientations with symmetrically equivalent ground states separated by an energy barrier. The ferroelectric polarization can be reversed under an electric field. Most studies of polarization reversal focus on domain wall properties and dynamics [1–3], particularly the growth of one domain at the expense of another as a wall moves. The main distinction between this study and previous work is that we are considering coherent reorientation of a large region, without considering domain wall formation or movement. In recent experiments, electric field pulses on the order of 1 μs are applied with scanning probe tips [4]. Synchrotron radiation has also been used successfully for domain reorientation [5]. Generally, ferroelectric domain switching on the nanometer scale is practical via both electrical and optical methods. Nevertheless, optical switching on the nanometer scale using a fine optical aperture tip as in scanning near-field optical microscopy has so far proven difficult due both to limitations on optical focusing and to the small transmitted power [6]. In the current study, we do not consider the lateral confinement of radiation explicitly, investigating coherent ferroelectric domain switching using applied optical pulses with suitable pulse shapes. In order to decrease the switching time to picoseconds, it is very important to control coherence. The high frequency and large magnitude of the required pulses present challenges for experimental applications. It is therefore useful to explore theoretically how best to apply those ultrashort pulses beforehand.

II. MODEL AND COMPUTATIONAL DETAILS

We used the bond-valence (BV) model [7], which reproduces ferroelectric behavior fairly accurately with a simple interatomic potential. In this model, the valence of an atom is distributed among the bonds it forms, and the bond valences are correlated with the bond length through an inverse power relation, with the total atomic valence of each atom equal to the sum of its bond valences. We use this BV formalism to treat Pb-O and Ti-O chemical bonding. The total interatomic potential consists of three parts: the repulsive potential energy (E_r), the Coulomb potential energy (E_c) and the bond-valence potential energy (E_b).

$$E_b = \sum_{\beta=1}^{3} S_\beta \sum_{i=1}^{N_\beta} |V_{i\beta} - V_\beta|^{\alpha_\beta} \tag{1}$$

where

$$V_{i\beta} = \sum_{\beta'=1}^{3} \sum_{i'(NN)} \left(\frac{r_0^{\beta\beta'}}{r_{ii'}^{\beta\beta'}} \right)^{C_{\beta\beta'}} \tag{2}$$

$V_{i\beta}$ is the bond valence of the ith atom of type β (Pb, Ti, and O) calculated according to Brown's formulation [8]. NN means summation over the nearest-neighbor atoms, and N_β is the number of the β ions. V_β is the desired atomic valence of the β ion, and $\mathrm{r}_{ii'}^{\beta\beta'}$ is the distance between the ith β ion and the i'th β' ion.

The electric field pulses are on the scale of hundreds of femtoseconds, and we use the same electric field pulse shape for all the simulations. The pulse shape integrates to zero (as required for optical pulses), with a large-amplitude short duration pulse followed by a lower-amplitude longer duration pulse in the opposite direction. The contribution of each atom to the spontaneous polarization is computed as the product of the Born effective charge [9] tensors Z^* and the atomic displacement vector. The local polarization in each cell, $\vec{P}_l$, is defined as the average of the atomic polarization of one Ti atom, its eight nearest-neighbor Pb atoms and its six nearest-neighbor O atoms. For PT, we set the tetragonal experimental lattice constants $a = 3.9$ Å, $b = 4.15$ Å [10].

III. RESULTS AND DISCUSSION

A suffficiently large electric field will reverse the polarization of all cells to the field direction. To switch the polarization from z to $-z$, the most direct way is to apply the opposite direction electric pulses ($-z$).

Applying a $-z$ direction electric field pulse starts the z component of the spontaneous polarization (P_z) to oscillate in time. The other two polarization components, P_x and P_y, are essentially zero during this short time period. A Fourier transform of P_z with respect to time shows that the oscillation period is about 240 fs, which corresponds to the 140 cm^{-1} soft mode frequency. The P_z oscillation period was found to be independent of pulse magnitude, indicating a fairly harmonic mode at these amplitudes.

However, in order to reverse the ferroelectricity, we must load the system with more energy to overcome the energy barrier. Success in augmenting the P_z oscillation with successive pulses strongly depends on the delay time between pulses. P_z coherence could be lost or magnified after the second pulse. We were able to carefully select the optimum timing each time we add the next pulse and achieve the polarization reversal within 15 ps after six pulses of amplitude 3000 MV/cm.

However, the reversed domain is readily able to flip multiple times, as a consequence of providing sufficient energy for the system to get over the barrier. We study the coupling between P_x, P_y, and P_z oscillations, as a mechanism to reduce z direction motion and quench the polarization into a single orientation. We also explore applying one additional $-z$ oriented pulse out of phase with P_z oscillations, to retard the motion after the system has crossed the barrier and trap the system into the desired polarization direction. At 0 K, our simulations gave a result of a completely flipped domain. The idea of an out-of-phase pulse for controlling final state is important for both the real case at 0 K and finite temperature.

It is well known [11] that polarization rotation can offer lower-energy pathways to polarization flipping than directly surmounting the barrier. We therefore investigate prospects for maintaining polarization coherence while rotating the polarization.

Corresponding simulations are performed to implement this proposed idea. Starting from a single x direction pulse, the simulation shows that both P_x and P_z oscillations are excited, corresponding to polarization rotation. Moreover this P_z oscillation is even bigger than the one after one $-z$ pulse. This phenomenon is quite promising. However, larger P_x resonant amplitude is needed.

Multiple x pulses (1000 kV/cm) are then applied, all at the optimum timing. The power spectrum shows that the period for P_z oscillation (54 cm^{-1}) is half that of P_x (107 cm^{-1}), which is more tangible evidence of polarization rotation in the xz plane. After the fourth x pulse, the polarization could rotate as much as 45° from the z-axis. In other words, P_x can equal or exceed P_z at the turning points of the rotation. We emphasize how well the polarization rotation trajectory avoids the highest energy barrier ($P = 0$), and approaches the lower saddle points.

After four x pulses, when the system approaches the turning point, a 2000 kV/cm $-z$ pulse was applied to push the system over the saddle point. This polarization rotation approach is more efficient then the former method, in terms of either the number of pulses or their peak magnitudes.

The width of the pulses is another issue we're concerned with. We proved that there is an optimal pulse width, with significanly longer or shorter pulses being less effective for domain reorientation. The preferred width is found to be about 200 fs to 300 fs, which is close to a half period of P_x rotation.

As for the finite temperature, we anticipate that maintaining coherence will be more challenging than the success reported here. More random fluctuations will make the final state even more difficult to predict. However, the impulsive, short-time response of the system may suppress the effect of fluctuations, allowing coherent flipping faster than the coupling of polarization to other modes. This issues is currenlty under investigation.

IV. CONCLUSIONS

We have shown that we are able to coherently switch the ferroelectric domain with strong picosecond optical fields. Using solely antiparallel fields can flip polarization coherently, and exciting polarization rotation with transverse pulses does so more efficiently. Both the timing and pulse width play important roles during the flipping process. Our BV model for coherent ferroelectric orientation can be applied universally to other ferroelectric materials. Compared with PT, ferroelectrics with shallower potential wells should be easier to switch.

V. REFERENCES

[1] B. Meyer and D. Vanderbilt, Phys. Rev. B **63**, 205426 1 (2001).

[2] S. V. Kalinin, C. Y. Johnson, and D. A. Bonnell, J. Appl. Phys. **91**, 3816 (2002).

[3] T. Tybell, C. H. Ahn, and J.-M. Triscone, Appl. Phys. Lett. **75**, 856 (1999).

[4] T. Tybell, P. Paruch, T. Giamarchi, and J.-M. Triscone, Phys. Rev. Lett. **89**, 097601 (2002).

[5] A. Grigoriev, D. H. Do, D. M. Kim, C. B. Eom, B. Adams, E. M. Dufresne, and P. G. Evans, PHYSICAL REVIEW LETTERS **96**, 187601 (2006).

[6] L. M. Eng, Nanotechnology **10**, 405 (1999).

[7] Y.-H. Shin, V. R. Cooper, I. Grinberg, and A. M. Rappe, Phys. Rev. B **71**, 054104 (2005), ISSN 0163-1829, URL `http://dx.doi.org/10.1103/PhysRevB.71.054104`.

[8] I. D. Brown, in *Structure and Bonding in Crystals II*, edited by M. O'Keeffe and A. Navrotsky (Academic Press, New York, New York, 1981), pp. 1–30.

[9] R. D. King-Smith and D. Vanderbilt, Phys. Rev. B **47**, 1651 (1993).

[10] G. Shirane, S. Hoshino, and K. Suzuki, Phys. Rev. **80**, 1105 (1950).

[11] H. Fu and R. E. Cohen, Nature **402**, 281 (2000).

Dynamics of polarization around domain walls under external fields

Young-Han Shin,[1] Ilya Grinberg,[2] I-Wei Chen,[3] and Andrew M. Rappe[†2]

[1]*Department of Materials Science and Engineering, POSTECH, Pohang, Republic of Korea*
[2]*Makineni Theoretical Laboratories, Department of Chemistry, University of Pennsylvania, Philadelphia, USA*
[3]*Department of Materials Science and Engineering, University of Pennsylvania, Philadelphia, USA*

[†]Phone: (215) 898-8313; Fax: (215) 573-2112; E-mail: rappe@sas.upenn.edu

In the previous ferroelectric workshop in 2006 we showed how the polarization reversal process of ferroelectric materials could be studied in the multi-scale strategy which made possible for us to study dynamics of polarization around the ferroelectric domain walls through the following steps:

- Pseudopotential density-functional theory (DFT) calculations to generate reference structures for optimization of the classical potential parameters
- Molecular dynamics (MD) simulations under the bond-valence potential formalism
- Stochastic study from the nucleation and growth rates from MD simulations

Such a model study clarifies physical phenomena which are hidden behind the real complex system, and it enables us to tackle large systems such as a moving domain wall within the current computer power.

In this presentation, we will use this strategy to show how the polarization reversal process behaves at the atomic level, and show the predicted relation between overall domain wall speed and external electric field compares with the experimental data. Considering differences in composition and the presence of defects in experimental materials, there is a quite reasonable agreement between theory and experiment. Our theoretical results are in particularly good agreement with the experiments of Gruverman *et al.*[1] who used 20/80 PZT films very similar in chemical composition to the pure PT in our study.

In addition, we are going to present how simple understandings of the critical nucleus on the ferroelectric domain walls are approachable with the Landau-Ginzburg-Devonshire (LGD) theory considering the polarization gradient around the domain boundary. The total free energy difference ΔU between a monodomain crystal and one with periodic domain walls and stripe domains is

$$\Delta U = U - U_0 = W_g + W_E + W_e + W_l$$

where U_0 is the single domain free energy, W_g is the gradient energy due to the dipole-dipole interaction, W_E is the depolarizing energy, W_e is the elastic energy, W_l is the local energy contribution from LGD theory. The free energy difference around the nucleus on the domain wall can be represented with the z component of the polarization vector

$$P_z(x,y,z) = \frac{P_s}{2}\left(f^-(x,l_x,\delta_x)\left(\frac{1}{2}f^-(y,l_y,\delta_y)f^-(z,l_z,\delta_z)-1\right)+f^+(x,l_x,\delta_x)\right)$$

Figure 1: The critical nucleus size and the energy barrier during the nucleation process.

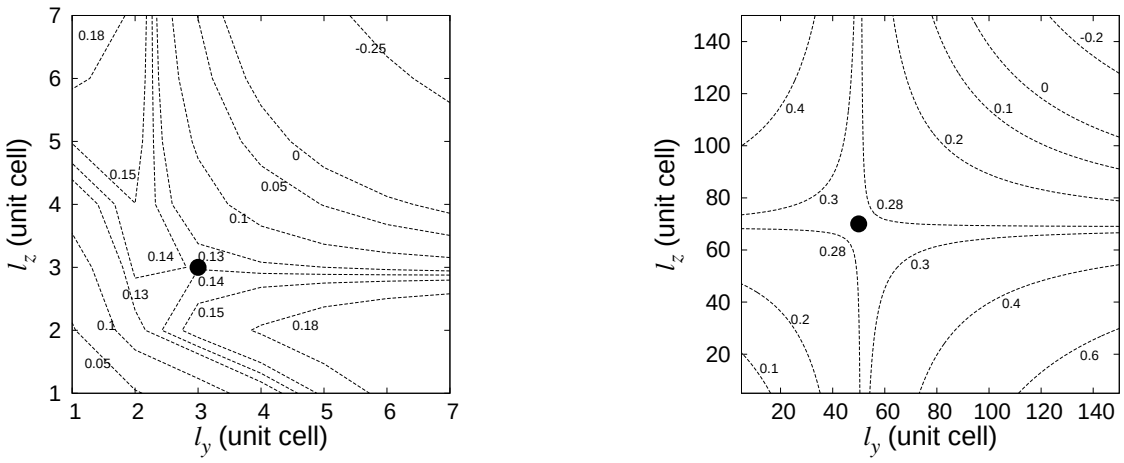

(a) $PbTiO_3$ (b) $BaTiO_3$

, where $f^{\pm}(a,b,c) = \tanh\left(\frac{a+b/2}{c/2}\right) \pm \tanh\left(\frac{a-b/2}{c/2}\right)$, l_k corresponds to the length of the nucleus to the k direction, and δ_k corresponds to the diffuseness to the k direction. When the external field E is applied to the 180° domain wall, the critical nucleus will be formed on it. The shape and size of the critical nucleus can be determined by solving the equation $\partial \Delta U / \partial l_k = 0$. The energy barriers for the critical nucleus formation of $PbTiO_3$ are shown in Figure 1 (a), and it is very close to the result from our multiscale calculation. To check the transferability of our model we applied it to $BaTiO_3$, and it also gives a good agreement with the experiments (Figure 1(b)).

This work is supported by the Office of Naval Research, the National Science Foundation and the U. S. Army Engineer Research and Development Center. Computational support was provided by the U. S. Department of Defense.

---

[1] Gruverman, A., Rodriguez, B. J., Dehoff, C., Waldrep, J. D., Kingon, A. I., Nemanich, R. J. & Cross, J. S. Direct studies of domain switching dynamics in thin film ferroelectric capacitors. *Appl. Phys. Lett.* **87**, 082902 (2005).

Growth and Structural Properties of Crystalline $LaAlO_3$ on Si (100)

J. W. Reiner[1], A. Posadas[1], M. Wang[2], T. P. Ma[2], C. H. Ahn[1]

[1]Department of Applied Physics, Yale University, New Haven, CT 06520-8284
[2]Department of Electrical Engineering, Yale University, New Haven, CT 06520-8284
Phone: (203)432-1816; Fax: (203)432-7044; e-mail:james.reiner@yale.edu

Silicon dioxide has been the gate dielectric in complementary metal oxide semiconductor technology (CMOS) for decades. As transistor scaling continues, the SiO_2 thickness will be the first transistor length scale to reach atomic dimensions of less than 1 nm. Fabricating devices with an SiO_2 layer only two atomic layers thick presents serious challenges with regard to gate leakage currents and process uniformity [1]. Because of these challenges, many alternative gate dielectrics have recently been studied, including amorphous hafnium and zirconium oxides, nitrided SiO_2, $SrTiO_3$[2], $SrHfO_3$, and $LaAlO_3$[3, 4]. Among the requirements for a useful gate dielectric are a large dielectric constant compared to SiO_2, a large band gap, large band offsets with silicon, and chemical stability in a silicon heterostructure. $LaAlO_3$ appears to be a promising material as judged by these requirements. However, attempts to fabricate crystalline $LaAlO_3$ films on silicon, which requires high temperature deposition or post annealing, have failed due to interfacial reactions between the $LaAlO_3$ and silicon. Crystalline $LaAlO_3$ on Si has been achieved with 2 nm SrO and 5 nm $SrTiO_3$ buffer layers, but with a 4-5 nm amorphous interfacial layer developing at the Si interface [4].

We present results for a crystalline $LaAlO_3$/Si MOS capacitor with an extremely thin 1 nm epitaxial $SrTiO_3$ buffer layer and no detectable SiO_2 at the oxide-silicon interface. The $LaAlO_3$/Si heterostructures were grown in a custom oxide molecular beam epitaxy (MBE) system equipped with a reflection high energy electron diffraction (RHEED) system. The growth chamber base pressure of 2×10^{-10} mbar was achieved using cryopumps. Sr, Ti, La, and Al metals were evaporated from Knudsen cells and reacted with molecular oxygen to form the epitaxial $SrTiO_3$ and $LaAlO_3$ films on Si (001) wafers. The metal evaporation rates were calibrated using a quartz crystal microbalance, which could be moved into and out of the Si wafer position. To create the buffer layers required for crystalline $LaAlO_3$ growth, a single SrO monolayer and two $SrTiO_3$ monolayers were deposited on the Si wafers. Having fabricated this 1 nm $SrTiO_3$ buffer layer, epitaxial $LaAlO_3$ was deposited at a wafer temperature of 700 °C to create films between 13 nm and 100 nm thick.

The crystallinity of the $LaAlO_3$ films was assessed during and after growth by RHEED, x-ray diffraction (XRD), and cross-sectional transmission electron microscopy (TEM). Analysis of RHEED images taken during growth indicates the presence of intensity oscillations in the specular intensity. XRD measurements confirm the crystallinity of the $LaAlO_3$ films. The rocking curves at the $LaAlO_3$ (002) peak are typically 0.15° FWHM. The RHEED and XRD measurements do not exclude the possibility that either during the $SrTiO_3$ growth, or especially the $LaAlO_3$ growth, an amorphous SiO_2 has developed at the oxide-silicon interface. This SiO_2 layer could be created by oxygen diffusing to the interface and reacting with the silicon during growth. For this reason, cross-sectional TEM studies were carried out on select $LaAlO_3$/Si heterostructures. One resulting image is presented in Figure 1, showing a very thin transition layer between the crystalline $LaAlO_3$ and silicon consistent with the 2 monolayers of $SrTiO_3$ we expected based on our growth process.

We have also employed inelastic tunnelling spectroscopy (IETS) to assess whether any SiO_2

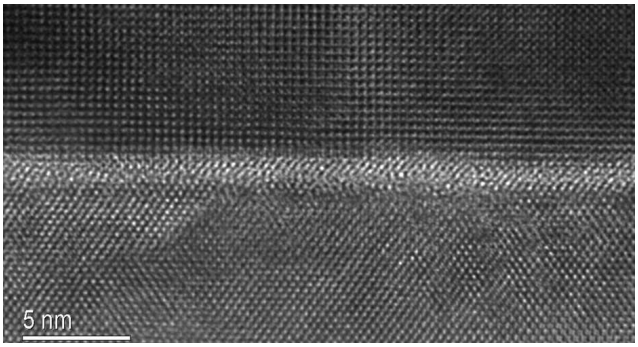

Figure 1: Cross-sectional TEM of crystalline $LaAlO_3$ film on Si (001) surface with a 2 monolayer $SrTiO_3$ transition layer.

is present in our $LaAlO_3$/Si structures. IETS consists of a high sensitivity I-V measurement of a capacitor structure performed at liquid helium temperatures. In the present case, we fabricated these structures by depositing 3000 Å of aluminum on top of our $LaAlO_3$ films, which were grown on degenerately doped n-type silicon. Aluminum top electrodes were then patterned using standard photolithographic techniques and an aluminum etchant. Inelastic modes which contribute to the current through this structure appear in an IETS spectrum as peaks at voltages that corresponds to the energies of the inelastic modes. In particular, Si-O phonon modes should appear in a voltage range of 0.15–0.18 eV. No peaks are apparent in the voltage range corresponding to Si-O phonons, indicating that no SiO_2 layer is present within the detection limits of this technique.

In conclusion, we have demonstrated that $LaAlO_3$ can be grown epitaxially on a Si (001) surface without any detectable amorphous SiO_2 layer by employing a 2 unit cell $SrTiO_3$ buffer layer. RHEED, XRD, TEM and IETS measurements indicate a highly crystalline $LaAlO_3$ film. TEM and IETS measurements indicate an abrupt interface between the $LaAlO_3$ and Si for samples fabricated under the growth conditions described. The absence of SiO_2 is crucial to achieving a suitable gate stack for CMOS applications. Additional requirements for a gate stack include low interface trap density and high channel mobility, issues that are currently under study. Looking beyond the gate dielectric problem, the use of extremely thin $SrTiO_3$ buffer layers provides a method to bring the rich functionality observed in complex oxide systems onto a silicon platform.

C.A. acknowledges primary support from the National Science Foundation under the MRSEC DMR 0520495 and ONR, along with support from the Packard and Sloan Foundations.

References

[1] H. Wong, H. Iwai, Microelectron. Eng. **83**, 1867 (2006).

[2] R. McKee, F. Walker, M. Chrisholm, Science **293**, 468 (2001).

[3] L. F. Edge, D. G. Schlom, R. T. Brewer, Y. J. Chabal, J. R. Williams, S. A. Chambers, C. Hinkle, G. Lucovsky, Y. Yang, S. Stemmer, M. Copel, B. Holländer, J. Schubert, Appl. Phys. Lett. **84**, 4629 (2004).

[4] W. F. Xiang, H. B. Lu, Z. H. Chen, X. B. Lu, M. He, H. Tian, Y. L. Zhou, C. R. Li, X. L. Ma, J. Crystal Growth **271**, 165 (2004).

Measurement of Born-Oppenheimer Potentials in Hydrogen Bonded Solids Using Neutron Compton Scattering----George Reiter, University of Houston

Neutron Compton scattering, by measuring the momentum distribution of protons in hydrogen bonded solids, provides a powerful new local probe of their structure.[1] In its first use in a ferroelectric, it was possible to demonstrate that the protons in KDP were, in fact, tunneling above the transition temperature.[2] Tunneling shows up in, n(p), the momentum distribution of the ground state as an oscillation, whose period is determined by the separation of the wells. The momentum distribution along the bond and the 1-D potential that gives rise to it are shown in Fig 1., along with the spatial wave function, and the first few predicted energy levels. The dotted lines are the rms error in n(p).

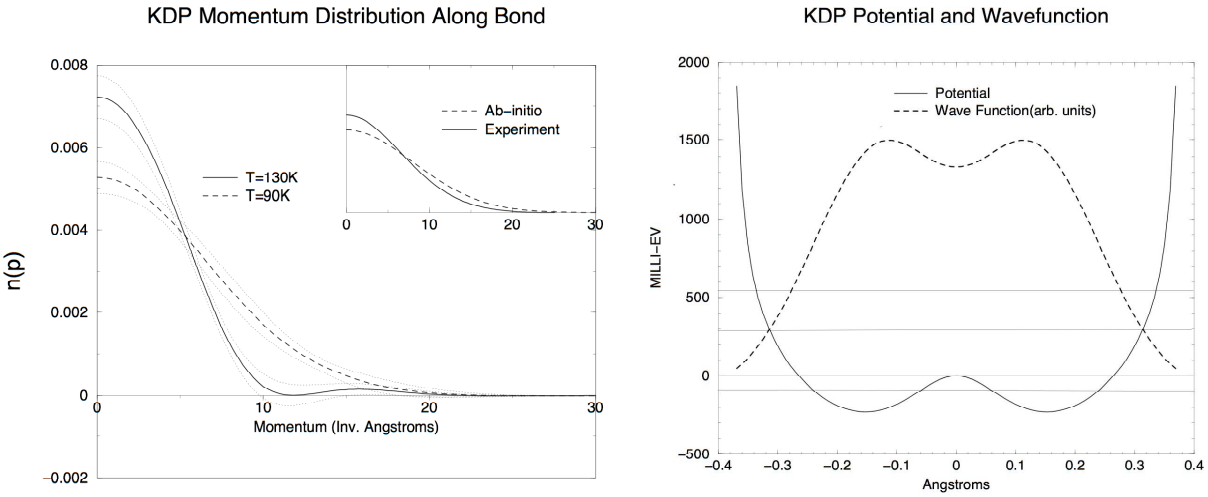

We have subsequently found that there is no coherent tunneling in DKDP, presumably because the tunnel splitting is less than the temperature.

More recent experiments on the RDP-ADP system, in which the replacement of Rubidium by ammonium ions frustrates the ferroelectric transition and leads to a structural spin glass, confirm the fact that the ground state is a coherent superposition of the particle in both wells, although in this case, due to the perturbing effect of the ammonium , the wells are asymmetric. This shows up as an incomplete oscillation. Remarkably, the asymmetry disappears at low temperatures (<4K), presumably because the ammonium delocalizes coherently in the cage it is in. The momentum distribution data along the bond direction for an ammonium concentration of 35% is shown in Fig 2, in the spin glass phase at 4K and 20K.

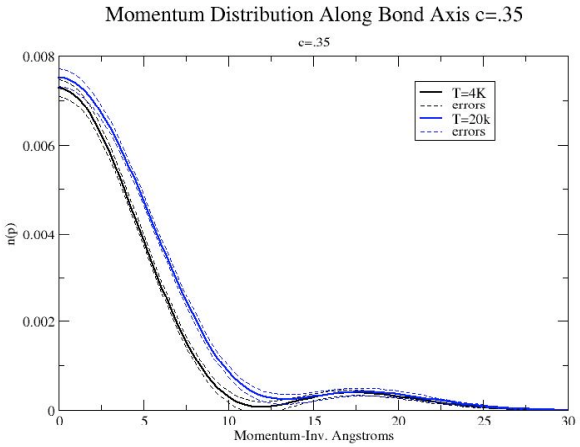

In some cases, this probe can provide complete information on the local structure by measuring directly the 3-D Born Oppenheimer potential.[3] We show below the first such measurement of this kind (in any material) in the "zero dimensional " hydrogen bond network in $Rb_3H(SO_4)$. The measurements were done at 10K, 70K, 300K and 350K Fig. 3 shows the coordinate system used to describe the proton in the bond, and the potential in the y-z plane that results from the measurment at 10K. There is no double well, consistent with the absence of a ferroelectric transition, and in contradiction to results obtained from light scattering and lower energy inelastic scattering measurements[4]. NMR results predict barriers that do not perturb the wavefunctions enough for us to

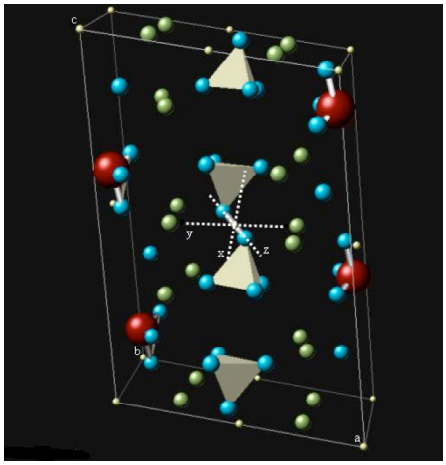

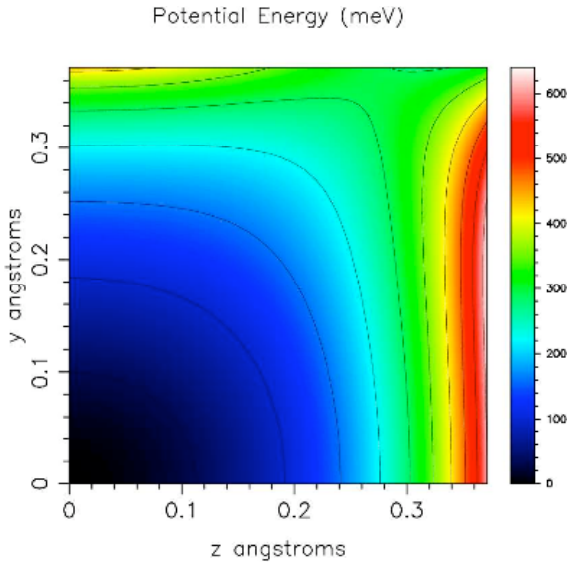

see.[5]

The implications of these measurements for theoretical models of the phase transition in KDP like materials will be discussed as well, if time permits.

References:

1. C. Andreani, D. Colognesi, J. Mayers, G. F. Reiter, and R. Senesi, Adv. Phys. 54, 377 (2005).
2. G. Reiter and R. Silver, Phys. Rev. Lett. 54, 1047 (1985).
3. G. F. Reiter, J. Mayers, and P. Platzman, Phys. Rev. Lett. 89, 135505 (2002).
4. F. Fillaux, A. Lautie, J. Tomkinson, and G. Kearley, Chem. Phys. 154, 135 (1991)
5. U. Mikac, D. Arˇcon, B. Zalar, J. Dolinˇsek, and R. Blinc, Phys. Rev. B 59, 11293 (1999).

Domain Structure of Graded Ferroelectric Multilayers and Films

A.L.Roytburd

University of Maryland; e-mail: roytburd@wam.umd.edu

Unusual properties of graded ferroelectric films, particularly the polarization offset and enhanced dielectric and pyroelectric responses, have been a subject of extensive experimental and theoretical investigations for more than a decade. Here we present the first theory of a polydomain graded ferroelectric multilayers and films. The theory is based on a model of a graded multilayer as an ensemble of electrostatically interacting single-domain and polydomain layers. Each polydomain layer contains specific equilibrium domain fractions depending on the applied electric field. The multilayer is polarized through changing domain fractions and transition between the polydomain and single-domain states of the layers.

Consider the polarization of a multilayer consisting of the sequence of layers with increasing spontaneous polarization, p_{01}, p_{02} …p_{on} and relative thicknesses, $\alpha_1,\alpha_2...\alpha_n$. In the absence of external field in the short circuited multilayer layer 1 with minimal spontaneous polarization is in a single-domain state, all other are in polydomain states. The minimum of free energy is reached if $P_1=P_2…P_n$ with $P_1=p_{01}$ and $P_i=p_{0i}(1-2\beta_i)$, i=2…n. Then, domain fractions at zero field are $\beta_i=1/2(1-p_{0i}/p_{01})$. To minimize the interlayer energy, 180° domains should form wedge-like macroscopical domains (Fig. 1). With increasing field layer 2 transforms to a single-domain state, then layer 3 transforms and so on, until all layers become single-domain ones. The change of polarization proceeds by movement of the boundary between a single-domain part and a polydomain part of the multilayer, i.e. by growth or shrinkage of wedge domains.

In linear approximation this process can be described formally by the set of the following equations:

$$\frac{1}{\varepsilon_k-\varepsilon_0}(P_k-p_{ok})=E+\frac{1}{\varepsilon_0}(\overline{P}-P_k)\ ,\quad \overline{P}=\sum_{k=1}^{n}\alpha_k P_k\ , \tag{1}$$

for single-domain layers if $k\le i$ and

$$0=E+\frac{1}{\varepsilon_0}(\overline{P}-P_k),\qquad P_k=(1-2\beta)p_{ok} \tag{2}$$

for polydomain layers, $i > k \ge n$. The solutions of these equations for a multilayer containing i single-domain layers is:

$$D^{(i)}=\varepsilon^{(i)}E+P_r^{(i)},\ \beta_k=1/2(1-D^{(i)}/p_{0k})\ \text{if}\ k>i,\ \beta_k=0\ \text{and if}\ k\le i, \tag{3}$$

where $\varepsilon^{(i)}=\left(\sum_{k=1}^{i}\frac{\alpha_k}{\varepsilon_k}\right)^{-1}$ is the dielectric constant of the multilayer, and $P_r^{(i)}=\varepsilon^{(i)}\sum_{k=1}^{i}\frac{\alpha_k}{\varepsilon_k}p_{0k}$ is the remanent polarization of the multilayer at the field E, $E_{ci-1}<E<E_{ci}$, where $E_{ci-1}=(p_{0i}-P_r^{(i)})/\varepsilon^{(i-1)}$.

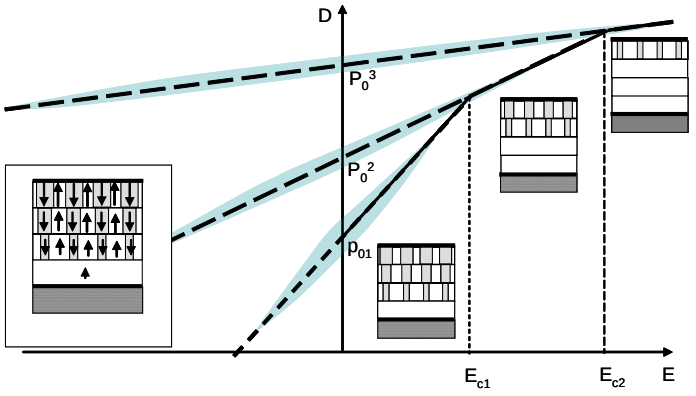

Figure 1. Polarization of a graded multilayer with four layer

Since the stiffness of the polydomain layers close to zero, the external field is concentrated in the single-domain part so polydomain layers amplify response of single domain ones. Therefore, at a low field the response of a polydomain part is controlled by change of polarization of a small single-domain part. There are two effects of non-linearity in this system. First, due to the concentration of field in the first single-domain layer, it losses stability and the polarization of a multilayer is switched at the reverse field with the magnitude much less than a coercive field for a single-domain layer. Second, when the decreasing fraction of the minor domain in polydomain layer becomes small, the energy of domain walls and non-uniform internal fields should decrease stability of a polydomain layer and enhance its transition to single domain state. Due to irreversibility of the transition from a polydomain to a single-domain state, partial hysteresis loops generated by AC field are observed in graded films.The width of the loops is determined by the dissipation of energy due to domain wall movement.

The presented model can be expanded to continuously graded films and Eq.(3) becomes:

$$D = \frac{E}{\int_0^z \frac{d\xi}{\varepsilon(\xi)}} + \frac{\int_0^z \frac{P(\xi)}{\varepsilon(\xi)} d\xi}{\int_0^z \frac{d\xi}{\varepsilon(\xi)}} \tag{4}$$

Here z is the coordinate of the boundary between single domain and polydomain parts of the film, where $D=P_0(z)$. In Fig. 2 the dependence D(E) is presented for the simple model of a graded film $\varepsilon(\xi) = \varepsilon, \quad P_0(\xi) = P_0 + \Delta P \xi$. Then, $D_{PD} = P_0 + \sqrt{2E\varepsilon\Delta P}$ and becomes $D_{SD} = E\varepsilon + P_0 + \frac{\Delta P}{2}$ when all polydomain layers transform into single-domain state. The change of the energy of domain walls accompanying growth and shrinkage of wedge domains can be taken into account by introducing a local effective field on the boundary, z, between polydomain and single-domain part of a film. It makes the movements of this boundary irreversible and results in the hysteresis of polarization.

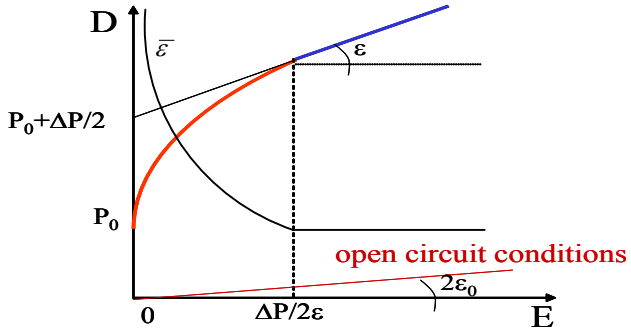

Figure 2. D(E) for short-circuit graded films with infinite suceptibility at zero field. D(E) for an open-circuit film is shown for comparison. $\bar{\varepsilon}$ is a dielectric constant of the film.

The polydomain model of a continuously graded film gives the principle explanation of the peculiarities of dielectric, piezoelectric and pyroelectric behavior of graded ferroelectrics. Expansion of the theory to the graded ferroelastics and ferromagnetics is discussed.

Polar Behavior and Ferroelectricity in Perovskites From *A*-Site Size Disorder

D.J. Singh[1], C.H. Park[1,2] and D.I. Bilc[1]
[1]Materials Science and Technology Division, Oak Ridge National Laboratory, Oak Ridge, TN, 37831-6032
[2]Department of Physics, Pusan National University, Busan, 609-735 Korea
e-mail: singhdj@ornl.gov

Here we report density functional calculations for various perovskites, ABO_3, examining in particular the effect of *A*-site size disorder. The Goldsmith tolerance factor, $t=(r_O+r_A)/2^{1/2}(r_O+r_B)$ where r_A, r_B, and r_O are the ionic radii of Shannon for the *A*-site, *B*-site and *O* ions, respectively, is generally useful in understanding trends in perovskite structures. Some of the most interesting and useful ferroelectrics are perovskites with Pb on the *A*-site and $t<1$. In contrast, almost all non-lead containing perovskites with $t<1$ occur in non-ferroelectric crystal structures that can be derived from the ideal cubic perovskite structure by combinations of zone boundary modes consisting of rotations and other distortions of the BO_6 octahedra. This difference is well understood in terms of the stereochemical activity of Pb, specifically covalency of Pb^{2+} with neighboring O ions. Interestingly, first principles calculations for $t<1$ perovskites with non-ferroelectric tilted ground state structures show that, while the indeed the correct structures are predicted, ferroelectric structures with off-centered *A*-site ions are nearby in energy.

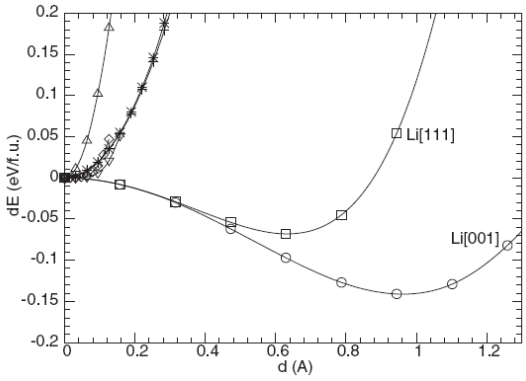

Figure 1. Energy vs individual atomic displacements of hypothetical perovskite $K_{1/2}Li_{1/2}NbO_6$ in a ordered 10 atom supercell. Note that there is a strong instability against Li off-centering, and that [001] displacements are favored.

The implication of this result is that *A*-site driven ferroelectricity could occur much more commonly if there were a chemical way of suppressing octahedral rotation in perovskites. Density functional calculations show that the ferroelectric and tilt distortions have very different characters: the metastable ferroelectric distortion in $t<1$ perovskites is dominated by *A*-site off-centering, while the tilts are coordinated rotations of the corner sharing BO_6 octahedra. Both instabilities are driven by the fact that the *A*-site ion is too small for its site. However, each off-centering involves only a single site, while the tilts involve several *A*-sites depending on the specific tilt pattern. Thus, one possibility for suppressing the rotations with a smaller effect on ferroelectric off-centerings, is the use of size disorder, specifically the use of alloying two or more ions with different sizes onto the *A*-site. Our results show that this mechanism works in some, but not all, perovskites. In particular, density functional calculations show that ferroelectricity can be induced in $(K,Li)NbO_3$ if it can be made

perovskite, and also in various perovskites with heavier 3*d* *B*-site ions. One such case is (La,Lu)($Mn_{0.5}Ni_{0.5}$)O_3. This material is of particular interest because it is a robust ferromagnetic insulator. Our supercell calculations show that the Lu, which is the small *A*-site ion in this material will off-center, and that either ferroelectricity or relaxor behavior is likely.

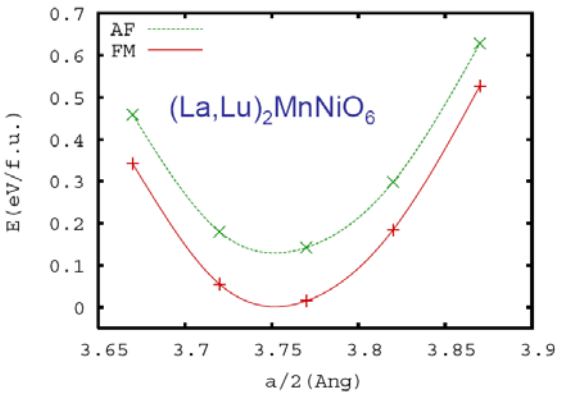

Figure 2. Energy of ferromagnetic and antiferromagnetically ordered double perovskite $(La,Lu)_2MnNiO_6$ showing robust ferromagnetism.

Thus, it is possible to induce *A*-site driven ferroelectricity in some $t<1$ perovskites without relying on Pb via *A*-site size disorder. This ferroelectricity is dominated by off-centering of the small *A*-site ions. These tend to displace along [001] directions. This is in contrast to *B*-site off-centering, which generally favors [111] directions and rhombohedral ferroelectric ground states in the absence of strain coupling. This competition may provide a useful way of modifying piezoelectrically active morphotropic phase boundary systems and designing new systems.

This work was supported by the Department of Energy, via the ORNL LDRD program, and by the Office of Naval Research.

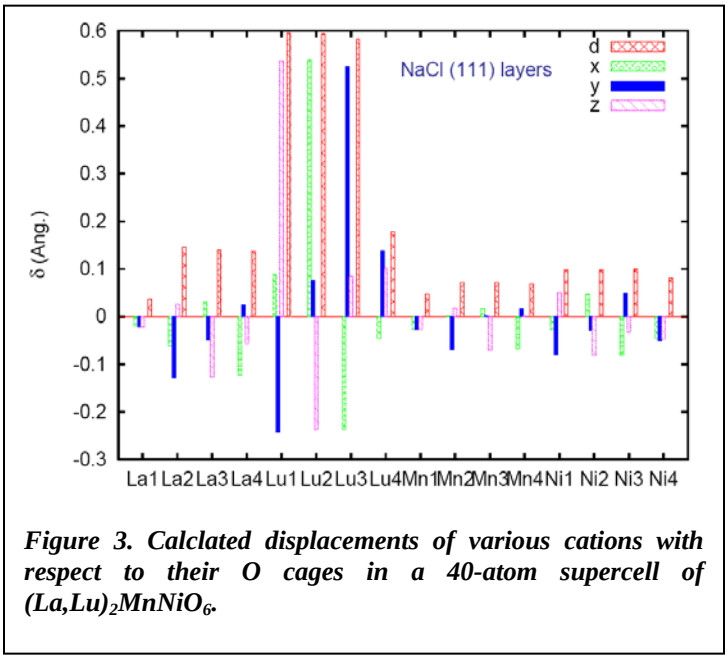

Figure 3. Calclated displacements of various cations with respect to their O cages in a 40-atom supercell of $(La,Lu)_2MnNiO_6$.

Phase field modeling of domain structures in nanocomposite ferroelectric multilayers

Julia Slutsker[1] and Andrei Artemev [2]

[1]*National Institute of Standards and Technology, Gaithersburg, USA, e-mail: julias@nist.gov*
[2]*Department of Mechanical and Aerospace Engineering, Carleton University, Ottawa, Canada*

The formation of domain structures in differently patterned multilayers with a nanocomposite structures containing ferroelectric components has been studied using a phase field method based on the microelasticity theory and the Fourier spectral analysis of electrostatic interactions. The effects of the depolarizing electric field, the thickness of the film, and the misfit between a film and a substrate on the domain pattern and switching properties have been analyzed.

The three component order parameter, η_p, describes the ferroelectric transition from a cubic phase to a tetragonal phase and the polarization vector is proportional to the order parameter, $P_i(\mathbf{r}) = P_0 \cdot \eta_p(\mathbf{r})$, where P_0 is determined from the saturation polarization for single domain equilibrium state. The transformation self-strain in a ferroelectric material is proportional to the second power of an order parameter:

$$\varepsilon_{ij}^{\,0}(\mathbf{r}) = \sum_{p=1}^{p=3} q_{ij}(p) \cdot \eta_p(\mathbf{r})^2 \qquad (1)$$

where q_{ij} is a electrostrictive coefficient tensor. This equilibrium field can be obtained by solving time-dependent Ginzburg-Landau equation with fast Fourier transform implementation for the energy of dipole-dipole interaction:

$$\frac{\partial \eta_p}{\partial t} = -L \frac{\delta F}{\delta \eta_p} + \xi_p \qquad (2)$$

where L is a kinetic coefficient and ξ_p is the Langevin noise term. The free energy functional, F, includes the Ginzburg-Landau-Devonshire potential, energy of elastic interactions and energy of electrostatic interactions.

The example of the phase field modeling of a domain structure in a ferroelectric rod embedded into an elastic matrix with dielectric properties of a vacuum are presented in Fig.1.

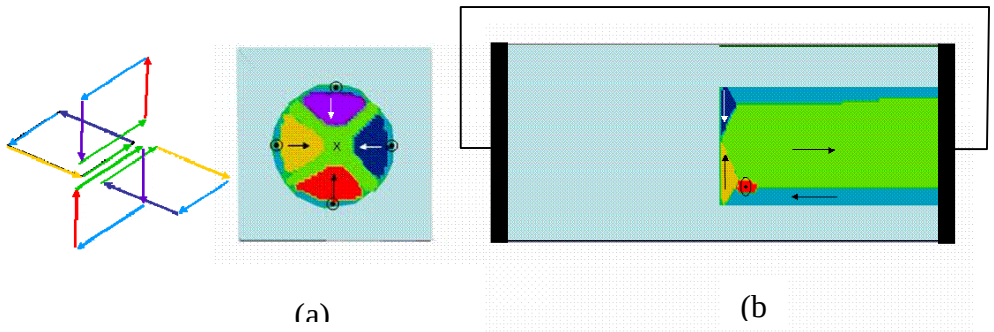

Figure 1. Domain structure in a ferroelectric nano-rod embedded into an elastic plate with dielectric properties of vacuum under short-circuit conditions. (a) plane-view and the corresponding schematic picture of three-dimensional close circuit of 90° domains (left), (b) cross-section. The directions of polarization vectors are shown by arrows.

The main features of domain structure in the rod are a closed circuit of 90° domains. This pattern is electrostatically equivalent to a vortex configuration which is a typical element in the ferroelectric nanorods, nanodisks and nanowires obtained by the first-principles-based simulations [1,2]. The phase field simulations have been performed for a generic cubic-tetragonal transformation in the ferroelectrics with parameters close to those of $PbTiO_3$. The mechanical constraint has been created by the matrix with a dielectric constant of a vacuum, $\tilde{\varepsilon}_0$, and the elastic moduli of a ferroelectric rod. It has been assumed that the gradient coefficient tensor is isotropic, $\beta_{ij}=\beta\delta_{ij}$, and does not depend on an order parameter.

The same simulation has been performed for a constrained ferroelectric layer with a variable ratio between energies of electrostatic, $\frac{1}{2} P_0^2/\tilde{\varepsilon}_0$, and elastic interactions, $\frac{1}{2} \varepsilon_{ij}^0 C_{ijkl} \varepsilon_{kl}^0$ (Fig. 2). There is a trend to form a closed circuit of 90° domains and to eliminate a heirarchical 90° domain structure with decreasing a relative contribution of the elastic interaction energy. The similar trend in a domain pattern formation is expected with decreasing size of confined ferroelectric crystals. The formation of a hierarchical 90° domain pattern results in decreasing the bulk electrostatic energy of depolarizing field and increasing the interface energy, while formation of a vortex-like closed circuit of 90° domains is accompanied by the disclination type distortion and increasing bulk elastic energy. Therefore, since decreasing size of a confined ferroelectric crystal results in decreasing contribution of the bulk energy in respect to the interface energy, it makes preferable relaxation of depolarizing field by the formation of closed circut of 90° domains.

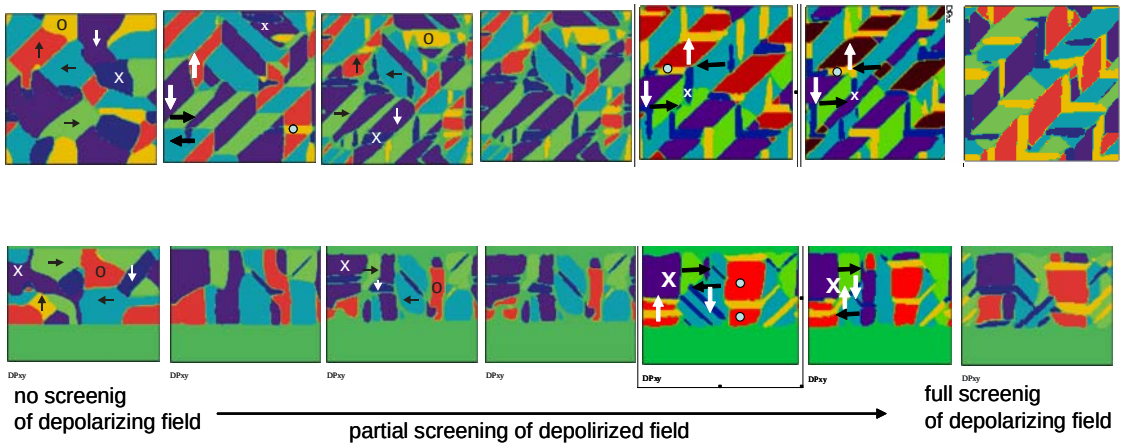

Figure 2. Domain patterns in a ferroelectric film with variable ratio between elastic and electrostatic interaction energies corresponding to the screening of depolarizing field. The closed circuit of 90° domains forms in the film with lowering the energy of elastic interaction or with decreasing screening of depolarizing field.

The results of phase field simulations demonstrate that the phase field method can be applied to the analysis of domain patterns in nano-ferroelectric composites, thus allowing us to describe ferroelectric films on different scale levels.

1. I.V.Naumov, L.Bellaiche and H.Fu, “Unusual Phase Transitions in Ferroelectric Nanodiscks and Nanorods”, Nature 432, 737-739 (2004)

2. I.Ponomareva, I.I.Naumov and L.Bellaiche, “Low-dimensional ferroelectrics under different electrical and mechanical boundary conditions:atomistic simulations”, Phys.Rev.B, 72, 214118, (2005)

Effects of Chemistry on the Structure and Properties of $PbTiO_3$-$Bi(B^IB^{II})O_3$ Solid Solutions

David M. Stein, Matthew R. Suchomel, and Peter K. Davies
Dept. of Materials Science and Engineering, University of Pennsylvania, Philadelphia, PA 19104
Phone: 215-898-1013; Fax: 215-573-2128; email: davies@upenn.edu

The discovery of the $PbTiO_3$-$BiScO_3$ perovskite system renewed research focus on $PbTiO_3$-$BiBO_3$ type solid solutions as possible low-lead or enhanced property replacements for $Pb(Zr,Ti)O_3$ (PZT) in piezoelectric and ferroelectric applications.[1] Predictions of enhanced tetragonality and other interesting properties in systems such as $BiGaO_3$ have provided additional motivation for research into novel Bi-perovskites, and recently high pressure synthesis techniques were used to prepare the highly tetragonal perovskite $BiCoO_3$.[2,3] Furthermore, first principles studies confirm that Bi^{3+} ions play a crucial role in the enhanced properties and polarizability in these solid solutions.[4] While earlier research was guided by empirical crystal-chemical considerations, recent work in our group has illuminated the importance of the chemistry and bonding on the B-site lattice in determining the structure and properties of these solid solution systems[5,6,7]. This research suggests the possibility of using ternary solid solution systems to engineer enhanced properties at the morphotropic phase boundary (MPB). The results from two ternary systems are the focus of this paper.

Empirical correlations between the tolerance factor of the non-$PbTiO_3$ (PT) end member and both the T_C and the position of the MPB have successfully guided research in this field. In particular, correlating tolerance factor with T_C led to the discovery of $BiScO_3$.[1] Correlations also correctly predicted the position of the MPB in solid solutions of $Bi(Mg_{1/2}Ti_{1/2})O_3$ and $Bi(Mg_{1/2}Zr_{1/2})O_3$ with lead titanate.[8] However, such crystal-chemical considerations fail to account for the covalent interactions that are fundamental to the spontaneous polarizations that are the basis of ferroelectricity and piezoelectricity. Recent work has merged empirical guides with first principles calculations and found that increasing concentrations of ferroelectrically (FE) active B-site ions stabilize the tetragonal perovskite structure and shift the position of the MPB to a more $PbTiO_3$-deficient composition.[5]

This stabilization of a tetragonal structure is exhibited in the extreme case of the end member $Bi(Zn_{1/2}Ti_{1/2})O_3$ (BZT).[6] Based on simple crystal-chemical correlations the properties of Zn-containing end members should be similar to their Mg-containing counterparts.[8,9] However, BZT contains a B-site that is fully occupied by FE-active cations and our experimental studies revealed large and sustained increases in both *c/a* and T_C in PT-BZT solid solutions. Near the solubility limit (~50% BZT) the *c/a* reaches *~1.11* and the T_C exceeds 700°C. First principles calculations indicate that the enhanced tetragonality in PT-BZT is stabilized by displacements of Bi^{3+} and Zn^{2+} that are considerably larger than in their PT counterparts.[10] The importance of coupled interactions between the Bi^{3+} cations on the A-site and FE active cations on the B-site is confirmed by the structures and properties of the $PbTiO_3$-$Bi(Zn_{3/4}W_{1/4})O_3$ (PT-BZW) system.[7] While the Mg-containing counterpart decreases tetragonality and forms an MPB[11], the PT-BZW

system behaves similarly to BZT reaching a *c/a* of *~1.08* and a T_C of 530°C at the limit of solubility.

While much research into alternatives to PZT has focused on engineering an MPB closer to the PT end-member, these Bi/Zn based solid solutions offer new alternatives based on end-members with tetragonalities and T_Cs higher than PT.

Pseudo-binary solid solutions in the ternary PT-BZT-$BiScO_3$ system were prepared to monitor the effect of the enhanced tetragonality of the end-member on the position of, and properties at the MPB. In this system, the crystal chemistry of the Sc^{3+} cation overwhelms the FE-active nature of the B-site cations in the PT-BZT end member and the ferroelectric properties are not significantly different to the PT-$BiScO_3$ system.[12]

To minimize the crystal chemical effects, new pseudo-binary solid solutions have been prepared in the PT-BZT-$Bi(Mg_{1/2}Ti_{1/2})O_3$ (BMT) ternary system. These compositions exhibit three phase transitions. A transition near room temperature shows relaxor-like behavior while the two higher temperature transitions show no signs of frequency dispersion in the dielectric constant. The highest temperature transition has a critical temperature (~600°C) that is only weakly dependent on composition in contrast to most PT-based solid solutions. This behavior was observed, but not explored, in the PT-BMT system. These results and their implications for the design of a new high Tc MPB system will be discussed.

Acknowledgement: this work was supported by the Office of Naval Research through grant N00014-01-1-0860. We thank A. M. Rappe, I. Grinberg and J. W. Bennett for many useful discussions.

[1]. R. E. Eitel, C. A. Randall, T. R. Shrout, P. W. Rehrig, W. Hackenberger, and S.-E. Park, Jpn. J. Appl. Phys., Part 1: 40 5999 (2001).
[2]. P. Baettig, C. F. Schelle, R. LeSar, U. V. Waghmare, N. A. Spaldin, Chem. Mater., 17, 1376 (2005).
[3]. A. Belik, S. Iikubo, K. Kodama, N. Igawa, S. Shamoto, S. Niitaka, M. Azuma, Y. Shimakawa, M. Takano, F. Izumi, and E. Takayama-Muromachi, Chem. Mater., 18, 798 (2006).
[4]. J. Iniguez, D. Vanderbilt, and L. Bellaiche, Phys. Rev. B, 67, 224107 (2003)
[5]. I. Grinberg, M. R. Suchomel, P. K. Davies, and A. M. Rappe, J. Appl. Phys., 98, 094111 (2005).
[6]. M. R. Suchomel and P. K. Davies, Appl. Phys. Lett., 86, 262905 (2005).
[7]. D. M. Stein, M. R. Suchomel, and P. K. Davies, Appl. Phys. Lett., 89, 132907 (2006)
[8]. M. R. Suchomel and P.K. Davies, J. Appl. Phys. 96, 4405 (2004)
[9]. C. A. Randall, R. Eitel, B. Jones, T. R. Shrout, D. I. Woodward, and I. M. Reaney, J. Appl. Phys., 95, 3633 (2004)
[10]. I. Grinberg, M.R. Suchomel, W. Dmowski, S. E. Mason, H. Wu, P.K. Davies, A.M. Rappe, Phys. Rev. Lett., (in press)
[11]. C. J. Stringer, R. E. Eitel, T. R. Shrout et al., J. Appl. Phys., 97, 024101 (2005).
[12]. M. R. Suchomel, University of Pennsylvania, 2005.

Origin of the dielectric dead layer in nanoscale capacitors

Massimiliano Stengel, Nicola A. Spaldin
Materials Department, University of California, Santa Barbara, CA 93106-5050
Phone: (805) 562-9190; e-mail: stengel@mrl.ucsb.edu

When the thickness of an oxide film is reduced to few unit cells, its dielectric properties (which are relevant, e.g., for nonvolatile ferroelectric memories and as gate oxides in MOSFET transistors) start to deviate from those predicted by macroscopic models, and cannot be disentangled from the metallic or semiconducting contacts. One particularly important issue related to interfacial effects is the "dielectric dead layer", which plagues the performance of thin-film perovskite capacitors by substantially reducing the effective permittivity (κ) of the active high-κ material. The microscopic origins of this reduced permittivity, and in particular whether it stems from defects or from the fundamental properties of a metal/insulator interface, are not well understood.

To address this problem from first principles, we will first show how the macroscopic polarization (and the coupling to an external field) can be rigorously defined for a periodic metal-insulator heterostructure [1], by using techniques and ideas borrowed from Wannier-function theory [2]. We will then demonstrate our new method by calculating the dielectric

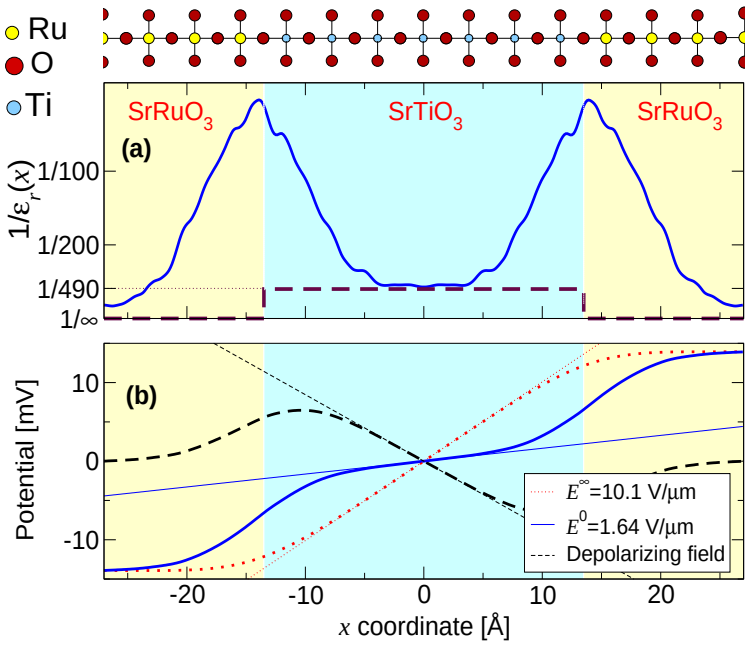

Figure 1: (a) Calculated inverse permittivity profile for the $SrTiO_3/SrRuO_3$ capacitor (solid curve) as compared to the classical picture (thick dashed curve) of a sharp transition between two ideal bulk materials; the calculated theoretical value of the static permittivity of bulk $SrTiO_3$ is 490. (b) Induced electrostatic potentials for an external bias $\Delta V = 27.8$ mV; the comparison between the dotted curve (only electrons are allowed to relax) and the solid curve (full structural relaxation in the presence of an applied field) evidences the *depolarizing field* induced by the ionic displacements (dashed curve).

properties of realistic $SrRuO_3/SrTiO_3/SrRuO_3$ nanocapacitors [3]. In particular, we demonstrate the existence of a dielectric dead layer (which is apparent in Fig. 1 as the impressive triangle-shaped peaks in the $1/\epsilon_r$ profile, and corresponds to an interfacial region with reduced permittivity compared to the bulk dielectric) and analyze its origin by extracting the ionic and electronic contributions to the electrostatic screening. We establish a correspondence between the dead layer and the hardening of the collective $SrTiO_3$ zone-center polar modes, and determine the influence of the electrode by repeating our calculations for $Pt/SrTiO_3/Pt$ capacitors.

Our results contribute to the fundamental understanding of the dielectric transition between high-κ insulators and metals, and are an important starting point for the development of more reliable phenomenological models. One thing we learn from this study is that the Thomas-Fermi screening length of the electrode material alone is not sufficient to account for the properties of the interface in a reliable way. The properties of the bulk materials are indeed chemically altered close to the interface, and the electrostatic screening is often a subtle balance of competing effects (in addition to the penetration of the electric field in the metal there is also a substantial penetration of the metallic states in the insulator), so that the overall dielectric response is difficult to predict without a full quantum-mechanical treatment of the junction. These results are also of direct technological relevance, in that they provide practical guidelines for minimizing the deleterious effects of the dielectric dead layer in nanoscale devices.

We are currently applying the same techniques to investigate multiferroicity and magnetoelectric properties at the interface between a ferromagnetic metal and a high-κ insulator; preliminary results for a *spin capacitor* will be presented.

References

[1] M. Stengel and N. A. Spaldin, cond-mat/0511042 (2005).

[2] M. Stengel and N. A. Spaldin, Phys. Rev. B **73**, 075121 (2006).

[3] M. Stengel and N. A. Spaldin, Nature (London) **443**, 679 (2006).

First Principles Determination of Positron Lifetimes in Materials

Hiroyuki Takenaka, David J. Singh
Oak Ridge National Laboratory, Oak Ridge, TN, 37831
Phone: 865-576-8675; Fax: 865-574-4143; e-mail: takenakah@ornl.gov

Positron lifetime measurements provide a sensitive probe of defects in materials. We are developing methodology for lifetime calculations in complex materials including oxides. Here we report the implementation of the method and tests of it. We report positron lifetimes for several materials. Electron charge densities and positron charge densities are obtained from first principles density functional theory calculations using the full potential linearized augmented planewave method within local density approximation. We apply the correlation potential and enhancement factors as parameterized by Boronski *et al.*[1] to obtain the potential sensed by the positron and the lifetime, respectively. We calculate the lifetimes for alkali metals, alkaline earth metals, transition metals, 14 group semiconductors, compound semiconductors, and various scintillators. Some results are shown in Table 1.

Now, we report trends in the lifetimes. First, we discuss elemental metals. Each alkali metal has the longest lifetime among atoms in the corresponding row of the periodic table. Because the alkali metals have the least number of valence electrons among the atoms, probability of the pair annihilation decreases. Furthermore, except for 8 group atoms, the lifetime increases as atomic mass increases in each group. Since this leads to strengthen attraction between electrons and nucleus, electrons exist around nucleus. Second, we discuss semiconductors. Semiconductors give rise to covalent charge bonding as well-known. The charge density is not delocalized, then, the positron lifetime increases. Now, we consider Si and Ge crystals, 14 group semiconductors. The lifetime of Ge is longer than that of Si because of mass. Next, we consider compound semiconductors, ZnO, GaAs, InP, and CdTe. We may recognize the lifetime of CdTe is the longest among them. Finally, we discuss scintillators, LaCl3, LuCl3, LaBr3, and LuBr3. The lifetime of the tri-bromides is longer than that of the trichlorides as same as mentioned above. Each lanthanide has the same number of valence electrons. The mass number of lutetium, however, is larger than lanthanum, contrary to this trend.

This work was supported by DOE, NA-22

---

[1] E. Boronski and R.M. Nieminen, Phys. Rev. B. 34, 3820 (1986)

Table 1: Positron lifetimes in [ps]

Li	301
Be	137
Na	322
Mg	234
Al	167
Si	214
K	378
Ca	288
Sc	197
Ti	146
V	116
Cr	102
Fe	103
Co	97
Ni	96
Cu	101
Zn	140
Ge	218
Rb	382
Sr	311
Y	216
Zr	158
Nb	122
Mo	106
Tc	99
Ru	92
Rh	98
Pd	106
Ag	127
Cd	157
CdTe	260
GaAs	218
InP	228
ZnO	144
$LaCl_3$	285
$LuCl_3$	284
$LaBr_3$	296
$LuBr_3$	290

Perfect Softening of Ferroelectric Mode in $SrTi^{18}O_3$

Masaki Takesada[1], Mitsuru Itoh[2], Akira Onodera[1], and Toshirou Yagi[3]
[1]Division of Physics, Graduate school of Science, Hokkaido University 060-0810, JAPAN
[2]Materials and Structures Laboratory, Tokyo Institute of Technology, 4259 Nagatsuta, Yokohama 226-8503, JAPAN
[3]Research Institute for Electronic Science, Hokkaido University 060-0812, JAPAN
Phonon: +81-11-706-4418; Fax: +81-11-706-3583; e-mail: mt@phys.sci.hokudai.ac.jp

The Strontium titanate $SrTiO_3$ has been considered as the typical quantum paraelectrics. The paraelectricity is kept until 0 K by the quantum fluctuation which prevents the ferroelectric order. [1] The Dynamics of the ferroelectric soft mode shows no freezing phenomena.[2,3] The first suggestion of the quantum-fluctuation effect in the ferroelectricity[1] has inclined many researchers to elucidate the physical origin of the quantum paraelectricity. Recently, by the substitution of ^{16}O in $SrTiO_3$ to its isotope ^{18}O the ferroelectric phase transition was discovered on $SrTiO_3$ at 23 K. [4] The ferroelectric soft mode in $SrTi^{18}O_3$ has been investigated to elucidate the phase transition mechanism related to the quantum fluctuation by many research groups [5-10]. However, any acceptable result has not been reported for the ferroelectric phase transition mechanism in $SrTi^{18}O_3$. According to these results about the lowest energy phonon mode, theoretical and experimental studies suggested the non-displacive phase transition mechanism in $SrTi^{18}O_3$. The previous works seem to give divergent conclusions from the insufficient analyses. In the present paper we demonstrate the perfect softening of the ferroelectric mode in $SrTi^{18}O_3$ by Raman scattering.

The light scattering experiment was performed by a Sandercock type tandem Fabry-Perot interferometer on six-pass stage. The finesse is more than 100. An Ar ion laser with a longitudinal single mode was used as a light source at a wavelength of 514.5 nm and a power of 100 mW. The scattering phonon wave vector q was parallel to the [001]c axis of the cubic phase. The value of isotope concentration x in the sample studied was 95 %. The sample was mounted in an optical cryostat cooled by liquid helium. The temperature was stabilized within an error of 0.01K.

In the VV scattering geometry the Raman spectra have been observed as a function of temperature. The spectra show a drastic change near T_c. The observed spectra above Tc have two components below 5 cm^{-1} and around 10-15 cm^{-1}, which are assigned to be the ferroelectric soft E_u mode and the A_{2u} mode, respectively. [11] With decreasing temperature, the spectra of the E_u mode shift to the central component critically and a drastic increase of intensity with temperature approaching to T_c. The spectra of the Raman inactive E_u mode have been observed owing to local symmetry breaking. The lowest frequency phonon mode (E_{u1}) shows continuous hardening below Tc from zero frequency with decreasing temperature. Both of the temperature dependences of the modes obey the Curie-Weiss law near T_c.

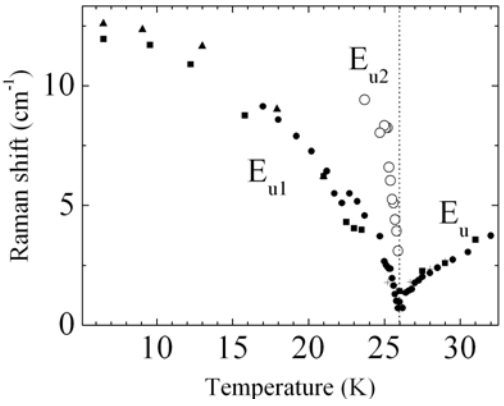

Fig. 1 The temperature dependence of the perfect softening ferroelectric mode in $SrTi^{18}O_3$.

In conclusion the E_u mode of the ferroelectric strontium titanate $SrTi^{18}O_3$ shows a perfect softening at T_c. The mechanism of the phase transition is concluded to be an ideal displacive type with perfect softening of the Slater type polar E_u mode. In the preset paper, we show a good agreement between the experimental results of the present and the previous reports [5-10] without a very low frequency region below 5cm^{-1}. An ambiguity of the previous reports is cleared.

References

[1] K. A. Muller and H. Burkard, Phys. Rev. B **19** 3593 (1979).
[2]Y. Yamada and G. Shirane, J. Phys. Soc. Jpn. **26** 396 (1969).
[3] K. Inoue, Ferroelectrics **52** 253 (1983).
[4] M. Itoh, R. Wang, Y. Inaguma, T. Yamaguchi, Y. –J. Shan, and T. Nakamura, Phys. Rev. Lett. **82** 3540 (1999).
[5] K. Abe, K. Yamashita, Y. Tomita, T. Shigenari, R. Wang and M. Itoh, Ferroelectrics **272** 155 (2002).
[6] H. Hasebe, Y. Tsujimi, R. Wang, M. Itoh and T. Yagi, Phys. Rev. B **68** 014109 (2003).
[7] T. Shigenari, K. Abe, K. Yamashita, T. Takemoto, R. Wang, and M. Itoh, Ferroelectrics, **285** 41 (2003).
[8] Y. Minaki, M. Kobayashi, Y. Tsujimi and T. Yagi, J. Korean. Phys. Soc., **42** S1290 (2003).
[9] Y. Yamada, N. Todoroki, and S. Miyashita, Phys. Rev. B 69 24103 (2004).
[10] T. Shigenari, K. Abe, T. Takemoto, O. Sanaka, T. Akaike, Y. Sakai, R. Wang, M. Itoh, Phys. Rev. B **74** 174121 (2006)
[11] M. Takesada, M. Itoh and T. Yagi, Phys. Rev. Lett. **96** 227602 (2006).

Soft Mode Dynamics in Quantum Ferroelectric ^{18}O-exchanged $SrTiO_3$ Studied by Raman Scattering

Hiroki TANIGUCHI, [1]Toshirou YAGI and Mitsuru ITOH
Materials and Structure Laboratory, Tokyo Institute of Technology, Yokohama 226-8503, Japan
[1]Research Institute for Electronic Science, Hokkaido University, Sapporo 060-0812, Japan
Phone & Fax: +81-45-924-5626; e-mail: taniguchi.h.aa@m.titech.ac.jp

Quantum phase transition in an inhomogeneous system has attracted increasing interest in recent years [for example Ref. (1) and (2)]. Several works indicate the smeared transition in the quantum phase transition with quenched disorder. However, the clear mechanism remains an open question. This situation seems to be due to a complexity of the system with the inhomogeneity and a difficulty to obtain reliable experimental results on it. In order to understand the nature of the quantum phase transition in the inhomogeneous system correctly, a simple model system has been desired.

In this point of view, ^{18}O-exchanged $SrTiO_3$ (STO18) is promising material. $SrTiO_3$ is a quantum paraelectric whose ferroelectricity is suppressed by quantum fluctuation in a low temperature region.[3] The exchange of ^{16}O with its isotope ^{18}O induces the ferroelectricity at a finite temperature T_c.[4] A T_c vs x (x is the exchange rate of ^{18}O) phase diagram shows good correspondence to a theoretical prediction for the quantum phase transition reported by Schneider *et al*.[5] The important point here is that ^{18}O is chemically equivalent to ^{16}O, therefore STO18 has only mass fluctuation of the oxygen atoms as an inhomogeneity. Thus STO18 is considered to be a quite simple and suitable material for the investigation of the effect of an inhomogeneity on the quantum phase transition. Motivated by this fact, a series of light scattering studies are performed, however the essential nature is still under discussion.[6, 7]

In the present study, we perform a Raman scattering experiment on STO18 as a function of the exchange rate x. The result clearly shows a gradual change of a soft mode behavior with increasing x, from quantum paraelectric like temperature dependence to classical ferroelectric like one [Fig. 1]. In the vicinity of the critical exchange rate for the ferroelectricity, on the other hand, the softening of soft mode becomes strongly smeared in association with microscopic paraelectric-ferroelectric phase separation. This experimental fact strongly indicates a novel dynamic critical

behavior at QCP in the ferroelectric phase transition of STO18. Finally we obtained experimentally a phase diagram for the quantum ferroelectric phase transition of STO18 on the basis of soft mode dynamics. The newly found anomalous soft mode dynamics in the vicinity of QCP is discussed in connection with the inhomogeneity of the system.

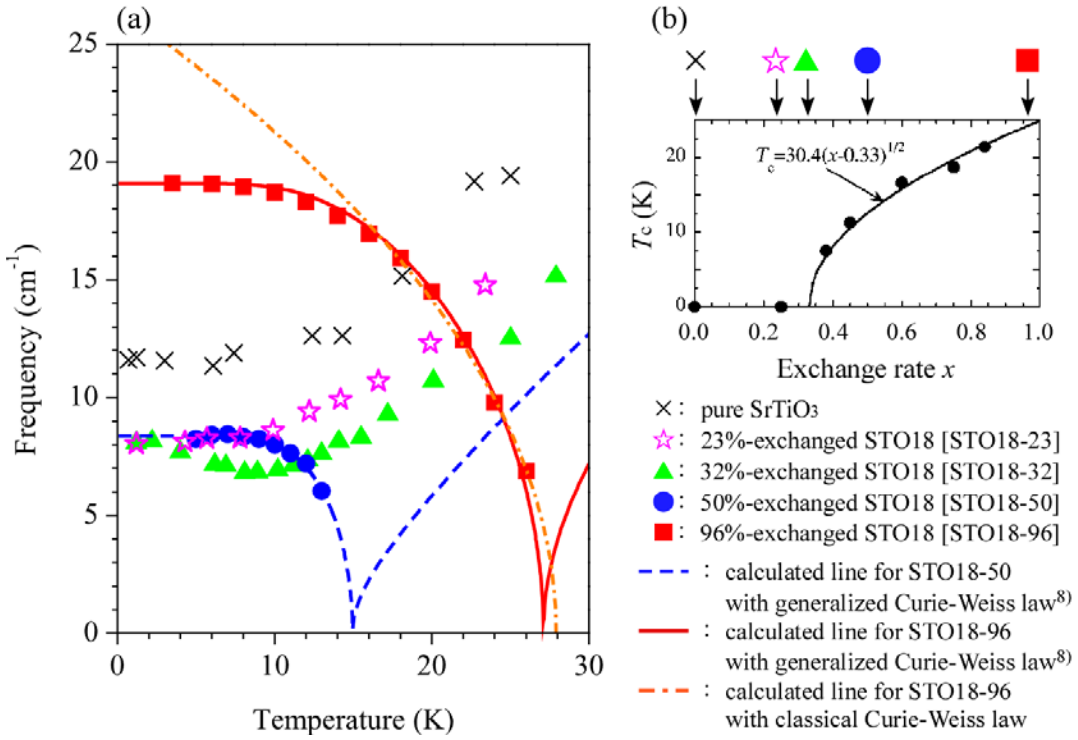

Fig.1: (a) Temperature dependencies of the soft mode in pure $SrTiO_3$ and STO18 with various exchange rates. (b) A phase diagram for STO18 obtained by the dielectric measurement. [4)]

REFERENCES:

1) T. Vojta: Phys. Rev. Lett. **90** (2003) 107202.

2) M. Vojta: Rep. Prog. Phys. **66** (2003) 2069.

3) K. A. Muller *et al.*: Z. Phys. B **84** (1991) 277.

4) R. Wang *et al.*: Phys. Rev. B **64** (2001) 174104.

5) T. Schneider *et al.*: Phys. Rev. B **13** (1976) 1123.

6) H. Taniguchi *et al.*: Phys. Rev. B **72** (2005) 064111.

7) M. Takesada *et al.*: Phys. Rev. Lett. **96** (2006) 227602.

8) S. A. Prosandeev *et al*. Phys. Rev. B **21** (1999) 14489.

Origin of Colossal Dielectric Properties of $CaCu_3Ti_4O_{12}$

Yoshiaki Uesu and Masakazu Mitsugi
Department of Physics, Waseda University, 3-4-1 Okubo, Shinjuku-ku, Tokyo, Japan
Phone:+81-3-5286-3446; Fax: +81-3-3202-4962; e-mail: uesu93@waseda.jp

$CaCu_3Ti_4O_{12}$(CCTO) exhibits an extremely large dielectric constant of about 80000 in a single crystal at room temperature, and a flat temperature dependence between 100K and room temperature in the frequency range from 10Hz to 1MHz [1]. Concerning the origin of the huge dielectric response, however, there exist two basically different understandings; one insists the extrinsic origin due to the effect of depletion layers between CCTO sample and electrodes [2], and another claims the intrinsic origin due to a structural or electronic disorder [3]. To estimate the effect of depletion layers, it was proposed to use a multilayer structure with CCTO interposed between insulating films [4].

Based upon the idea, we synthesize thin films of CCTO interposed between $CaTiO_3$ (CTO) films. It is also expected that this type of structure could reduce a high dielectric dissipation factor (tanδ) of CCTO. The CTO/CCTO/CTO/$SrRuO_3$ multilayer thin films are deposited on (001) substrates of $SrTiO_3$(STO) by the PLD method. A $SrRuO_3$(SRO) thin film with thickness of 40nm is used as a bottom electrode for dielectric measurements. From the capacitances of the multilayer thin films with different thicknesses of CTO, we obtain a capacitance free from the effect of the depletion-layers by extrapolating the CTO thickness to zero. This process is repeated by changing CCTO thicknesses, from which we eliminate the extra-capacitance at CCTO/CTO interfaces. Finally we obtain the inherent dielectric constant of CCTO.

CCTO thin films are deposited at 500C instead of 750-850C as reported in the previous papers and annealed at 800C for 30 minutes. The process makes the films surface smooth and keeps the high crystallinity of CCTO as shown in Fig.1. This is quite necessary because the dielectric response of a multilayer thin film especially for thinner one cannot be accurately measured on a rough surface. The orientations of the multilayer thin films are investigated by XRD after cooling the films to room temperature with cooling rate of 10C/min and the result is shown in Fig.2. Both CCTO and CTO films are well oriented along the (001) direction of STO. The dielectric responses are measured for different combinations of thicknesses of CCTO (40nm, 140nm) and CTO (16nm-124nm). Fig.3 shows the frequency dependence of capacitances of the multilayer thin films with CCTO thickness fixed at 140nm and CTO thickness varied from

40nm to 124nm. To obtain the inherent capacitance of CCTO, we eliminate the extra capacitance due to the charge effect at CCTO/CTO interfaces, and finally determine the inherent dielectric constant ε_{CCTO} as 500±150. The value is almost same order of magnitude as the value obtained by the first principle calculation (70~120) [5]. Therefore, the extremely large dielectric constant of CCTO could be mostly originated from the extrinsic nature such as a depletion layer and/or interface effects but an intrinsic contribution may still exist in the apparently large dielectric constant.

[1] M. A. Subramanian, D. Li, N. Duan, B. A. Reisner, and A. W. Sleight, *J. Solid State Chem.* **151**, 323 (2000)

[2] P. Lunkenheimer, V. Bobnar, A. V. Pronin, A. I. Ritus, A. A. Volkov, and A. Loidl, *Phys. Rev. B* **66,** 052105 (2002)

[3] W. Kobayashi and I. Terasaki, Appl.Phys.Lett. **87,** 032902 (2005)

[4] M. H. Cohen, J. B. Neaton, L. He, and D. Vanderbilt, *J. Appl. Phys.* **94,** 3299 (2003)

[5] L. He, J. B. Neaton, M. H. Cohen, D. Vanderbilt, and C. C. Homes, *Phys. Rev. B* **65**

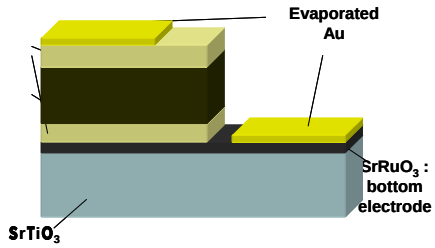

Fig.1 Scematic illustration of CTO/CCTO /CTO/SRO/STO multi- layer thin film.

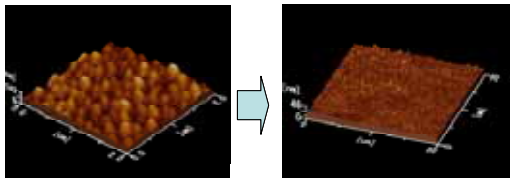

(a) (b)

Fig.2 AFM images of CCTO/SRO/STO films. CCTO thickness is 140 nm, deposited at 800˚C (a) and at 500˚C (b).

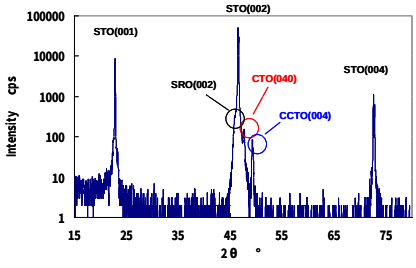

Fig.3 XRD patterns of the CTO/CCTO/CTO/SRO multilayer thin film on a (001) substrate of STO. The thickness of CCTO and CTO is 400nm and 200nm, respectively.

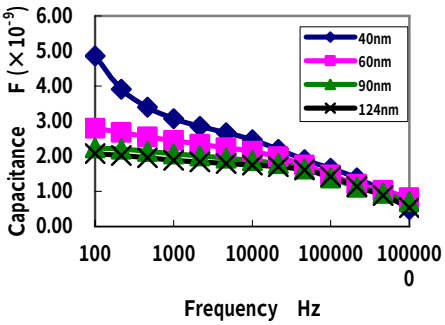

Fig.4 Frequency dependence of capacitances of the multilayer thin films composed of CCTO(140nm) and CTO with different thicknesses.

Finite electric fields and non-linear responses in ferroelectrics

David Vanderbilt, Oswaldo Diéguez, Xifan Wu, and Karin Rabe
Department of Physics and Astronomy, Rutgers University, USA
Massimiliano Stengel
Materials Department, University of California at Santa Barbara, USA
Phone: 732-445-2514; Fax: 732-445-4400; Email: dhv@physics.rutgers.edu

Until recently, a fully first-principles treatment of a bulk insulator in a finite electric field $\mathcal{E}$ was problematic. The difficulties arise from the fact that the usual central assumption of solid state physics – namely, the periodicity of the crystal potential – is violated, and in such a way that the system does not have any truly well-defined ground state, in a finite electric field. Approximate methods have partially succeeded in circumventing these difficulties. For example, when the dominant contribution to the electric polarization arises from lattice displacements, as opposed to electronic distortions *per se*, it is sufficient to compute electric polarizations at $\mathcal{E} = 0$ and incorporate the information about its coupling to lattice displacements into effective-Hamiltonian parameters[1] or into dynamical effective charges.[2,3] In the latter approach, for example, one takes into account that there is an extra force on each atom equal to its dynamical charge tensor Z^* times the field $\mathcal{E}$, but makes the approximation of computing Z^* at zero field. In surface slab studies,[4] it is also possible to apply an electric field to the slab by inserting an external dipole layer in the vacuum region, but this trick would not work for bulk or superlattice structures.

A fundamental advance came in 2002 when it was realized[5,6] that the electric field could be included in a bulk first-principles calculation by minimizing the Nunes-Gonze[7] electric enthalpy functional $E - \mathcal{E} \cdot P$, where E is the usual zero-field Kohn-Sham functional and P is the Berry-phase polarization.[8] This approach has allowed for direct calculations of the structural and electronic properties of insulators in finite electric fields.

Before such a method could become truly useful for ferroelectric materials, however, an additional modification was necessary. The problem arises from the double-well structure of the energy surface of a ferroelectric, and the fact that for small electric fields, there are three competing solutions, located in the majority well, in the minority well, and near the saddle-point. Moreover, the last of these is an unstable solution that cannot be found using minimization methods at fixed electric field. Instead, we have introduced an approach[9] based on mapping out $E(P)$, the energy as a function of polarization. In this approach, the electric field $\mathcal{E}$ appears in the guise of a Lagrange multiplier, so that one also obtains the field-vs.-polarization curve $\mathcal{E}(P)$, which we refer to as an "electric equation of state." In fact, since the displacement field is trivially given as $D = \epsilon_0 \mathcal{E} + P$, it is also straightforward to numerically construct other electric equations of state such as $P(\mathcal{E})$, $D(\mathcal{E})$, or $P(D)$.

I will discuss two applications of these new approaches. First, the polarization reversal in KNO_3 takes place via a very unusual mechanism involving the rotation of nitrate groups.[9] We map out the energy E, nitrate group rotation angle θ, and electric field $\mathcal{E}$ as a function of P along the rhombohedral axis. If time permits, a simple model that explains the qualitative features of the behavior will be introduced.

Second, I will discuss our recent work attempting to compute and analyse the nonlinear dielectric behavior of short-period superlattice structures composed of materials such as $SrTiO_3$ and $BaTiO_3$. In this context, we find it especially convenient to focus on the $P(D)$ equation of state, because (i) $P(D)$ is typically a single-valued function, and (ii) D is uniform throughout the superlattice. Moreover, using a new approach for computing the individual polarizations p_i of each layer i, based on a one-dimensional Wannier-function analysis,[10] we compute $p_i(D)$ and study its dependence upon the local compositional environment. From such an approach, we hope to build robust and predictive models for the nonlinear electrostatic properties of superlattices in finite field and, for example, to use such models to predict the $C-V$ characteristics of superlattices of arbitrary layer sequence.

[1] L. Bellaiche, A. García, and D. Vanderbilt, "Electric-field induced polarization paths in $Pb(Zr_{1-x}Ti_x)O_3$ alloys," Phys. Rev. B **64**, 060103 (2001).

[2] N. Sai, K.M. Rabe, and D. Vanderbilt, "Theory of structural response to macroscopic electric fields in ferroelectric systems," Phys. Rev. B **66**, 104108 (2002).

[3] H. Fu and L. Bellaiche, "First-principles determination of electromechanical responses of solids under finite electric fields," Phys. Rev. Lett. **91**, 057601 (2003); I.I. Naumov and H. Fu, "Phonon structure in $SrTiO_3$ under finite electric fields: First-principles density functional approach," Phys. Rev. B **72**, 012304 (2005).

[4] B. Meyer and D. Vanderbilt, "Ab initio study of $BaTiO_3$ and $PbTiO_3$ surfaces in external electric fields," Phys. Rev. B **63**, 205426 (2001).

[5] I. Souza, J. Íñiguez, and D. Vanderbilt, "First-principles approach to insulators in finite electric fields," Phys. Rev. Lett. **89**, 117602 (2002).

[7] P. Umari and A. Pasquarello, "Ab initio molecular dynamics in a finite homogeneous electric field," Phys. Rev. Lett. **89**, 157602 (2002).

[7] R.W. Nunes and X. Gonze, "Berry-phase treatment of the homogeneous electric field perturbation in insulators," Phys. Rev. B **63**, 155107 (2001).

[8] R.D. King-Smith and D. Vanderbilt, "Theory of polarization of crystalline solids," Phys. Rev. B **47**, 1651 (1993).

[9] O. Diéguez and D. Vanderbilt, "First-principles calculations at constant polarization," Phys. Rev. Lett. **96**, 056401 (2006).

[10] X. Wu, O. Diéguez, K.M. Rabe, and D. Vanderbilt, "Wannier-based definition of layer polarizations in perovskite superlattices," Phys. Rev. Lett. **97**, 107602 (2006).

Polar Nanoclusters in (1-x) $PbMg_{1/3}Nb_{2/3}O_3$ - x $PbSc_{1/2}Nb_{1/2}O_3$ Across the Ferroelectric Phase Transition

Robert L Vold*, Gina L Hoatson, and M. Vijayakumar
Department of Physics and Department of Applied Science*,
College of William and Mary, Williamsburg, VA 23187-8795, USA

Solid solutions with composition (1-x)$PbMg_{1/3}Nb_{2/3}O_3$ – x $PbSc_{1/2}Nb_{1/2}O_3$ (PMSN) are among the more promising ferroelectric materials. Local structural disorder in these materials plays a vital role in their ferroelectric behavior. In order to shed more light on local structural changes that occur across the ferroelectric phase transition, high field (17.6Tesla) ^{93}Nb MAS & 3Q-MAS NMR studies were carried out as a function of temperature on pure PMN and also on annealed PMSN samples with compositions x = 0.2, (a relaxor ferroelectric), and x = 0.6, (a normal ferroelectric).

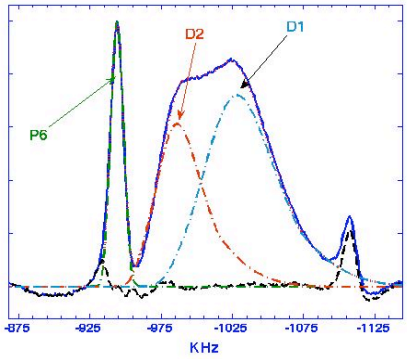

Figure 1: ^{93}Nb MAS NMR spectrum of PMN at T = 350 K, ν_R = 30 kHz, and 17.6T.

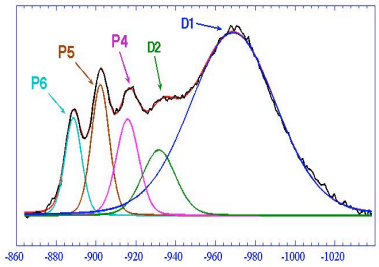

Figure 2: ^{93}Nb MAS NMR spectrum of 0.8PMN-0.2PSN at T = 370 K, ν_R = 30 kHz, and 17.6T.

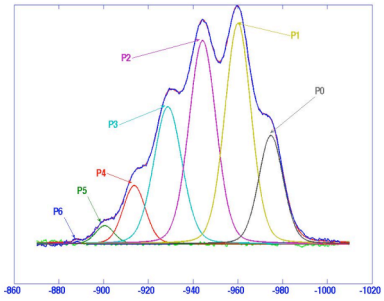

Figure 3: ^{93}Nb MAS NMR spectrum of 0.4PMN-0.6PSN at T = 375 K, ν_R = 30 kHz, and 17.6T.

^{93}Nb magic angle spinning (MAS) spectra obtained at temperatures well above the phase transition are shown in Figures 1-3. Up to seven narrow components are observed, P0,…P6, as well as two distribution peaks, D1 and D2. These peaks can be unambiguously assigned to specific next nearest B-site neighbor (nBn) configurations[1]. The distribution peaks represent niobium ions in configurations that contain at least one Nb^{5+} cation in the shell of next nearest B-site neighbors: D1 includes configurations that contain at least one Nb^{5+} cation and zero or one Mg^{2+} cations; D2 includes configurations with 2-5 Mg^{2+} cations and variable numbers of Nb^{5+} and Sc^{3+} cations; and P0,…P6 are assigned to single configurations with no niobium cations and the indicated number of Mg^{2+} cations. The assignments are based on a self-consistent analysis of integrated MAS intensities, determined by deconvolution as indicated in the figures. The results, confirmed by 3QMAS spectra, are provide direct evidence for the now widely accepted random site model ordering proposed by Davies and coworkers [2].

The peak positions in MAS spectra are determined by a combination of isotropic chemical shifts, δ_{iso}^{CS}, and the isotropic second order quadrupole shift, δ_{iso}^{2Q}. Line widths include major contributions from anisotropic second order quadrupole broadening as well as inhomogeneous distributions $\Delta\delta_{iso}^{CS}$ and $\Delta\delta_{iso}^{2Q}$. Rapid spinning, $\upsilon_R \geq 30$ kHz, suppresses contributions from dipolar coupling.

For pure PMN, isotropic chemical shift and quadrupole coupling parameters were determined for each peak as a function of temperature by least squares fitting, using peak frequencies observed in 3QMAS spectra to constrain the parameters. The temperature dependence of the mean quadrupole coupling constants, $\langle C_Q \rangle$ found for P6, D1, and D2 in PMN is shown in Figure 4. For P6 (blue triangles) and D2 (red circles) C_Q increases gradually with decreasing temperature; this is normal behavior for ionic crystalline solids. However, for D1 the temperature dependence of C_Q is much stronger. It is relevant that the onset of bulk remnant polarization in PMN occurs near 270 K.

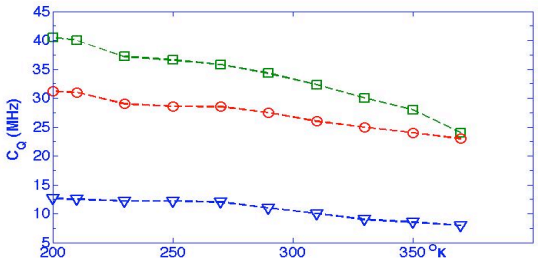

Figure 4: Temperature dependence of C_Q for peaks P6 (blue), D2(red) and D1 (green) in pure PMN. Dashed lines are drawn to guide the eye.

In annealed ("ordered") PMSN samples, there is a crossover from relaxor to normal ferroelectric behavior near PSN mole fraction $x = 0.5$ [3]. The temperature dependence of mean C_Q for the various peaks in annealed 0.4PMN-0.6PSN is shown in Figure 5. Just as in pure PMN, only D1 shows significant temperature dependence. As expected, C_Q drops sharply for this peak above the phase transition, where off-centering is suppressed.

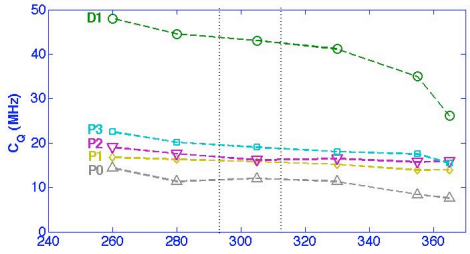

Figure 5: Temperature dependence of C_Q for peaks P0 …P3 and D1 in 0.4PMN-0.6PSN. Vertical bars indicate the 5-95% limits of remnant bulk polarization. Dashed lines are drawn to guide the eye.

A complete discussion of these results may be found in references [4] and [5]. In all three samples, only D1 displays significant temperature dependence across the paraelectric to ferroelectric phase transition. The observed changes in C_Q and δ_{iso}^{CS} for this peak arise primarily from temperature dependent changes in Nb-O bond lengths and angles that occur upon formation of polar nanoclusters. Our results demonstrate that the polar nanoclusters in these materials consist predominantly of nBn configurations assigned to D1, namely, those with at least one Nb^{5+} cation and zero or one Mg^{2+} cations. As temperature decreases, Nb^{5+} ions in nBn configurations with increasing numbers of Mg^{2+}, originally in D2, move off center and join the polar nanoclusters.

Acknowledgements

We thank Prof. Peter Davies (University of Pennsylvania) useful discussions and for providing the PMSN and other samples. This work was supported by grants from the Office of Naval Research and the National Science Foundation.

References

[1] D.H.Zhou, G.L.Hoatson, R.L.Vold, J. Magn. Reson. **167** (2004) 242-252; G.L.Hoatson, D.H.Zhou, F.Fayon, D.Massiot, R.L.Vold, Phys. Rev. B **66** (2002) 224103.
[2] M. K. Akbas and P. K. Davies, Journal of the American Ceramic Society **83**, 159 (2000).
[3] L. Farber and P. K. Davies, J. AM. Ceramic Society **86**, 1861 (2003).
[4] M. Vijayakumar, G. L. Hoatson, and R. L. Vold, Phys Rev B **in press** (2006)
[5] R. L. Vold, G. L. Hoatson, and M. Vijayakumar, Phys. Rev. B **(submitted)** (2007).

FORMATION AND DYNAMICS OF POLAR NANOREGIONS IN RELAXOR FERROELECTRICS

B.E. Vugmeister

Datamir Inc., Clifton, New Jersey 07012, USA
e-mail: vugmeister@datamir.net

Nowadays there is more and more evidences that relaxor ferroelectrics represent new state of matter, intermediate between *non-equilibrium dipole glass* and regular ferroelectrics [1]. However, till recently the theory has been developed [1,2] only for experiments involving long wave length polarization (e.g. linear and nonlinear dielectric response in the applied electric field).

We present here the mesoscopic theory of relaxor ferroelectrics which generalizes our previous approach to explain for the first time *formation of polar nanoregions* (PNR) and dynamics of both long wave length polarization contributing to the dielectric response, and the *local polarization dynamics* determining NMR spin lattice relaxation and the transverse component of the neutron scattering intensity.

The main assumption of the theory is the existence of *off-center ions* below Burns temperature and their interaction with *highly polarizable lattice* of relaxor materials. Such interaction leads to the crossover from the displacive type of polarization behavior to order-disorder type, characterized by the appearance of the dynamic central peak in Raman and neutron scattering.

We show that in the central peak regime off-center ions form *short range reorienting clusters* with the size $r_c > a, a$ is the lattice constant. Each cluster involves simultaneous displacements of other atoms adjacent to a given off-center ion, and the effective dipole moment d^* of each cluster exceeds significantly the proper off-center ion dipole moment. The relaxor behavior can be thought then to arise from the mutual interactions of such *giant dipole moments* accompanied by the effect of compositional disorder.

A consequence of the compositional disorder is the *distribution of cluster relaxation times* and *quenched random fields* resulting in the suppression of ferroelectric phase transition due to strong local field fluctuations.

We show that the effect of local field fluctuations could be included in a self-consistent manner with the use of the developed self-consistent random field theory, and calculate the structure factor of polarization determining transverse neutron scattering.

Complexity of polarization dynamics in relaxors caused by the *coexistence of the critical dynamics*, a common feature of pretransitional phenomena, and the *glassy dynamics* of polar clusters.

Interrelation between the dynamics of long wavelength fluctuations and local polarization dynamics provides an important test to distinguish between the different models of relaxor behavior. Till now, the mostly used model considers each PNR as an independent rigid relaxator characterized by a single exponential relaxation function. It implies that the observable experimental characteristics are the average values over the different PNR which fluctuate as a whole. Then the average and local polarization should obey the same relaxation law, and NMR relaxation time T_1 should be proportional to the imaginary part of the dielectric susceptibility measured at NMR frequency. However, this scenario is not realized in PMN (see Fig. 1) and apparently in other relaxors as well. The temperature slope of ϵ'' is much sharper than the slope of T_1, and the position of the maximum of T_1^{-1} and ϵ'' do not necessarily coincide. We prove that the nature of this inconsistency is that PNR are not tight binding entities, and the local polarization could propagate along PNR by the diffusion type mode similarly to that in regular ferroelectrics. At the temperatures where dynamics of the average polarization undergoes critical slowing down, the diffusion type relaxation of local polarization dominates and partially smoothes the effect of the critical slowing down on the local

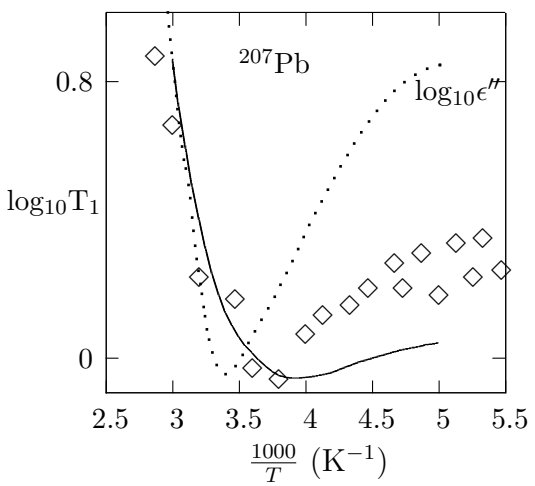

Fig.1

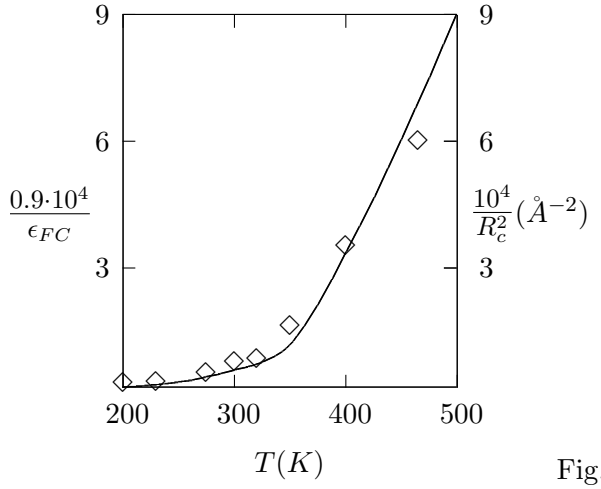

Fig.2

Fig.1. Experimental (Blinc et al., Phys. Rev. B **63**, 024104 (2001)) and theoretical (solid line) temperature dependence of ^{207}Pb NMR spin lattice relaxation time T_1 in PMN at Larmor frequency 79.4 MHz. Dotted line reproduces the temperature dependence of $\log_{10}\epsilon''(\omega)$ at ω =112MHz (Grigalaitis et al, J. Phys. IV **128**, 127 (2005)). Vertical positions of the dotted and solid lines are adjustable parameters.

Fig.2. Experimental temperature dependences (Levstik et al, Phys. Rev. B 57, 11204 (1998), Viehland et al, Phys. Rev. B 46, 8003 (1992)) of the inverse static dielectric permittivity in PMN (solid line) and square of the inverse correlation length of PNR (Vakhrushev et al, Physica B 156-157, 90 (1989))

polarization dynamics.

We show that with the neglect of correlations between relaxation times of different short range clusters, the effect of the distribution of cluster relaxation times on polarization dynamics could be described in terms of *continuous time random walk* stochastic process which has been widely explored for the analysis of different transport phenomena and aging effects in disordered solids.

Using self-consistent random field theory and continuous time random walk approximation, a relationship is established [3] between the average polarization dynamics contributing to the low frequency dielectric response, and the local polarization dynamics determining NMR spin lattice relaxation time. The length scale (correlation length) R_c of PNR is estimated from the obtained universal relationship between the parameters of the soft mode dispersion curve and the static dielectric permittivity, and is in agreement with the experiment in PMN (e.g., $R_c \approx$10nm at T=300K) and other relaxors (see table below for comparison).

Crystal	T	$(R_c/r_c)_{Teor}$	$(R_c/r_c)_{Exper}$	Method
PMN	300K	15.3	19.1	neutron[4]
KTN 1.2%	15.5 K	4.6	5	raman[5]
KTN 15%	125 K	11.8	12	raman[5]
KLT 4%	55 K	2	4.5	raman[5]

Also the theory reproduces qualitatively a trend in the soft mode hardening at low temperatures (as a result of nonlinear interactions of off-center ions with the lattice polarization), and the coexistence of local and long range polar order due to incomplete freezing of local polarization.

The obtained reasonable agreement of the theory with the body of experiments in relaxor suggests that the theory captures essential physics of relaxor ferroelectrics, and could be used for the characterization of new relaxor materials.

1. B.E. Vugmeister and H. Rabitz, Phys. Rev. B **57**, 7581 (1998);
2. B.E. Vugmeister and H. Rabitz, Phys.Rev. B **61**, 14448 (2000); **65**, 024111 (2002).
3. B.E. Vugmeister, Phys. Rev. B **73**, 174117 (2006).
4. S. B. Vakhrushev, B. E. Kvyatkovksy, A. A. Naberezhnov et al, Physica B 156-157, 90 (1989).
5. P. DiAntonio, B. E. Vugmeister, J. Toulouse, and L. A. Boatner, Phys. Rev. B **47** 5629 (1993).

Non-ferroelectric aging in PMN

M.B. Weissman and Eugene V. Colla,
Department of Physics, University of Illinois at Urbana-Champaign.
Phone: 217-333-7897; Fax: 217-333-9819; e-mail mbw@uiuc.edu

The central question in the physics of relaxor ferroelectrics such as $PbMg_{1/3}Nb_{2/3}O_3$ (PMN) is how the underlying frozen disorder prevents the formation of long-range ferroelectric order while allowing the formation of polar nanoregions (PNRs) on a scale of several nm. We have argued previously, e.g. [1, 2], that there is a second type of order, similar to that proposed for martensitic systems[3], involving glassy states of unit-cell scale displacements orthogonal to the mid-range ferroelectric polarization and/or in regions lacking such polarization. One of the principle symptoms of such an additional form of glassiness is distinctive spinglass-like aging effects, much less sensitive to applied field than one would expect for a glass of PNR-scale dipoles. [1, 2, 4] Here we show that in a collection of PMN samples whose linear and non-linear dielectric behaviors are quite diverse, the low temperature aging effects are very nearly identical. Our interpretation is that although the dielectric response must be dominated by PNRs, the aging is coming from some distinct degrees of freedom, for which the other components of the unit-cell displacements remain the best candidate, since such aging effects are absent in the frozen state of uniaxial relaxors[5].

The four samples described here (a longer report with more description of the sources is available[6]) were all single crystals of nominally good quality. However, they showed a range of dielectric properties. The temperature T_P of the peak in ε'was 249K, 252K, 267K and 265K for samples A-D, respectively. Samples A, B, and D not only had lower T_P but also showed significant reductions in ε' compared with C. When cooled in large electric fields, only sample C showed the abrupt forced ferroelectric transition reported[2, 7-9] for several other PMN samples with similar dielectric properties. Sample D also showed a small sharp step in ε' on cooling the vicinity 172-191K on each cool-down. This step, of unknown origin, also showed up as a depolarization spike when field-cooling.

Aging experiments were run by cooling at zero field to 180K, aging for around ten hours, further cooling to 120K, then reheating, all while measuring ε' and ε". Despite the variety of dielectric behaviors and the variety of empirical phase diagrams, the reduction in ε" during the initial aging is very similar for the four samples, as shown in Fig. 1. Furthermore, all four samples showed similar spinglass-like aging 'holes' with memory, as illustrated for two samples in the inset to Fig.1. The reduction in ε during aging shows up only near the aging temperature, and is largely preserved under subsequent cooling, though not under warming above the aging temperature In sample D, this effect was not noticeably different in a run in which the abrupt step in ε' occurred before the aging procedure and in a run in which it occurred after aging but before read-out of the memory on reheating.

.

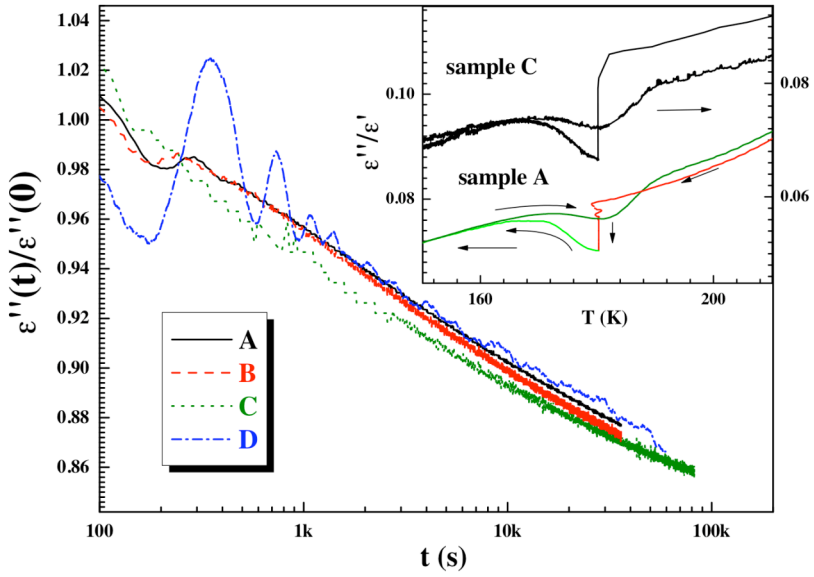

Figure 1. The aging of ε″(100 Hz) is shown as a function of time t spent at 180 K after rapid cooling from 400 K. The wiggles for t < 1000 s just come from temperature oscillations.. The inset shows the development of an aging hole at 180 K in samples A and C. The aging time was 10 hours, before cooling to 120 K and then reheating.

We conclude that although the properties of the PNR, which are the only thermodynamically plausible source of the high e, are strongly sensitive to some sample-dependent property (perhaps long-range correlated strain), the source of the aging effects is not. That fits well with the hypothesis that the glassy aging effects are dominated by collective states of much smaller units than the PNR. What remains to sort out is how important this glassy order is in the thermodynamics of the relaxor state.

We thank our collaborators, P.M. Gehring, Guangyong Xu, Haosu Luo, P. Gemeiner and Brahim Dkhil both for samples and for thoughtful advice. This work was funded by NSF DMR 02-40644 and used facilities of the Center for Microanalysis of Materials, University of Illinois, which is partially supported by the U.S. Department of Energy under grant DEFG02-91-ER4543.

[1] M. B. Weissman, E. V. Colla, and L. K. Chao, in *Fundamental Physics of Ferroelectrics 2003*, edited by P. K. Davies and D. J. Singh (AIP, Williamsburg, Virginia (USA), 2003), Vol. 677, p. 33.
[2] E. V. Colla and M. B. Weissman, Phys. Rev. B **72**, 104106 (2005).
[3] S. Kartha, T. Cast'an, J. A. Krumhansl, and J. P. Sethna, Phys. Rev. Lett. **67**, 3630 (1991).
[4] L. K. Chao, E. V. Colla, and M. B. Weissman, Phys. Rev. B **74**, 014105 (2006).
[5] L. K. Chao, E. V. Colla, M. B. Weissman, and D. D. Viehland, Phys . Rev. B **72**, 134105 (2005).
[6] E. V. Colla, M. B. Weissman, P. M. Gehring, G. Xu, H. Luo, P. Gemeiner, and B. Dkhi, Phys. Rev. B **75**, 024103 (2007).
[7] G. Schmidt, H. Arndt, G. Borchhardt, J. v. Cieminski, T. Petzsche, K. Borman, A. Sterenberg, A. Zirnite, and V. A. Isupov, Phys. Stat. Sol. (a) **63**, 501 (1981).
[8] E. V. Colla, E. Y. Koroleva, N. M. Okuneva, and S. B. Vakhrushev, Ferroelectrics **184**, 209 (1996).
[9] B. Dkhil and J. M. Kiat, J. Appl. Phys. **90**, 4676 (2001).

First-principles study of in-plane strain effects on the polarization in $PbTiO_3/SrTiO_3$ superlattices

Yanpeng Yao and Huaxiang Fu
Department of Physics, University of Arkansas, Fayetteville, AR 72701

Strain can affect the polarization of ferroelectric materials. Various studies have been conducted to investigate the polarization of ferroelectric thin films on substrate of different degree of lattice mismatch, when the films are made of one perovskite material [1]. For ferroelectric superlattices that consist of two substances of rather dissimilar polarization properties, such as $PbTiO_3/SrTiO_3$ superlattices (where PT is strongly ferroelectric while ST is incipient ferroelectric), the understanding of how its polarization may be altered by inplane strain, and of how this response in superlattices deviates from the response when each individual constituent alone is subject to the in-plane strain, remains rather limited [2].

Here we perform first-principles density functional calculations to study the structure and polarization response of $PbTiO_3/SrTiO_3$ 1x1 superlattice under varied inplane strain. The superlattice is chosen to be grown along (001) crystallographic direction, and is assumed to be tetragonal. Calculations are carried out using pseudopotential method with mixed bases. For a given inplane strain, the out-of-plane lattice constant and atomic positions are relaxed. Polarizations are calculated using the Berry phase approach. The LDA-calculated unstrained structural parameters for bulk materials are a=3.877Å, c/a=1.031 for $PbTiO_3$, and a=3.855Å, c/a~1 for $SrTiO_3$. As a starting point, we first determine the structure and polarization of strained bulk $PbTiO_3$. The polarization is found to increase with the decreasing inplane lattice length, and the slope of $P_3 \sim \eta_1$ curve is determined to be 628μC/cm^2, which is comparable with the value of 804μC/cm^2 reported in Ref.1. For PT/ST superlattice, the equilibrium inplane lattice constant is calculated to be 3.877Å, which is interestingly close to the value of pure tetragonal $PbTiO_3$. This superlattice has very small polarization which is close to zero. As the inplane lattice constant is compressed to 3.85Å by 0.07%, only a nominal polarization of 0.11C/m^2 appears, as compared to the large value of ~0.6C/m^2 in bulk $PbTiO_3$. Further calculations on $PbTiO_3/SrTiO_3$ superlattices are in progress.

[1] C. Ederer and N. A. Spaldin, Phys. Rev. Lett. 95 (2005) 257601.
[2] M. Dawber, C. Lichtensteiger, M. Cantoni, M. Veithen, P. Ghosez, K. Johnston, K.M. Rabe, and J.-M. Triscone, Phys. Rev. Lett. 95 (2005) 177601.

RE-ENTRANT RELAXOR BEHAVIOR IN A NEW SOLID SOLUTION OF (1-x)BaTiO3–xAgNbO3

C. Lei and Z-G. Ye[a)]

Department of Chemistry, Simon Fraser University,
8888 University Drive, Burnaby, BC, V5A 1S6, CANADA
[a)] Phone:604-291-3351, Fax: 604-291-3765, Email: zye@sfu.ca

In our research on lead-free relaxor materials, a new perovskite solid solution system of (1-x)$BaTiO_3$–$x$$AgNbO_3$ (with x = 0 to 0.10) was prepared for the first time in the form of ceramics by solid state reaction. The structure, dielectric properties and ferroelectric polarization are investigated. It is found from the temperature dependence of dielectric constant that, with increasing $AgNbO_3$ amount (x) in the solid solution, the para- to ferro-electric phase transition takes place between 120 and 130 ^{o}C, which is associated with the transition in pure $BaTiO_3$ (BT). The two other dielectric peaks, corresponding to the low temperature phase transitions in BT, tend to merge and become a single peak in the solid solution with $x \geq 0.03$. These peaks show dielectric relaxation satisfying the Vogel-Fulcher law, indicating typical relaxor behavior (Fig. 1). The Curie-Weiss law applies to all the compositions up to a constant temperature of T_d, below which the deviation starts to appear.

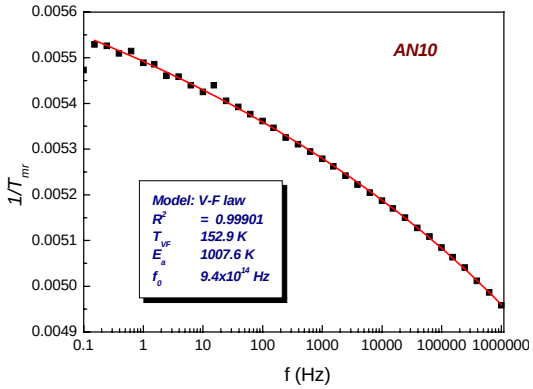

FIG. 1. The inverse temperatures of real permittivity maxima as a function of frequency of 0.9BT-0.1AN ceramics. Solid curve represents the fitting to the Volgel-Fulcher law.

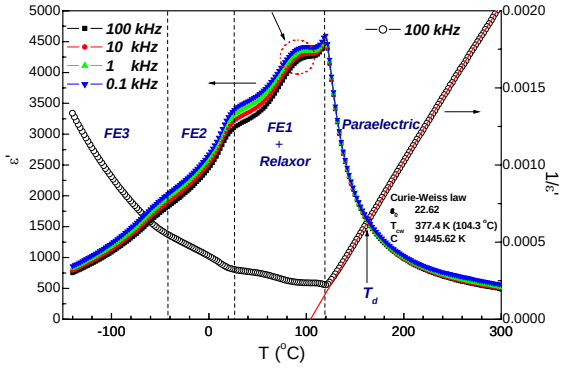

FIG. 2. Temperature dependence of the real part of the dielectric permittivity (ε') of the 0.99$BaTiO_3$-0.01$AgNbO_3$ ceramics measured at different frequencies upon cooling, and the reciprocal of dielectric constant ($1/\varepsilon'$) as a function of temperature at 100 kHz. Solid line is the fitting to the Curie-Weiss law.

The most interesting feature of this solid solution lies in that it exhibits re-entrant phenomenon, which means that the relaxor state occurs after the para- to ferro-electric

phase transition upon cooling, i.e., inside the ferroelectric phase (see Fig. 2 as an example). Such a re-entrant disordered phase, predicted theoretically long ago for magnetic spin glass (SG) by Sherrington and Kirkpatrick,[1] was found in many amorphous metallic magnets and SG alloys.[2] The term "re-entrant", something of a misnomer, means here that the cluster-glass state re-enters the disordered phase from ferromagnetic (FM) state, since the re-entrant SG (RSG) does not re-enter the normal (i.e. paramagnetic) state at T_{xy} (the FM-SG phase transition temperature).[3] Indeed, recent results reveal that the FM order does not collapse across T_{xy}, leading to coexisting FM and SG orderings.[2] Although the phenomenon is general in FM systems, no good theoretical model has been found yet. This unusual phase transition phenomenon was only reported recently in the $Ba_{0.9}Bi_{0.067}(Ti_{1-x}Zr_x)O_3$ solid solution as the first (di)electric analogy[4] (and no equivalent example has been reported for the canonical lead-based relaxor ferroelectrics). Moreover, the relaxor state arises from a tetragonal phase rather than from a cubic phase as observed in conventional relaxors. Fig. 3 shows the experimental XRD pattern (open circles) and deconvoluted phases of the {200} reflection at selected temperatures of 0.99BT-0.01AN sample. The phase diagram of (1-x)BT-xAN system was also established from dielectric spectroscopic analysis (see Fig. 4).Thus, the (1-x)$BaTiO_3$–$xAgNbO_3$ system provides an additional and interesting example of the re-entrant relaxor behaviour.

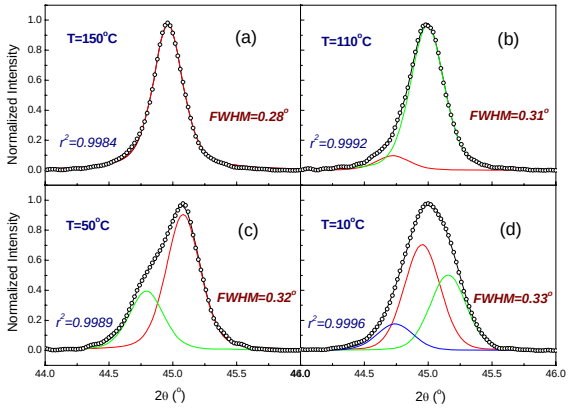

FIG. 3. Powder XRD pattern of the (200) peak in 0.99BT-0.01AN ceramics at selected temperatures, and the deconvolution of the peak profile with different phase components.

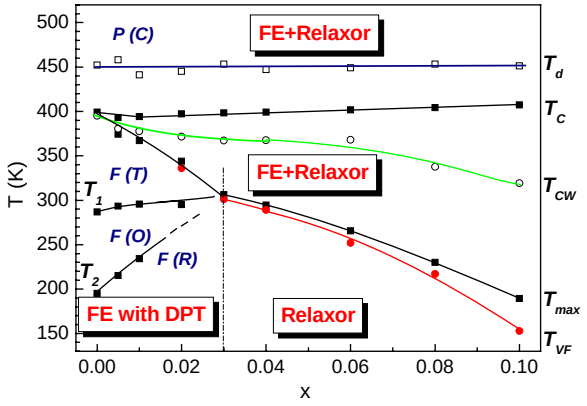

FIG. 4 Phase diagram of (1-x)BT-xAN system established from dielectric spectroscopic analysis.

The authors would like to thank Dr. A. A. Bokov for helpful discussion. This work was supported by the U.S. Office of Naval Research (Grant No. N00014-06-1-0166).

[1] D. Sherrington and S. Kirkpatrick, Phys. Rev. Lett. **25,** 1792 (1975).

[2] D. H. Ryan, in *Recent Progress in Random Magnets*, edited by D. H. Ryan (World Scientific Publishing Co. Pte. Ltd. 1992), pp. 1-40.

[3] J. A. Mydosh, in Spin Glasses: and experimental introduction, (Taylor & Francis Ltd 1993).

[4] A. Simon, J. Ravez and M. Maglione, *Solid State Sci.*, **7**, 925 (2005).

Quasi-ferroelectric State in $Ba(Ti_{1-x}Zr_x)O_3$ Relaxor

A.A. Bokov[1], M. Maglione[2], and Z.-G. Ye [1]

[1] Department of Chemistry, Simon Fraser University, Burnaby, BC, V5A 1S6, Canada
[2] ICMCB—CNRS, 33608 Pessac, France
Phone: 604-291-3351; Fax: 604-291-3765; e-mail: zye@sfu.ca

The determinative property of relaxors is the extraordinary large, diffuse and frequency-dispersive maximum in the temperature dependence of dielectric permittivity (ε). This maximum is believed to originate from the polarization of nanosize regions inside which permanent ferroelectric-like order exists. The relaxor behavior has been studied elaborately in lead-containing crystals with perovskite-type structure where the evolution of the high-temperature cubic ergodic relaxor phase upon cooling is known to occur in one of the two ways. In some relaxors, e.g. in $(1-x)Pb(Mg_{1/3}Nb_{2/3})O_3 - xPbTiO_3$ with large x, the ergodic phase transforms into a ferroelectric phase at a Curie temperature which is usually several degrees below the temperature of the permittivity maximum, T_m. In some others, the canonical relaxors, e.g. in $Pb(Mg_{1/3}Nb_{2/3})O_3$, the structure remains macroscopically cubic (nonpolar) but a glassy nonergodic relaxor phase appears. The ergodicity becomes broken because of the dipolar interactions, which lead to a cluster glass state where the dipole moments of polar nanoragions are frozen in random directions.

In the present work we report the discovery a new type of relaxor behavior. In the perovskite $Ba(Ti_{0.675}Zr_{0.325})O_3$ (BTZ_{325}) solid solution which was known to be relaxor with a cubic structure (space group $Pm\bar{3}m$) down to low temperatures the dielectric dipole dynamics is, however, found not to be subject to any critical slowing-down and freezing. This implies that in contrast to other known relaxors the low-temperature state in BTZ_{325} is neither dipolar glass nor ferroelectric. Nevertheless, such a state is nonergodic, and it can be called quasi-ferroelectric state.

To study the dipole dynamics in BTZ_{325} ceramics we used the dielectric spectroscopy in a wide frequency range of $10^{-2} - 10^6$ Hz. The ceramics exhibits the basic characteristics of relaxors including very large and diffuse peak of $\varepsilon'(T)$ with a strong dispersion at the low-temperature side and the Vogel-Fulcher (VF) shift of T_m as well as two relaxation processes in the high-temperature ergodic relaxor phase, namely the Kohlrausch-Williams-Watts (KWW) relaxation which is related to the main contribution to the $\varepsilon'(T)$ peak and the Curie-von Schweidler (CS) relaxation which becomes significant only at the lowest studied frequencies. Using the method of fitting of dielectric spectra at selected temperatures developed in [1] the relaxation parameters are determined and their temperature dependencies are analysed. It is found that in the temperature vicinity of $T_m \sim$ 190 K the parameters of KWW relaxation (the characteristic relaxation time τ_{KWW} and stretching exponent β) and the CS relaxation exponent n obey the VF-type temperature relations: $\tau_{KWW} = \tau_0 \exp\left[E_\tau / \left(T - T_f\right)\right]$, $\beta = \beta_0 \exp\left[- E_\beta / \left(T - T_f\right)\right]$ and $n = n_0 \exp\left[- E_n / \left(T - T_n\right)\right]$ (see figures where the fitted VF

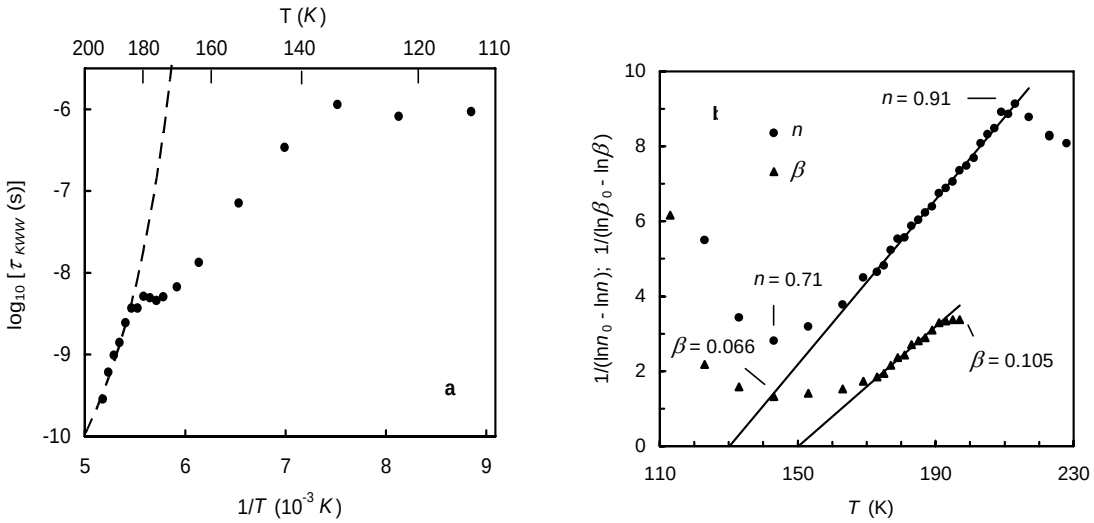

dependences are shown by lines). If these relations persisted down to the lowest temperatures, they would indicate freezing of the KWW and CS spectra at T_f and T_n, respectively [1]. However, the VF relations are violated at ~170 K so that at lower temperatures τ_{KWW} becomes almost temperature-independent, while β and n even increase upon cooling, indicating that the freezing of dipole dynamics does not take place and the system of dipoles (presumably the dipole moments of polar nanoregions) giving rise to dielectric response remains ergodic. However, the pyro- and piezoelectric effects in poled samples and the ferroelectric-type hysteresis loops are observed in BTZ, hinting at the nonergodicity of the low-temperature state.

To account for the full set of experimental data we suggest the existence of two types of polar nanoregions in the low-temperature quasi-ferroelectric phase: dynamic nanoregions which are responsible for the $\varepsilon'(T)$ peak and dielectric relaxation and static nanoregions determining the ferroelectric properties. The polar regions coexist with the non-polar Zr-rich nanoregions which have recently been found in EXAFS experiments [2].

This work was supported by the U.S. Office of Naval Research (Grant No. N00014-06-1-0166).

[1] A. A. Bokov and Z.-G. Ye, Phys. Rev. B **74** 132102 (2006).
[2] C. Laulhe, F. Hippert, J. Kreisel, M. Maglione, A. Simon, L. Hazemann and V. Nassif Phys. Rev. B **74**, 014106 (2006).

Pressure-Induced Non-canonical Relaxor State in $Pb(Mg_{1/3}Nb_{2/3})O_3$–$PbTiO_3$ Crystals

A.A. Bokov[1], A. Hilczer[2], M. Szafrański[2], and Z.-G. Ye[1]
[1] Department of Chemistry, Simon Fraser University, Burnaby, BC, V5A 1S6, Canada
[2] Institute of Physics, Adam Mickiewicz University, 61-614 Poznań, Poland
Phone: 604-291-3351; Fax: 604-291-3765; e-mail: zye@sfu.ca

The effect of hydrostatic pressure on ferroelectric (FE) phase transitions has been studied for some time. In perovskites, which are the best-known displacive ferroelectrics, the stability of the FE phase is reduced under pressure so that a linear decrease of the Curie temperature is observed. The interest in this field has been renewed thanks to a number of interesting and sometimes unexpected discoveries in the past decade. It was found that pressure can change not only the intensity of the interactions responsible for the FE ordering, but also their type. In particular, in ferroelectrics with a compositionally disordered structure (e.g. perovskite solid solutions) a moderate pressure leads to the crossover from ferroelectric to relaxor behavior [1]. The crossover has been explained by the qualitative change of interactions among reorientable polar nanoregions that are present in the high-temperature phase of these materials. The critical (crossover) pressure has been derived theoretically in the framework of the coupled spherical random bond – random field phonon model [2] as the pressure above which the characteristic relaxation time diverges and the FE phase transforms into the spherical glass phase. It is believed that the mechanism of the FE-to-relaxor crossover upon varying the degree of crystalline disorder by chemical substitution and by increasing pressure is essentially the same and the analogy is helpful in elucidating the nature of relaxor ferroelectricity [1]. Experimentally, however, only some characteristics of pressure-induced relaxor behavior were confirmed, namely, it was shown that with increasing pressure a comparatively sharp and non-dispersive dielectric anomaly corresponding to FE phase transition at T_C gradually decreases and broadens and conventional relaxor dispersion appears. On the other hand, the freezing of the dielectric spectrum and the restoring of the cubic crystal symmetry in the low-temperature state have not been verified.

In the present work we study the effect of pressure on the dielectric response in the perovskite $0.69Pb(Mg_{1/3}Nb_{2/3})O_3$–$0.31PbTiO_3$ (PMN-0.31PT) single crystal. A sharp FE transition exists under ambient conditions and the crossover to the relaxor-type behavior is observed at high pressure. However, the behavior is found to be very different from that in pure PMN. In particular, increasing pressure does not induce any changes in the dielectric spectrum which might indicate the approach of the system to the nonergodic dipolar (or spherical) glass state. This implies that the high pressure generates a new relaxor state which distinguishes itself from the low-temperature state observed in canonical relaxors at atmospheric pressure.

The complex dielectric permittivity is measured in the frequency ranges of 10^{-2} – 10^6 Hz and pressure up to 0.8 GPa. The normalized permittivity $\varepsilon'/\varepsilon_m$ versus a reduced temperature, $T - T_m$, where ε_m is the value of ε' at T_m is plotted in Fig. 1. Interestingly, at $T > T_C$ all data points collapse onto a single master curve, which means that the shape of

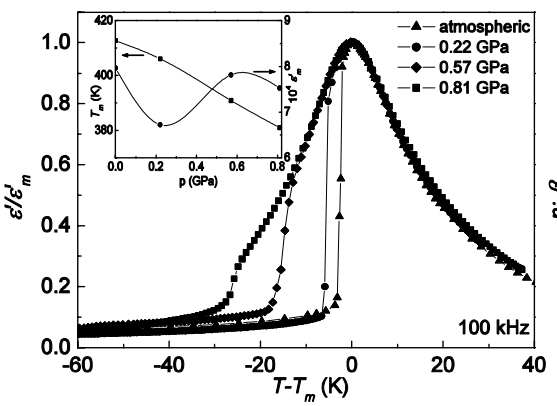

Fig.1

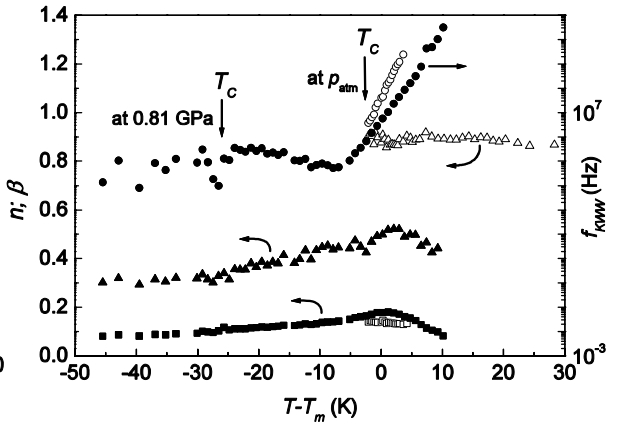

Fig.2

the $\varepsilon'(T)$ peak does not change with pressure. The peak merely moves to lower temperatures. This is the first important difference between the relaxor behavior induced by pressure and that observed as a result of FE-to-relaxor crossover upon varying composition. The latter is accompanied, as a rule, by the increase of $\varepsilon'(T)$ diffuseness.

The dielectric spectra at selected temperatures are fitted using the method developed in [3], and two relaxation processes in the high-temperature ergodic relaxor phase were found, namely, the Kohlrausch-Williams-Watts (KWW) relaxation which is related to the main contribution to the $\varepsilon'(T)$ peak and the Curie-von Schweidler (CS) relaxation which becomes significant only at low frequencies. The relaxation parameters are determined and analysed. Fig. 2 shows the temperature dependences of characteristic relaxation frequency f_{KWW} (circles) and stretching exponent β (squares) for the KWW relaxation and the CS relaxation exponent n (triangles) at atmospheric pressure (unfilled symbols) and at 0.81 GPa (filled symbols). In contrast to canonical relaxors (e.g. PMN) where f_{KWW}, β and n tend to zero $T_f > 0$ following the Vogel-Fulcher law, indicating thereby the freezing of dipole dynamics at temperature T_f below which the glassy nonergodic relaxor state exists, in the pressure-induced relaxor state these parameters does not obey the Vogel-Fulcher law, furthermore they remain unchanged or slightly temperature-dependent below T_m. This means that the relaxor-type freezing of dipole dynamics in the low-temperature state does not occur despite the fact that some relaxor features, e.g. the Vogel-Fulcher frequency shift of T_m, are developed.

The properties of the pressure-induced relaxor state in PMN–0.31PT are further studied in this work and the results are explained in the framework of the microscopic model of FE phase transitions in crystals with quenched compositional disorder [4]. It would be interesting to apply similar methodology to study the FE-to-relaxor crossover in other crystals and to determine if the behavior observed in the PMN–0.31PT is general.

This work was supported by the U.S. Office of Naval Research (Grant No. N00014-06-1-0166).

[1] G. A. Samara and E. L. Venturini, Phase Transitions **79**, 21 (2006).
[2] R. Blinc, V. Bobnar, and R. Pirc, Phys. Rev. B **64**, 132103 (2001).
[3] A. A. Bokov and Z.-G. Ye, Phys. Rev. B **74** 132102 (2006).
[4] A. A. Bokov, J. Exp. Theor. Phys. **84**, 994 (1997).

Extremely slow kinetics and non-ergodicity of a relaxor $K_{1-x}Li_xTaO_3$

Hiroko Yokota and Yoshiaki Uesu
Department of Physics, Faculty of Science and Engineering, Waseda University
3-4-1 Okubo Shinjuku-ku Tokyo 169-8555, JAPAN
Phone: +81-3-5286-3446 ; Fax: +81-3- ; e-mail: hiroko-9bq@ruri.waseda.jp

$KTaO_3$ (KTO) is known to be one of the most typical quantum paraelectrics, in which quantum fluctuations suppress the low-lying soft-mode at low temperature and prevent a ferroelectric phase transition. A small addition of impurities or an application of external field can easily induce a polar state. Depending on impurities, the state could be in a long-range order (ferroelectric) or stays in a local order (dipole glass or relaxor). In KTO, the substitution of Li ions at K sites (KLT-*x*%) induces dipole moments originating from a strong off-center position of Li ions. Based on neutron diffuse scattering experiments and dielectric measurements, Toulouse et al. claim that KLT is a relaxor.[1,2] We performed SHG microscope (SHGM) observations to determine the polarization behavior[3], high precision X-ray diffraction studies to determine minute lattice strains and supplementary neutron scattering and dielectric measurements on KLT with different Li concentrations. These investigations also support that KLT is a relaxor. In the present paper, we report that KLT-3 with the critical concentration shows extremely slow kinetics under the electric field which is similar to a prototype relaxor $Pb(Mg_{1/3}Nb_{2/3})O_3$ and this phenomenon can be interpreted by the Avrami theory.

We use the SHG microscope to observe the time evolution of the order parameter because SHG is quite sensitive to the change in polarization. The sample is cooled down to 24K without an electric field *E*, and heated without *E* to a certain temperature at which a time evolution measurement is performed. When the temperature becomes stable, the electric field of 80V/mm is applied and the field-induced SH intensity is observed as a function of time. Figure 1 shows the results of KLT-3 at several temperatures below Curie temperature of 50K. Below 35K, SH intensity does not increase within the laboratory time. This fact indicates that this temperature range is a non-ergodic state. At 39.7K, SH intensity begins to increase dramatically after a long incubation time of 40 minutes. At 42 and 43K, the SH intensity increases steeply immediately after applying *E*, then gradually up to the saturation state. Thus the behavior is fundamentally different above and below 40K.

We analyze the peculiar phenomenon using the Avrami theory. In the Avrami theory, the total volume v of nuclei is described with fitting parameters k and n as

$$v = 1 - \exp(-kt^n) \qquad (1)$$

Assuming that the SH intensity is proportional to v, we fit the time evolution of SH intensity using eq.(1). The results at 42K and 39.7K are shown in Fig.2, from which fitting parameters k and n are determined. The same fitting procedure is also performed with the data obtained at 43K. The determined exponent n is about 0.5 above 40K and between 4 and 5 at 39.7K. According to Avrami, n changes depending on nucleation and growth velocities. If we presume that nucleation and growth velocities are constant with respect to time, n takes 2, 3 or 4 depending on the domain shape, linear, plate-like and polyhedron, respectively. When the number of nuclei is constant and domains grow with the diffusion-controlled velocity, n takes 0.5. The present analysis discloses that the exponent n changes from 0.5 to about 4 at 40K. This indicates that the temporal behavior above 40K is governed by the diffusion-controlled process with a constant nuclei number, while domains grow in the three-dimensional directions with the nucleation number proportional to time below 40K.

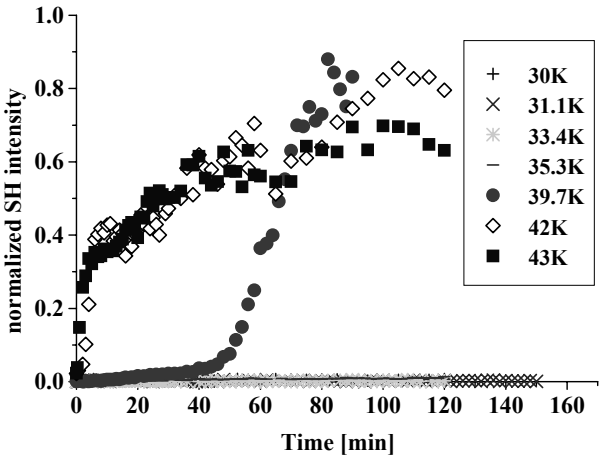

Fig.1 Time evolution of SH intensities

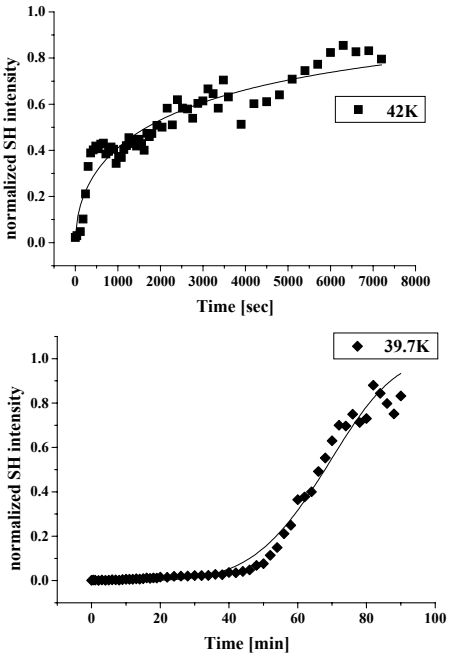

Fig.2 Fitting with the Avrami theory

[1] J. Toulouse, B. E. Vugmeister and R. Pattnaik, Phys. Rev. Lett. **73**, 25, 3467(1994)

[2] G. Yong, J. Toulouse, R. Erwin, S.M. Shapiro and B. Hennion, Phys.Rev. **B62**, 22, 14735(2000)

[3] H. Yokota, T. Oyama and Y. Uesu, Phys. Rev. **B72**, 144103(2005)

Distribution of Polarization Switching Times and Switching Dynamics in Polycrystalline $Pb(Zr,Ti)O_3$ Films

J. Y. Jo[1], H. S. Han[1], Jong-Gul Yoon[2], C. Y. Koo[3], S. H. Kim[3], and T. W. Noh[1]

[1]*ReCOE & FPRD, Department of Physics and Astronomy, Seoul Nat'l Univ., Korea*

[2]*Department of Physics, University of Suwon, Kyunggi-do 445-743, Korea*

[3]*R&D center, INOSTK Inc., Korea*

Phone:+82-2-883-1385; Fax:+82-2-875-1222; e-mail : jgyoon@ suwon.ac.kr

Polarization switching in ferroelectric materials has been investigated intensively for the understanding of domain reversal process. The subject is becoming more important to ferroelectric memory devices for low-voltage/high-speed operation. Kolmogorov-Avrami-Ishibashi (KAI) model, which is based on nucleation and growth of opposite domains, has been successful in describing the switching kinetics of ferroelectric single crystals and epitaxial films. However, the KAI model is not satisfactory for a quantitative explanation of the switching kinetics in polycrystalline thin films. In this work, we will present a quantitative description of switching kinetics in polycrystalline $PbZr_{0.3}Ti_{0.7}O_3$ (PZT) thin films and discuss about Lorentzian distribution of internal field.

The switching kinetics in polycrystalline PZT film was investigated at various fields and temperatures by measuring polarization ($\Delta P=P_{sw}-P_{ns}$) with the pulse fields of widths between 200 ns and 1 ms, as shown in Figs. 1(a) and 1(b). Application of the KAI model, where normalized $\Delta P(t)=1-\exp[-(t/t_0)^n]$, to our experimental data resulted in unphysical n values smaller than 1, as shown in Fig. 2(a). Correct description of switching kinetics was not possible especially for our low-field and low-temperature experiments as can be seen in Figs. 1(c) and 1(d). As an alternative approach, Lorentzian distribution of $\log t_0$ for the characteristic switching times t_0 in KAI model provided a quantitatively good explanation of our polarization switching data, as shown in Fig. 2(b). Since t_0 is sensitive to an applied field, distribution of the switching times might be directly related to the distribution of internal field. We suggest that the field from randomly distributed (nano)domains in polycrystalline films induces variations in local field. Figure 3 shows that the logarithm of center and width of the Lorentzian switching time distribution are proportional to $1/E_{ext}$ in low-field region. We will discuss switching dynamics of ferroelectric domains in conjunction with randomness and switching-field distribution in polycrystalline and epitaxial thin films.

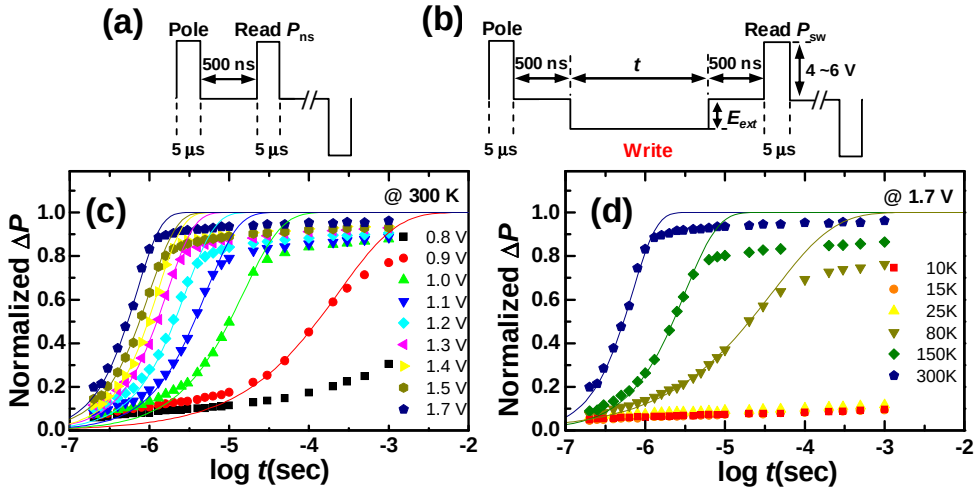

Figure 1. Time(*t*)-dependent polarization switching behavior. Pulse trains to measure (a) non-switched polarization and (b) switched polarization. Normalized switchable polarization (*ΔP*) (c) under various electric fields and (d) under various temperatures. Solid symbols and solid lines correspond to experimental results and fitting results using KAI model, respectively.

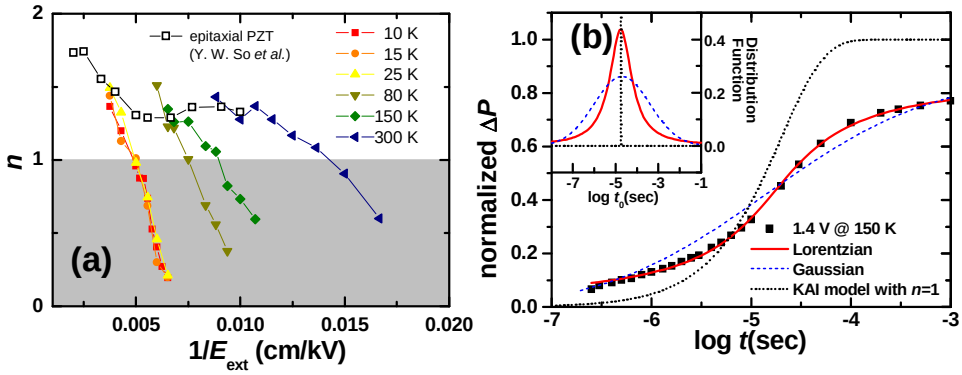

Figure 2. (a) Dimension (*n*) at various electric fields and temperatures under KAI model. Note that *n* values smaller than 1 are unphysical. (b) Normalized *ΔP* with (solid symbols) experimental data and (lines) fitting results. Inset shows distribution functions for log t_0, respectively. Delta distribution function corresponds to KAI model.

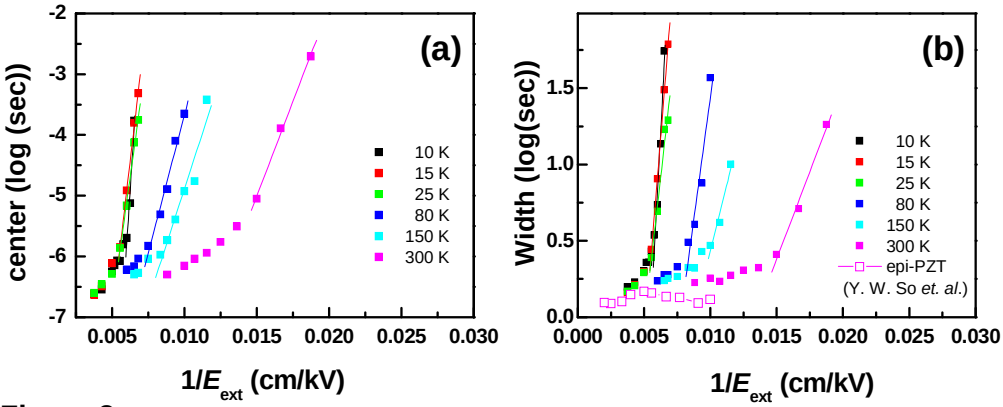

Figure 3. In Lorentzian distribution functions fitting with experimental results, (a) the center and (b) width under various E_{ext} and temperatures. In low E_{ext} region, center and width values are proportional to 1/ E_{ext}.

Thermo-Electromechanical Response of a Ferroelectric Perovskite from Molecular Dynamics Simulation

Xiaowei Zeng [1,2], R. E. Cohen [2], Youping Chen [3], James D. Lee[1]
[1] Department of Mechanical and Aerospace Engineering,
The George Washington University, Washington, DC 20052
[2] Carnegie Institution of Washington, Washington, DC 20015
[3] Department of Mechanical and Aerospace Engineering, University of Florida,
Gainesville, Florida 32611
Phone: 202-994-5945; Fax: 202-994-0238; E-mail: xwzeng@gwu.edu

Based on a shell model potential obtained from first principles calculations, molecular dynamics (MD) simulations are performed to investigate the electromechanical response of a ferroelectric perovskite under finite temperature and electric field. The microscopic paths by which homogeneous polarization reorientation process takes place in a ferroelectric perovskite are characterized. The microscopic switching path shows that the 180^0 switching of polarization consists of two consecutive 90^0 rotations. From our shell model potential, we found the transition from ferroelectric tetragonal to paraelectric cubic to occur at a temperature of 600 K, which underestimates the experimental T_c value of 763 K. This result can be compared to earlier shell model potentials for $PbTiO_3$ that showed T_c of 450 K [1] and 900 K [2].

The change of polarization in response to external electric field applied parallel to the c-axis (the direction of spontaneous polarization) is shown in Fig. 1(a). The polarization response is strongly nonlinear and history dependent. A small electric field applied opposite to the polarization direction results in an initial linear response of polarization parallel to the field. As the field is increased, the response becomes nonlinear and there is a discontinuous jump resulting in 180^0 polarization switching (hysteresis) in $PbTiO_3$ which are quantitatively similar to those seen in theoretical computations [3,4]

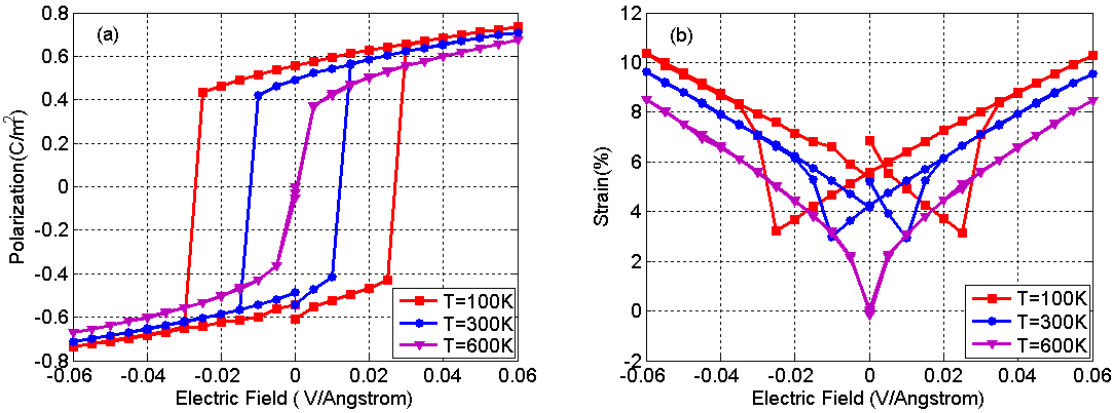

Figure 1 (a) Polarization-electric field (hysteresis loop) and (b) strain-electric field for $PbTiO_3$ as a function of electric field at zero pressure obtained from MD simulations.

The 180^0 switching described above is accompanied by homogeneous straining of the unit cell of the $PbTiO_3$ crystal. In Fig. 1(b) we also show the homogeneous strain

component $\varepsilon_{zz}=(c-a)/a$ as a function of the applied electric field. The butterfly shaped diagrams are qualitatively similar to those seen in theoretical computations [3] or experiments of other related materials, such as PLZT [5]. At different temperature, we find an essentially similar transition path with the exception that there is a slight offset due to the temperature difference. However, when temperature reaches T_c, a value of 600 K in our case, both polarization-electric and strain-electric curve become a line. Our results also show that the switching electric field at high temperature is smaller than that at low temperature.

As an important application of piezoelectric response, the most common coefficients d_{31} and d_{33} of ferroelectric tetragonal $PbTiO_3$ as a function of temperature has been presented in Fig. 2. The agreement with the available experimental data is quite good if we consider the difference between the theoretical and experimental transition temperature.

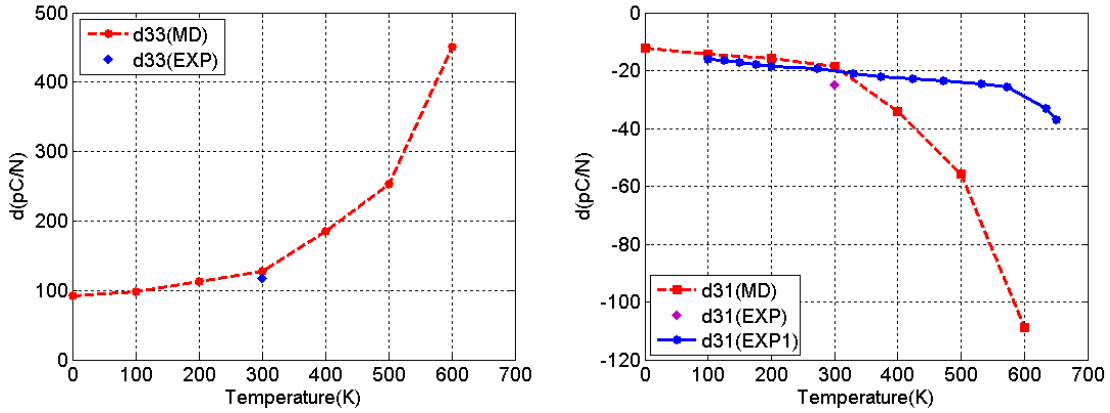

Figure 2 Piezoelectric charge coefficient d_{33} and d_{31} plotted vs temperature. The diamond-shaped data point is an experimental room temperature value and the circular data points and solid curve are the experimentally measured temperature dependence of d_{31} from Ref.6. The dashed curve is the MD simulation results.

The support to this work by National Science Foundation under Award Numbers CMS-0301539 and CMS-0428419 and Office of Naval Research grant N00014-02-1-0506 to REC are gratefully acknowledged.

[1] M. Sepliarsky and R. E. Cohen, Development of a shell model potential for molecular dynamics for $PbTiO_3$ by fitting first-principles results, in Fundamental Physics of Ferroelectrics 2002, R.E. Cohen, Editor. 2002, AIP: Melville, NY. p. 36-44.
[2] A. Asthagiri, Z. Wu, N. Choudhury, and R. E. Cohen, Advances in First-principles Studies of Transducer Materials, Ferroelectrics, **333**:69-78 (2006).
[3] E.B. Tadmor, U.V. Waghmare, G.S. Smith and E. Kaxiras, Polarization switching in $PbTiO_3$: an ab initio finite element simulation, Acta Materialia, **50**, 2989-3002 (2002)
[4] Na Sai, Karin M. Rabe, and David Vanderbilt, Phys. Rev. B, **66**, 104108 (2002)
[5] S. C. Hwang and R. M. McMeeking, Ferroelectrics, **207**, 465 (1998).
[6] V. G. Gavrilyachenko and E. G. Fesenko, Sov. Phys. Crystallogr. **16**, 549 (1971).

Domain Structures and Properties of Strained Epitaxial $BiFeO_3$ Thin films: Thermodynamic Analysis and Phase-field Simulations

J. X. Zhang,[1,*] Y. L. Li,[1,3] Y. Wang,[1] S. Choudhury,[1] Y. H. Chu,[2] F. Zavaliche,[2] Q. X. Jia,[3] D. G. Schlom,[1] R. Ramesh,[2] L. Q. Chen[1]

[1]Department of Materials Science and Engineering
Pennsylvania State University, University Park, PA 16802
[2]Department of Materials Science and Engineering,
and Department of Physics, University of California, Berkeley, CA 94720

[3]MST-STC, Los Alamos National Laboratory, Los Alamos, NM 87545
[*]Phone: (814) 865-0389; email: jzz108@psu.edu

$BiFeO_3$ has attracted a great deal of attention recently due to the coexistence of ferroelectricity and antiferromagnetism at room temperature. Domain structures and ferroelectric properties of epitaxial $BiFeO_3$ thin films could be dramatically different from the corresponding bulk single crystals due to the substrate constraint. In this work, $(001)_c$, $(101)_c$, and $(111)_c$ oriented $BiFeO_3$ ferroelectric thin films are studied using the phenomenological Landau theories (Fig. 1) and the phase-field simulations (Fig. 2). Our studies show that the substrate effect on ferroelectric polarizations and domain structures of $BiFeO_3$ thin films depends on the film orientations and the types of substrate strains. For $(001)_c$ oriented $BiFeO_3$ film, the normal substrate strains only rotate the polarization direction without changing its magnitude ($P_s = |\mathbf{P}|$) considerably, and twin-like domain structures were observed for the full range of substrate strains. While shear substrate strain will have a significant effect on the magnitude of the spontaneous polarization, and a single domain structure was observed for $(001)_c$ oriented films under a shear strain. For $(111)_c$ and $(101)_c$ oriented $BiFeO_3$ films, normal substrate strains can significantly alter domain structures and magnitudes of the spontaneous polarization. The simulation results may provide insight for strain engineering of $BiFeO_3$ ferroelectric thin films.

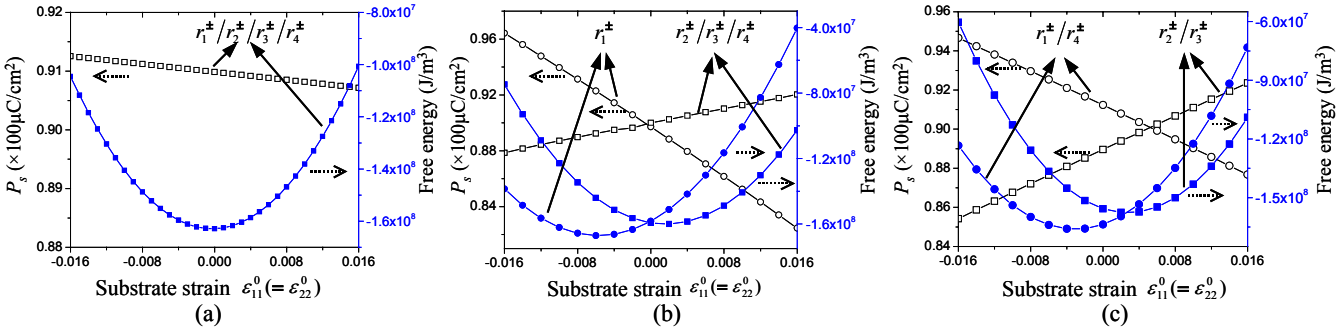

Fig. 1. Free energies and P_s of (a) $(001)_c$, (b) $(111)_c$, and (c) $(101)_c$ oriented $BiFeO_3$ thin films as a function of normal substrate strains. ($r_1^+ = [111]_c$, $r_2^+ = [\bar{1}11]_c$, $r_3^+ = [\bar{1}\bar{1}1]_c$, $r_4^+ = [1\bar{1}1]_c$, $r_1^- = [\bar{1}\bar{1}\bar{1}]_c$, $r_2^- = [1\bar{1}\bar{1}]_c$, $r_3^- = [11\bar{1}]_c$, and $r_4^- = [\bar{1}1\bar{1}]_c$)

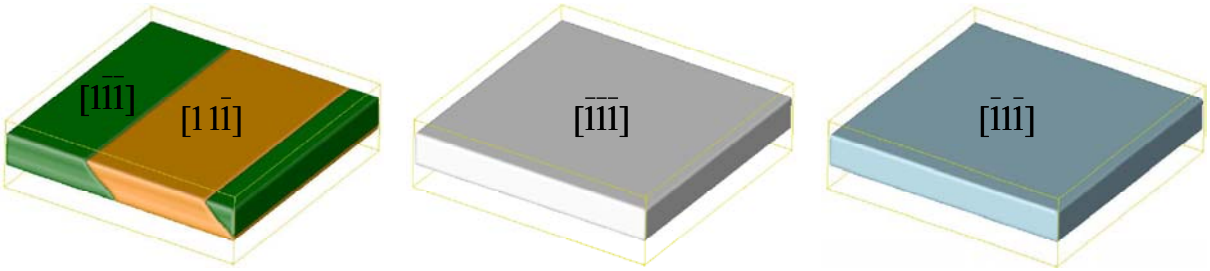

Fig. 2. Domain structures of (a) $(001)_c$, (b) $(111)_c$, and (c) $(101)_c$ oriented $BiFeO_3$ thin films. ($\bar{\varepsilon}_{11} = \bar{\varepsilon}_{22} = -0.015$, $\bar{\varepsilon}_{12} = 0$)